ENHANCED PROPYLENE PRODUCTION BY CATALYTIC CRACKING OF HYDROTREATED VGO OVER NOVEL FCC CATALYST ADDITIVES

BY

ABDELRAHMAN HUSSAIN

A Thesis Presented to the
DEANSHIP OF GRADUATE STUDIES

KING FAHD UNIVERSITY OF PETROLEUM & MINERALS
DHAHRAN, SAUDI ARABIA

In Partial Fulfillment of the
Requirements for the Degree of

MASTER OF SCIENCE

In

CHEMICAL ENGINEERING

SEPTEMBER 2015

KING FAHD UNIVERSITY OF PETROLEUM & MINERALS

DHAHRAN- 31261, SAUDI ARABIA

DEANSHIP OF GRADUATE STUDIES

This thesis, written by **ABDELRAHMAN I. HUSSAIN** under the direction his thesis advisor and approved by his thesis committee, has been presented and accepted by the Dean of Graduate Studies, in partial fulfillment of the requirements for the degree of **MASTER OF SCIENCE IN CHEMICAL ENGINEERING.**

Dr. Sulaiman Al-Khattaf
(Advisor)

Dr. Mohammed Ba-Shammakh
Department Chairman

Dr. Mohammed Ba-Shammakh
(Member)

Dr. Salam A. Zummo
Dean of Graduate Studies

Dr. Mohammad Hossain
(Member)

13/12/15

Date

Dedicated to my uncle Omar Siribbal,

his words of encouragement still ring in my ears

May almighty Allah bless his soul

ACKNOWLEDGMENTS

All Praises and gratitude to almighty Allah for giving me strength, endurance and patience to complete this work successfully. I thank him for guiding me to this point of my career and the uncountable favors he has bestowed on me.

Thereafter, I am thankful to King Fahd University of Petroleum and Minerals for giving me the chance to pursue my graduate studies. I would like to express my deepest gratitude to my thesis advisor Dr. Sulaiman Al-Khattaf for his excellent guidance, inspiration and motivation. I am very thankful for his support academically and emotionally. His insightful comments and encouragement gave me the power to move on and face all difficulties during this research. I also wish to extend my sincere gratefulness to my Committee members: Dr. Mohammed Ba-Shammakh and Dr. Mohammed Mozahar Hossain for their immense assistance and valuable suggestions.

I am very grateful to Dr. Abdullah Aitani for his kind assistance and professional advices. I am thankful for his patience in reading and commenting on many revisions of this work. My sincere thanks also goes to Dr. Nabil al Yassir for his countless efforts and assistance. I am very thankful for the long discussions that helped me to build the chemistry background related to my research. He was always willing to help and give his best advices. Many thanks to Dr. Jiří Čejka from J. Heyrovský Institute of Physical Chemistry for his valuable help and support.

I am also grateful to FCC lab staff: Mr. Mian Rahat, Mr. Mohammed Abdulbari and Mr. Ramzi Al-Shuqaih for assisting me in the experimental work and training me on different

catalyst evaluation techniques. They provided me with a professional and very joyful work environment.

Last, I am very thankful to my father, mother, brothers and my extended family for their moral guidance and caring throughout my life.

TABLE OF CONTENTS

LIST OF TABLES

LIST OF FIGURES

LIST OF ABBREVIATIONS AND NOMENCLATURE

FCC	:	Fluid Catalytic Cracking
MAT	:	Microactivity Test
VGO	:	Vacuum Gas Oil
E-Cat	:	Equilibrium Catalyst
USY	:	UltraStable Y zeolite
LPG	:	Liquefied Petroleum Gas
LCO	:	Light Cycle Oil
HCO	:	Heavy Cycle Oil
RON	:	Research Octane Number
HTC	:	Hydrogen Transfer Coefficient
C/O	:	Catalyst to Oil ratio
XRD	:	X-ray Diffraction
SEM	:	Scanning Electron Microscopy
FTIR	:	Fourier Transform Infrared
BET	:	Fourier Transform Infrared
$\mathbf{k_{ij}}$	:	Reaction rate constant for reaction of lump *i* to lump *j*

$\mathbf{k_{o\text{-}ij}}$	:	Pre-exponential factor for reaction of lump *i* to lump *j*
$\mathbf{E_{ij}}$	:	Apparent activation energy for reaction of lump *i* to lump *j*
t	:	Contact time
$\mathbf{t_{os}}$	:	Time on stream
$\boldsymbol{\alpha}$	:	Deactivation constant
$\boldsymbol{\varphi}$	:	Deactivation function
$\boldsymbol{Y_i}$	:	Weight fraction of lump *i*
T	:	Reaction temperature
$\mathbf{T_o}$	:	Average temperature of the experiments
R	:	Universal gas constant

ABSTRACT

Full Name : Abdelrahman Izzeldin Hassan Hussain

Thesis Title : Enhanced Propylene Production by Catalytic Cracking of Hydrotreated VGO over Novel FCC Catalyst Additives

Major Field : Chemical Engineering

Date of Degree : September 2015

Fluid catalytic cracking (FCC) process is a source of considerable amounts of global propylene as well as gasoline. Its product distribution is increasingly shifting to maximize propylene yield in order to meet high demand from petrochemicals users.

In this study, catalytic cracking of hydrotreated vacuum gas oil (VGO) was carried out in a microactivity test (MAT) unit. Commercial FCC USY catalyst (E-Cat) was used and modified by various zeolites with different pore structures and different Si/Al molar ratio. These zeolites included SSZ-74, SSZ-33, MCM-22, MCM-36, ZSM-5, TNU-9, IM-5, and ferrierite. At constant conversion and comparable Si/Al molar ratio, the highest propylene yield of ~11 wt.% was achieved over ferrierite and MCM-36 compared with 7 wt.% over E-Cat. An increase in light olefins yield over all additives was associated with a decrease in gasoline yield due to the cracking of gasoline-range reactive species. It was found that additives with lower ability to carry bimolecular reactions were more selective to light olefins. With increasing Si/Al molar ratio, both propylene and light olefins yields passed through maxima. Results of kinetic study showed that the additives helped to decrease activation energy for the cracking reaction of gasoline to gases.

ملخص الرسالة

الاسم الكامل:عبدالرحمن عزالدين حسن حسين

عنوان الرسالة: تحسين إنتاج البروبلين من عمليات التكسير الحفزي للزيت الفراغي عن طريق إضافات حفازات التكسير المميع

التخصص: هندسة كيميائية

تاريخ الدرجة العلمية:سبتمبر ٢٠١٥

تعتبر عملية التكسير الحفزي من العمليات الأساسية في صناعة تكرير البترول. حيث أنها أحد المصادر المهمة للإنتاج مادة البروبلين إلى جانب الجازولين. ومع ازدياد الطلب العالمي للبروبلين, تتواصل الجهود لتحويل ناتج عمليات التكسير الحفزي لزيادة إنتاج البروبلين لتلبية إحتياجات الصناعة البتروكيماوية.

في هذه الدراسة, تم إجراء التكسير الحفزي للزيت الفراغي في وحدة تفاعل كيميائي من نوع (MAT). حيث تم إستخدام حفاز مستخدم في مصافي البترول كأساس وتم تحسينها عن طريق اضافة مواد زيولايتية ذات تراكيب مختلفة وذات نسب سيليكا إلى ألومينا متفاوتة. وتضمنت الإضافات كل من SSZ-74, SSZ-33, MCM-22, MCM-36, ZSM-5, TNU-9, IM-5 و ferrierite. أظهرت النتائج عند نسب سيليكا الى الومينا متقاربة, أعلى نسبة بروبلين في المنتج النهائي كانت 11wt.% وتحصل عليها من زيولايت من نوع MCM-36 و ferrierite مقارنة ب 7 wt.% للحفاز الأساسي (غير المحسن). وتمت زيادة إنتاج الألوفينات الخفيفة عن طريق تكسير إضافي للمواد النشطة الموجودة في الجازولين. وتبين أن المواد الزيولايتية ذات القدرة الضعيفة لتنشيط تفاعل أنتقال الهيدروجين, ذات إنتاجية أعلى للبروبلين. وجد أن زيادة نسبة السيليكا الى الألومينا ذو فعالية في إنتاج البروبلين نتيجة لتثبيطها تفاعل أنتقال الهيدروجين. و أوضحت دراسة حركية تفاعل التكسير الحفزي للزيت الفراغي أن الإضافات الزيولايتية قادرة على تقليل طاقة التنشيط اللازمة لتفاعل تكسير الجازولين للمنتج الغازي.

CHAPTER 1

INTRODUCTION

1.1 Background

Propylene is an important building block for the petrochemicals industry. It is used in the production of polypropylene, propylene oxide, acrylo-nitrile, cumene, acrylic acid and other products [1,2]. Global demand for propylene increased from 65 million ton/year in 2009 to 84 million ton/year in 2013, and it is anticipated to reach 120 million ton/year by 2022 [3]. The high demand for propylene built a supply issue which is the reason for increasing propylene prices. Figure 1 shows global propylene production growth. Over 90% of propylene is obtained as by product from either steam cracking of hydrocarbons or fluid catalytic cracking (FCC) of vacuum gas oil (VGO). FCC units contribute about 35% to the global propylene production capacity and steam cracking produces about 50% [4,5]. The reminder of propylene is coming from on-purpose technologies. In light of the market conditions and the capability to achieve elevated propylene yield in an FCC unit, there is a desire to maximize propylene yield from these units to overcome the future supply gap.

Figure 2 shows the most important propylene derivatives. About two third of propylene is utilized in the production of polypropylene. Polypropylene became the leading polymer in manufacturing a variety of consumers and industrial products. For instance,

polypropylene accounts for a one third of plastics used in automobiles. It is used in electronic and electrical applications, toys, clothing, pipes and many other products.

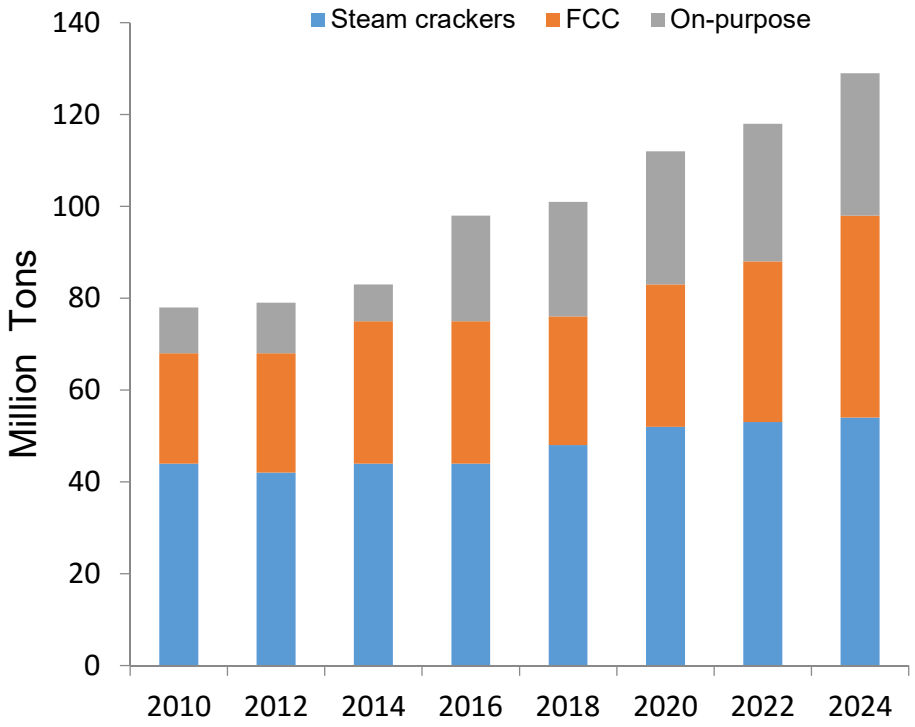

Figure 1 Propylene production capacity[3]

In the 1990s, polypropylene substituted other polymers due to its less expense which is driven by low propylene prices. This caused an increasing demand for polypropylene at 10% per year. However, in the recent years with the increase in propylene cost, polypropylene prices became in the same level of other polymers. The growth in polypropylene demand is now anticipated at average of 5% per year [6].

Acrylonitrile is the second derivative of propylene consumption. Its uses vary from elastomeric polymers to fiber applications. Acrylic fibers are the largest outlet of acrylonitrile.

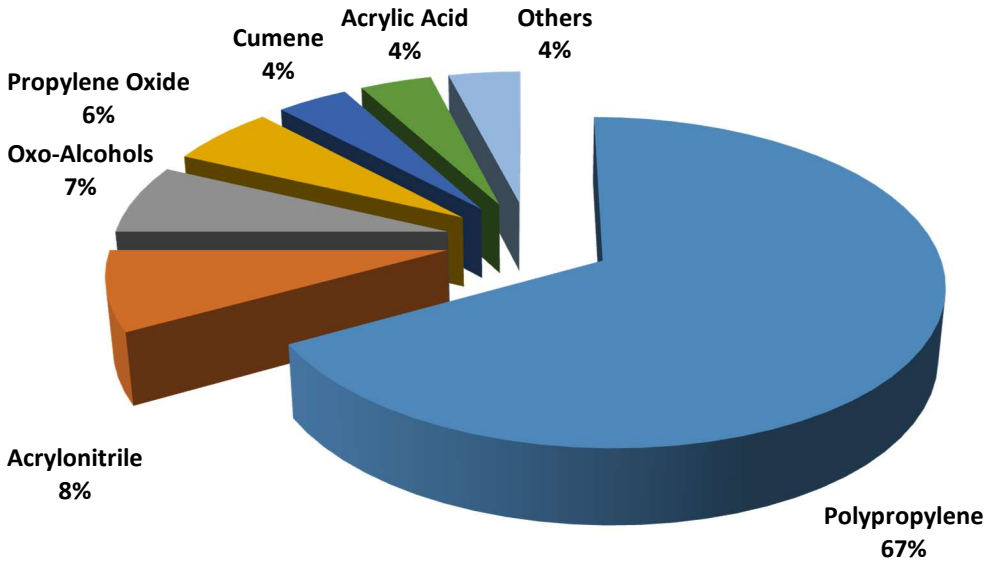

Figure 2 Propylene derivatives [6]

1.2 Main routes for propylene production

1.2.1 Steam Cracking

Steam cracking is the main route to produce propylene and other light olefins. Ethylene is produced as a main product while propylene as a byproduct. Steam cracking reactions

involve hydrocarbons bond breaking and is highly endothermic. Considerable amount of heat is required to derive the reaction to olefins production. Typical feedstocks for steam crackers are ethane, naphtha and LPG. The reactions favors high temperature and low pressure, for this, superheated steam is used to reduce hydrocarbons partial pressure. Steam crackers consist of several pyrolysis furnaces where, the feed is cracked in presence of steam. Typical operating conditions are 750-800 ^{o}C and 1-1.2 atm. The ratio of steam/hydrocarbons is around 0.5 and depends on the type of feed used wither gas or liquid. Steam crackers do not provide full control on propylene to ethylene ratio (P/E), the maximum value that can be obtained is 0.65. Above that, a severe drop in total light olefins occur which cause significant economical drawbacks.

1.2.2 Fluid Catalytic Cracking (FCC)

Fluid catalytic cracking process was originally developed to promote gasoline production by processing vacuum gasoil (VGO) and, in some cases, other feeds such as atmospheric reside. As the market conditions evolve, FCC units are being optimized to produce light olefins (mainly propylene). Conventional FCC units produce approximately 4 wt.%-6 wt.% propylene. Revamping operating conditions and catalyst system enhance propylene yield by 5 wt.%. However, new emerging FCC processes enabling over 20 wt.% propylene production.

1.3 FCC process description

The heart of the FCC unit is the reactor-regenerator section. Figure 3 shows a schematic diagram for a typical FCC reactor. The preheated feed is introduced to the bottom of the

riser reactor together with a regenerated hot catalyst. The regenerated catalyst cause the feed to instantly vaporize and the cracking reactions are taking place in the vapor phase.

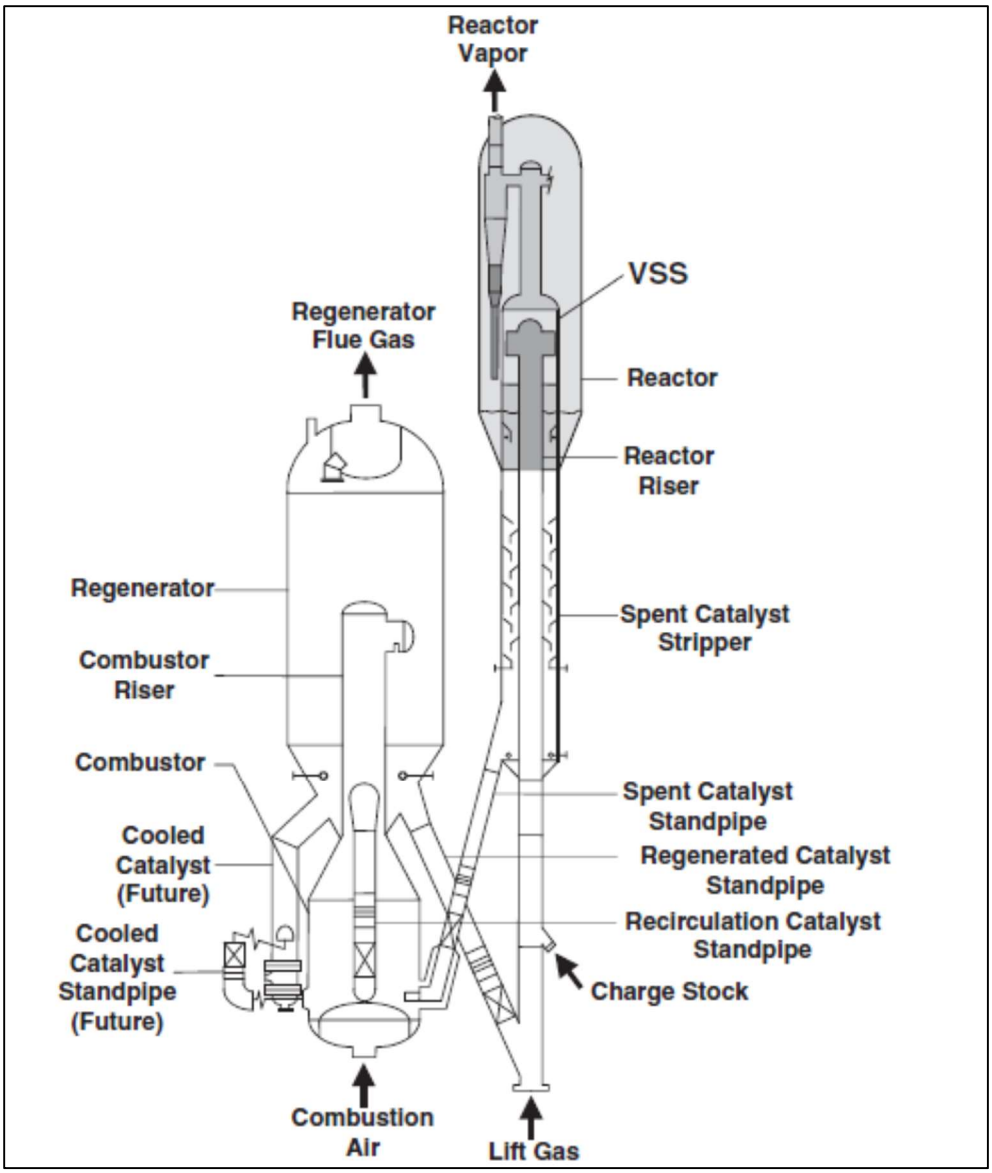

Figure 3 UOP FCC reactor-regenerator configuration [7]

The cracking reaction is endothermic and the heat required is supplied by the regenerated catalyst. The vapors carry the catalyst upward to the top of the riser where the reactions are completed. Typical contact time in the riser is 2–3 seconds. From the riser, the catalyst-hydrocarbons mixture is discharged to the reactor vessel, where the catalyst is rapidly separated from the cracked hydrocarbons through cyclone separation to minimize undesired secondary reactions. Reactor effluent is directed to other FCC sections for products separation and recovery. The spent catalyst drops from the reactor into a stripping section, where some remaining hydrocarbons in the catalyst are removed by steam. After that, the spent catalyst moves through a standpipe to the regenerator.

During the cracking reactions, coke is produced and deposits on the catalyst which causes sever catalyst deactivation. The deactivated catalyst (spent catalyst) is reactivated in the regenerator by continuously burning the coke off the catalyst using hot air. Coke combustion is exothermic reaction and the heat generated is absorbed by the catalyst particles to support the endothermic cracking reactions in the riser reactor. The regenerated catalyst is then circulated back to the riser reactor.

1.4 Increasing propylene yield from FCC units

The main advantage of FCC units is the high flexibility it provides in processing variety of low-cost hydrocarbons feedstocks and product yields. Variety of operating conditions, catalyst systems and additives can be tuned to meet current market demands. All these aspects make propylene more important to refinery and FCC unit economics. High propylene yield from FCC units result from high VGO conversion and selective cracking.

In industrial practice, this is achieved by several solutions such as, increasing operation severity, naphtha recycle, dedicated FCC catalysts and additives.

Increasing operation severity i.e. high temperature and high catalyst/oil (C/O) ratio, favors the conversion and hence, promote light olefins yield. However, employing high reaction temperature has the disadvantage of increasing competing thermal cracking relative to catalytic cracking. Thermal cracking is the main source of undesired dry gas. Increasing C/O ratio has the advantage of compensating the negative effect of high temperature operation.

The above mentioned solutions to increase propylene yield are more reliable in designing new units or revamping existing one. However, the easiest and more efficient method, especially for operating units, is the use of dedicated FCC catalyst and zeolite additives. The use of specialized catalyst containing ZSM-5 zeolite is a widely used method to enhance propylene yield. ZSM-5 additive cracks gasoline range olefins to light olefins taking advantage of its shape-selectivity. Figure 4 shows the role zeolite additives in increasing propylene yield. Zeolite additives can be combined into the base FCC catalyst as an active component in the catalyst matrix or as a separate additive. However, separate additives provide more flexibility in changing the ratio between the base catalyst and additives. This is important with the changing operating conditions and objectives in commercial units [8]. Catalytic cracking processes such as deep catalytic cracking (DCC) utilize ZSM-5 based catalyst at sever conditions to enhance propylene yield. The enhancement in propylene yield was up to 20-25 wt.% compared to 4-6 wt.% for conventional FCC units [9].

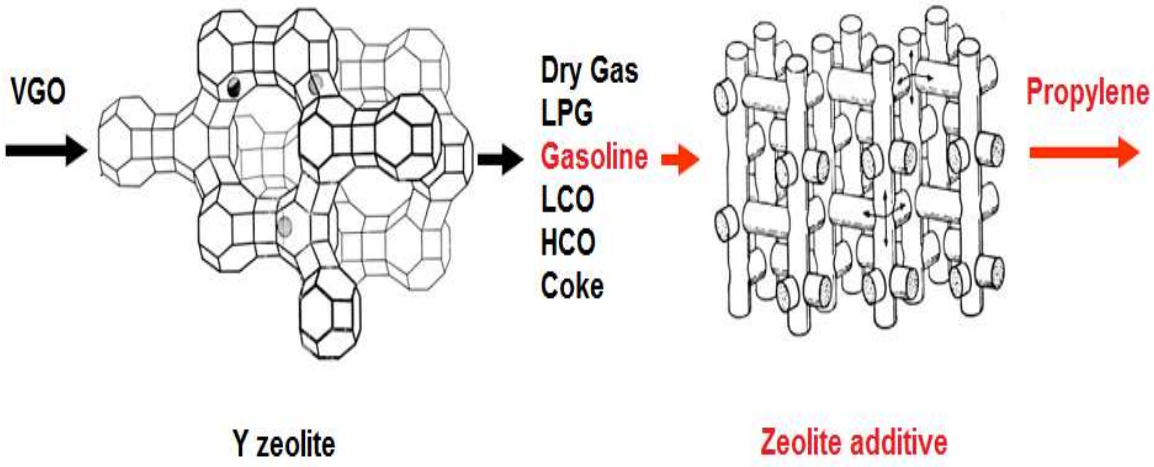

Figure 4 The role of zeolite additives in enhancing propylene yield

1.5 Microactivity evaluation of FCC catalyst

Extensive research and development focused on FCC technology since its invention in 1940s and up today, proposed quite different formulation of catalysts to meet the ever changing operating environments. This made an ongoing and cost effective process for evaluating FCC catalyst very essential. In this regard, the main tool that is extensively used in FCC catalyst evaluation is the Microactivity Test (MAT) unit. This method provides simple and quick technique with reproducible results. The unit is very cost effective as it only needs few grams of catalyst and oil feed compared to pilot plants, where larger amounts of testing materials are required. MAT unit provides the benefit of accessing catalyst activity and selectivity independently of other operating variables in FCC unit. Furthermore, MAT unit is used to assess the reactivity of different hydrocarbons and process variables such as temperature and C/O ratio.

Due to different fundamentals between MAT and commercial units, the absolute yields obtained from MAT runs cannot be used directly to predict catalyst performance in commercial units. However, it provides means to distinguish the performance characteristics of different catalysts when the data are used in comparative manner. Detailed description and methodology of catalyst evaluation using MAT is provided in Chapter 3.

1.6 Thesis objective

The primary objective of this work is to investigate the performance of a series of zeolite materials having different acidic and textural properties as FCC catalyst additives to enhance propylene yield.

The specific objectives are:

1. Investigate the effect of zeolite pore topology on catalyst activity and selectivity.
2. Investigate the effect of zeolite Si/Al molar ratio on propylene selectivity.
3. Study the effect of pore topology and Si/Al molar ratio on activation energies in VGO catalytic cracking.

CHAPTER 2

LITERATURE REVIEW

2.1 FCC catalyst

Historically, developments in catalytic cracking catalyst introduced significant advances to process technology [10]. Increasing the catalyst efficiency continuously changed the type of reactors employed in the process. Catalyst activities were raised significantly over the years and units were redesigned to take full advantage of emerging catalyst technologies [11,12]. New design changes utilized the feed riser as a sole conversion vessel; and the fluidized-bed as a stripper to separate the catalyst from the products.

Commercial FCC catalysts are in the form of spray-dried spherical particles. These catalysts are used in acidic matrix consists of 30-40% zeolite material. Other components of the catalyst matrix include filler and binder to provide physical integrity and mechanical strength to resist process severe conditions and fluidization [7]. Zeolite is the key component in FCC catalyst; it determines the product selectivity and accounts for most of the catalyst activity. As a result, the catalyst performance depends greatly on the type and quality of the zeolite used [13].

Zeolite X and zeolite Y were used in FCC catalysts since 1960s [10,14]. While both have the same crystalline structure, zeolite Y has higher Si/Al molar ratio, greater hydrothermal stability and better selectivity than zeolite X. For these properties, zeolite Y became the dominant zeolite for FCC catalyst [14]. Y zeolite is a three dimensional zeolite contains super cages (1.3 nm diameter) accessible through 12-membere ring with

0.74 nm diameter. Most of the catalytic activity occurs in these cages. The large pore structure of Y zeolite allows the processing of large molecules of heavy feedstocks [15]. Furthermore, it provides high surface area and sufficient acidic character required for catalytic cracking reactions [16]. In order to balance the activity, stability and product quality, Y zeolite was used in several forms such as; Ultrastable Y (USY) and rare earth exchanged Y zeolite (RE-USY) [10,17]. USY FCC catalysts produce more light olefins and higher octane gasoline compared to RE-USY. However, RE-USY catalyst has better activity and stability than USY catalyst [14,15].

2.2 Reaction mechanism

Catalytic cracking reactions follow carbonium ion mechanism [18]. Carbonium ion is generated from both Brønsted and Lewis acid sites [18,19]. Brønsted acid site forms carbonium ion from donation of a proton to an olefin molecule:

$$R\text{-}CH{=}CH\text{-}CH_2\text{-}CH_3 + H^+ \text{ (a proton from Brønsted acid site)} \rightarrow R\text{-}C^+H\text{-}CH_2\text{-}CH_2\text{-}CH_3$$

Lewis acid site form carbonium ion from removal of an electron from paraffin molecule:

$$R\text{-}CH_2\text{-}CH_2\text{-}CH_2\text{-}CH_3 \text{ (removal of } H^- \text{ at Lewis site)} \rightarrow R\text{-}C^+H\text{-}CH_2\text{-}CH_2\text{-}CH_3$$

After forming the carbonium ion, the reactions proceed through carbonium ion intermediates. These reactions include primary reactions (cracking of carbon-carbon bond) and secondary reactions of the cracked products. Figure 5 summarizes main FCC reactions according to molecular description. From this set of reactions, the most important ones are:

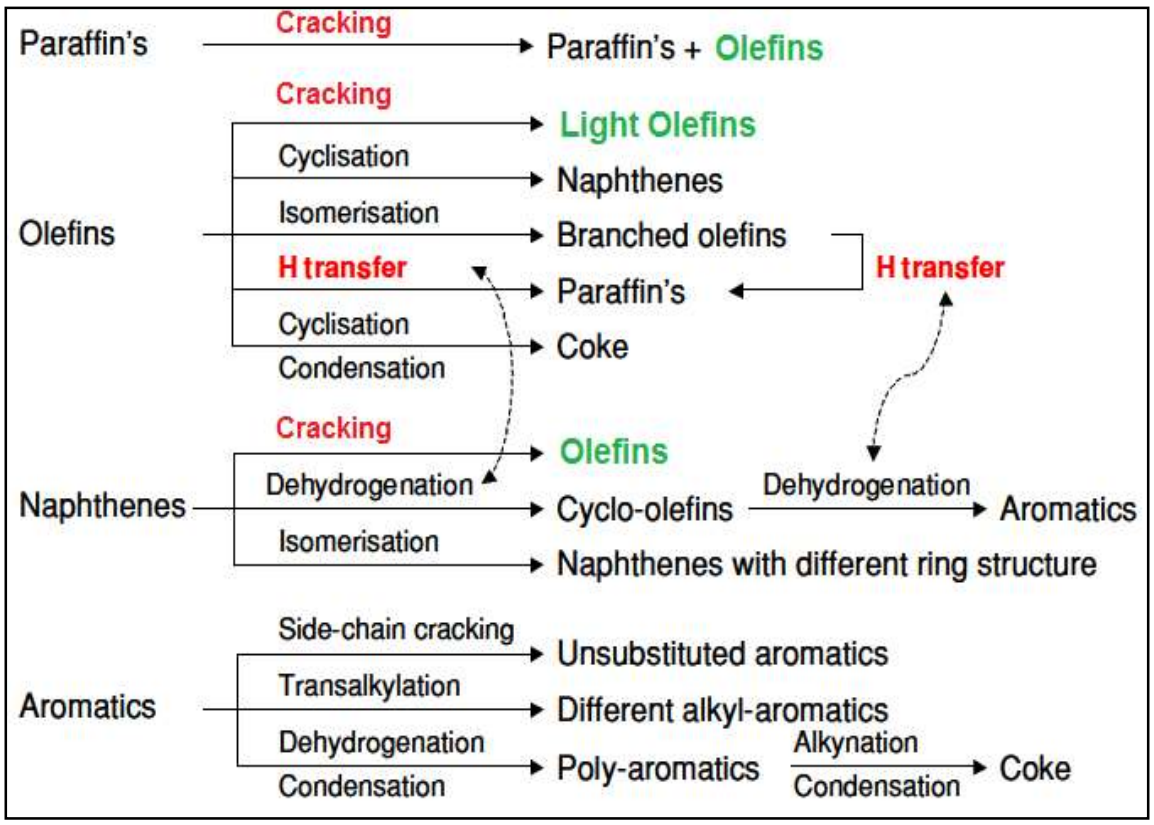

Figure 5 FCC main reactions [20]

i) Cracking reactions

Cracking of carbon-carbon bond (β-scission) is a monomolecular reaction favored at high temperatures. Long chain hydrocarbons are more active than short chain hydrocarbons. The rate of cracking reaction decreases with the decrease in chain length [18,20]. β-scission produce initially olefins as a product and new carbonium ion to continue the chain reactions.

ii) Hydrogen transfer reactions

Hydrogen transfer reactions are bimolecular reactions require the reactants to be in close proximity to a strong acid sites. These reactions hydrogenate olefins to paraffins and aromatics in two suggested pathways:

1. Two olefins are adsorbed on two close active sites. One olefin forms a paraffins and the other olefin forms cyclo-olefin. Cyclo-olefin is then hydrogenated with another olefin to paraffin and aromatic. Chain reaction then stops due to the extreme stability of aromatics.

$$\text{olefins} \rightarrow \text{paraffins} + \text{aromatics}$$

2. Naphthenes donate hydrogen and react with olefins to paraffins and aromatics.

$$\text{olefins} + \text{naphthenes} \rightarrow \text{paraffins} + \text{aromatics}$$

Since olefins are the most reactive species in gasoline fraction, hydrogen transfer reactions reduce gasoline overcracking and increase its stability [21].

iii) Coke formation

Coke formation do not affect propylene yield directly. However, it is with great impact on FCC operation. During catalytic cracking reactions, part of the feed is converted into coke. Coke formation causes deactivation of the catalyst by pore blockage, which limits the access to active sites [22]. The chemistry for coke formation is complex and not fully understood [10]. However, researchers found several factors affecting coke formation. Increases in acid sites density of the catalyst promote coke formation and causes faster deactivation [22,23]. Coke is easily formed in zeolites with large pore openings and cages. Severe catalyst deactivation is reported over zeolites having large cages accessible through small pores [24,25]. Also, zeolites with one dimensional pore structure exhibit faster deactivation. If the channel is blocked at any point, the whole channel becomes inactive [24,26]. This was observed over mordenite zeolite. For this reason, three dimensional zeolites are favorable in FCC reactions. This type of structure minimizes diffusion limitations caused by coke deposition [27].

From the above reactions chemistry, researchers found that the key feature to increase the production of light olefins in FCC process is to preserve the olefinic products resulting from beta scission primary cracking reaction [25,28]. Primary olefins are less stable and can be easily consumed through bimolecular reactions such as cyclization and hydrogen transfer reactions [23,25]. For this reason, The suppression of competing secondary reactions is critical for maximizing light olefins yield in FCC unit [24]. Since, bimolecular reactions are influenced by zeolite acidic properties and pore structure; they play a vital role in controlling product distribution.

2.3 Zeolite acidic properties

Zeolites activity and selectivity are greatly influenced by their acidic properties such as, acid sites type (Brønsted or Lewis), concentration, strength and location. Several studies investigated the effect of total number of acid sites on zeolites catalytic behavior [27]. A direct correlation exists between number of acid sites and product yields. Zeolites with high acid sites concentration produce more LPG and less gasoline. Over zeolites with low number of acid sites, the reaction of gasoline-olefins proceeds predominantly through isomerization and direct cracking to light olefins. Strong acid sites are needed to enhance the overcracking of gasoline to LPG-range olefins. As a result, zeolites with low concentration of strongly acid sites are favorable to produce light olefins [29], they provide high cracking activity with low hydrogen transfer ability. Many attempts were directed to optimize zeolite acidity to enhance propylene selectivity and balance its activity. One of the approaches is exchanging zeolites with alkaline earth elements. Zeolites were exchanged with several alkali metals such as Mg, Ca and Ba [30,31]. This method was effective in reducing acid sites and weakening acid strength. It decreased the

readsorption of cracked products such as propylene and ethylene on the acidic surface and allowed them to desorp as olefins. Phosphorus modification is one of the most common methods applied to zeolite ZSM-5 [13,32]. It significantly improves the hydrothermal stability by stabilizing lattice aluminum ions. This allows the zeolite to retain large fraction of its acidity after severe steaming [13].

Framework tetrahedral aluminum is the source of zeolite acidity. Therefore zeolite Si/Al molar ratio has major impact on its performance as catalysts [33]. Lu et al. investigated the effect Si/Al molar ratio of ZSM-5 as FCC catalyst additive in the cracking of C4 alkanes [30]. It was found a decrease in acid sites density and strength with the decrease in Si/Al molar ratio, while weak acid amounts increased. The study found that high Si/Al molar ratio (>80) was more beneficial in producing light olefins. The hydrogen transfer reactions were minimized due to lower number of acid sites. Other studies found that high Si/Al molar ratio increased zeolite hydrothermal stability [25,34]. Aluminum content extraction is limited due to its low content. This decreases framework collapse and hence, provides more stable crystal lattice [34].

2.4 Zeolite pore topology

Zeolites product selectivity, cracking rates and hydrogen transfer are directly correlated to their pore dimension and topology. Despite the effect of zeolite acidic properties and Si/Al molar ratio, it is the zeolite pore structure that plays the vital role in product selectivity. The historical success of ZSM-5 as FCC catalyst additive to enhance light olefins production, boosted investigations of other zeolites with novel topologies. Many researchers reported the utilization of different zeolite materials such as TNU-9[35], beta [36,37], mordenite[36], SSZ-33 [35], ITQ-13 [38] and MCM-22 [39,40]. While most of

these zeolites were active enough, ZSM-5 exhibited a higher selectivity towards light olefins. Table 1 presents different zeolites structure utilized as FCC catalyst additives found in the literature.

Table 1 Zeolites utilized as FCC catalyst additives

Zeolite additive	Advantages	Disadvantages
ZSM-5	High selectivity to propylene.	Low conversion.
Beta [37]	Increased propylene yield and middle distillates.	Fast deactivation.
SSZ-33 [35]	High VGO conversion.	Low selectivity to propylene and light olefins.
TNU-9 [35]	Increased propylene and light olefins yield.	Increase undesired dry gas yield, high gasoline penalty.
ITQ-13 [38]	Improved catalyst shape-selectivity to propylene.	High dealumination during calcination.
MCM-22 [40]	Good propylene yield enhancement with lower gasoline loss compared to ZSM-5	Less active compared with ZSM-5

A recent study compared the cracking behavior of heavy fuel oil over ZSM-5 and MCM-41 as additives to a base FCC equilibrium catalyst [41]. While ZSM-5 produced 62 wt.% light olefins, MCM-41 produced only 57 wt.%. The base catalyst produced 45 wt.% light olefins. Corma et al. reported the use of IM-5 zeolite in the catalytic cracking of VGO and naphtha [42,43]. In both cases, IM-5 showed a higher activity to light olefins production than ZSM-5 due to a lower dealumination rate. Bastiani et al. reported the use

of ferrierite as FCC catalyst additive to increase light olefins yield [44]. While ferrierite was more capable in suppressing hydrogen transfer reactions, ZSM-5 showed a higher activity. However, a mixture of the two zeolites gave optimal light olefins production, owing to the avoidance of excessive bimolecular reactions and elevated activity.

It can be concluded from the literature survey that there is always need to increase propylene yield from FCC process. Majority of previous work focused on catalyst rout and investigated novel zeolites to increase propylene yield. However, there are still zeolite structures that have not been investigated such as zeolite SSZ-74. An in-depth study that utilizes wide range of zeolite materials to reveal the effects of zeolite pore topology and Si/Al molar ratio on propylene yield will be with great importance.

CHAPTER 3

MATERIAL AND METHODS

3.1 Material preparation

3.1.1 Base catalyst

The base catalyst was a commercial equilibrium FCC USY catalyst (E-Cat) obtained from a domestic refinery. The E-Cat was calcined at 500°C for 3 h before further use. The textural properties of E-Cat are presented in Table 2.

Table 2 Properties of commercial equilibrium FCC USY catalyst (E-Cat)

Total surface area (TSA) (m^2/g)	135
Mesopore surface area (MSA) (m^2/g)	31.1
Pore volume (cm^3/g)	0.23
SiO_2	54.1
Al_2O_3	40.7
Re_2O_3 (wt.%)	2.03
Ni (ppm)	Neg.
V (ppm)	Neg.
Fe (ppm)	Neg.
Unit cell size (UCS) (Å)	24.29

3.1.2 Zeolite additives preparation

Eight different zeolite additives with different topologies: ZSM-5, SSZ-33, SSZ-74, MCM-22, MCM-36, Ferrierite, IM-5 and TNU-9 were used in this study. Table 3 summarizes basic structural features of the zeolites used.

Table 3 Zeolite structures under study [45]

Zeolite	Code	Pore type	Member ring	Pore diameter (nm)
Y [a]	FAU	Large	12	7.4×7.4
ZSM-5	MFI	Medium	10	5.1×5.5; 5.3×5.6
SSZ-33	CON	Large & Medium	12	6.4×7.0; 5.9×7.0
			10	4.5×5.1
SSZ-74	-SVR	Medium	10	5.5×5.7; 5.2×5.9; 5.2×5.6
IM-5	IMF	Medium	10	5.5×5.6; 5.3×5.4; 5.3×5.9; 4.8×5.4; 5.1×5.3
MCM-22; MCM-36	MWW	Medium	10	4.0×5.5; 4.1×5.1
Ferrierite	FER	Medium & Small	10	4.2×5.4
			8	3.5×4.8
TNU-9	TUN	Medium	10	5.5×6.0; 5.2×6.0; 5.4×5.5

[a] zeolite component in the base catalyst (E-Cat)

Zeolites ZSM-5 and ferrierite were acquired as follows:

ZSM-5 was acquired from Zeolyst; CBV3024E, nominal Si/Al (Si/Al) = 30 in NH_4-form.

Ferrierite was acquired from Zeolyst (CP914, Lot. No 2200-1) in ammonium form with Si/Al = 27.5.

Other zeolites were prepared by J. Heyrovský Institute of Physical Chemistry according to following procedures:

SSZ-33 zeolite was synthesized according to the patent of Zones [46]. N,N,N-trimethyl-8-ammonium tricyclo-[5.2.1.02.6]-decane hydroxide was employed as SDA. The starting gel had the following composition: 24.5 SDA-OH:22 NaOH:1$Na_2B_4O_7 \cdot 10H_2O$:161.5 SiO_2:7000 H_2O. The reaction was seeded at the 2 wt.% level with SSZ-33 synthesized in the previous run. The reaction gel was prepared from 1.2 M solution of SDA (11.2 g) diluted with 61 ml of distilled water and mixed with NaOH (0.48 g), $Na_2B_4O_7.10\ H_2O$ (0.42 g) and SiO_2 (5.4 g, Cab-O-Sil M-5). Synthesis was carried out in 90 ml Teflon-lined autoclaves at 160 °C for 4 days under agitation. Calcination in a stream of nitrogen (to 120 °C/2 h, to 540 °C/4 h, to 600 °C/6 h, heating rate 1 °C/min) was performed to remove the SDA. Transformation of B-SSZ-33 to Al-SSZ-33 was performed via four-step reflux in 0.25 M $Al(NO_3)_3.9H_2O$ solution at 95 °C for 3 h.

High-silica **SSZ-74** was synthesized in fluoride medium using 1,6-bis-(methylpyrrolidinium) hexane hydroxide as the organic SDA [47]. 64 g of SDA-OH solution was mixed with 12.6 g of TEOS and allowed to evaporate to the appearance of dryness for 5 days. Finally, LZ-210 zeolite (0.2 g) [48] as a source of Al, seeds of SSZ-74 zeolite (0.1 g), distilled water (3.7 g) and 40% HF (1.3 g) were added and stirred until the thick gel was formed. Crystallization proceeded in teflon-lined stainless steel 25 ml autoclaves at 170 °C for 6 days under agitation. Calcination was performed in a stream of air in stages to 580 °C (at 120 °C for 2 h, at 540 °C for 5 h and at 580 °C for 5 h) with a heating rate 1 °C/min.

IM-5 zeolite was prepared using the procedure of Corma et al. [49]. Starting gel had the molar composition: 10 SDA:17 Na_2O:6 NaBr:1.5 Al_2O_3:60 SiO_2:2400 H_2O. The organic SDA, 1,5-bis-(methylpyrrolidinium) pentane dibromide (22.4 g), NaOH (6.9 g), NaBr (3.5 g) and sodium aluminate (1.6 g, 53% Al_2O_3, 42.5% Na_2O) were dissolved in distilled water (241.9 g) and the clear solution poured onto 20.2 g of SiO_2 (ULTRASIL) and stirred for 30 min. Crystallization proceeded in teflon-lined stainless steel 90 ml autoclaves at 175 °C for 6 days under agitation. As-synthesized IM-5 was calcined in a stream of air at 580 °C for 6 h (heating rate 1 °C/min).

MCM-22 was synthesized according to the Ref. [50] using the gel with the molar composition: 10 HMI:2.5 Na_2O:Al_2O_3:40 SiO_2:580 H_2O.Ludox LS-30 (309.7 g), sodium aluminate (7.4 g, 53% Al_2O_3, 42.5% Na_2O), NaOH (50%, 4.8 ml) and hexamethyleneimine (HMI, 43.6 ml) were mixed together and the gel transferred to teflon-lined stainless steel 0.5 L autoclave (Parr Instrument) and heated at 143 °C for 4 days under agitation. As-made MCM-22P was calcined in a stream of nitrogen at 482 °C for 3 h (heating rate 1 °C/min) followed by calcination under air at 540 °C for 8 h (heating rate 1 °C/min).

MCM-36 was prepared from swollen MCM-22P by pillaring with TEOS. The synthesis of MCM-22P and MCM-36 was based on [50,51]. MCM-22P crystallized from the gel composition of: 10 HMI:2.5 Na_2O:Al_2O_3:30 SiO_2:580 H_2O. Ludox LS-30 (232.3 g), sodium aluminate (7.4 g, 53% Al_2O_3, 42.5% Na_2O), NaOH (50%, 4.8 ml) and HMI (43.6 ml) were mixed together and the gel transferred to teflon-lined stainless steel 0.5 L autoclave and heated at 150 °C for 5 days under agitation. Swelling of MCM-22P was performed with 25% CTMA-OH (20 ml/1 g of MCM-22P), and stirred overnight at room

temperature. Pillaring was carried out with 1 g of dried swollen zeolite in 10 ml of TEOS under stirring and heating under reflux at 85 °C overnight. Solids were isolated by centrifugation, mixed with water (100 ml/1 g) and stirred overnight. Calcination was carried out at 540 °C for 6 h with a heating rate 1 °C/min.

TNU-9 zeolite was prepared according to literature [52]using the molar gel composition: 4.5 SDA:11 Na_2O:0.5 Al_2O_3:30 SiO_2:1200 H_2O. At first, 1,4-bis-(methylpyrrolidinium) butane dibromide (48.2 g, SDA), $Al(NO_3)_3.9H_2O$ (10.4 g) and NaOH (24.8 g) were dissolved in distilled water (599.4 g).The obtained solution was poured onto 51.8 g of SiO_2 (Cab-O-Sil M-5) and stirred for 1 day. Crystallization proceeded in 1000 ml autoclave (Parr Instrument) at 160 °C for 10 days under agitation. As-synthesized TNU-9 was calcined in a stream of air at 580 °C for 12 h (heating rate 1 °C/min).

Framework topology for zeolites under study is given in Figures 6 and 7.

3.1.3 Catalyst preparation (E-Cat containing additives)

The NH_4-forms of individual zeolites were calcined in a stream of air at 550 ^oC for 5 h with temperature ramp of 3 ^oC/min to get the H-form. All calcined additives were pelletized, crushed and sieved, a fraction of 80-90 micron was taken. Catalysts were used as a mixture of 75 wt.% E-Cat and 25 wt.% additive. It was reported that the maximum increase in light olefins yield occurs at additive level of 25 wt.% with incremental increase in propylene yield [53]. Above 25% conversion of reactive gasoline-range species was complete, and the major effect of additive is dilution of the base cracking catalyst with severe lose in overall conversion [53].

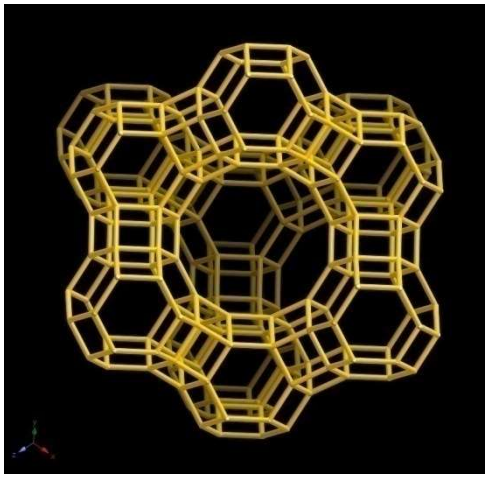

FAU

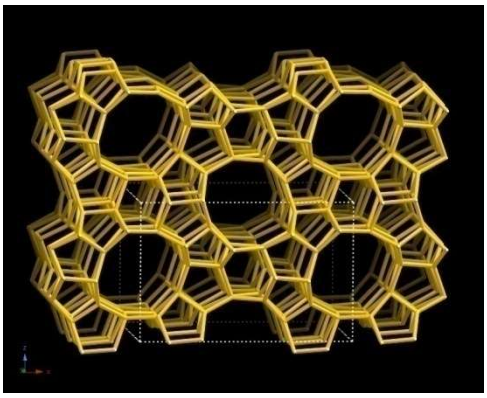

MFI

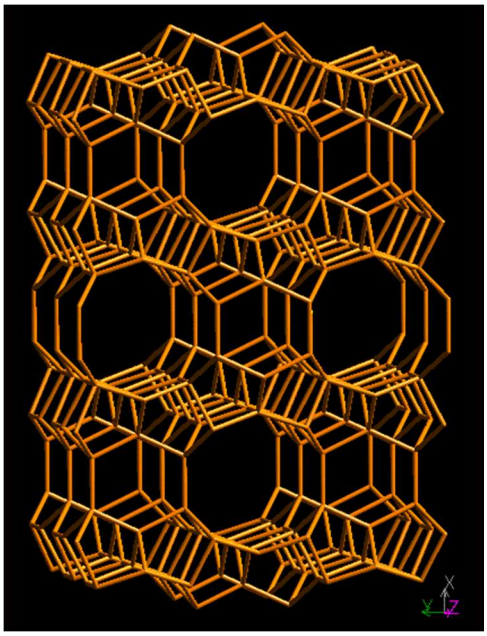

FER

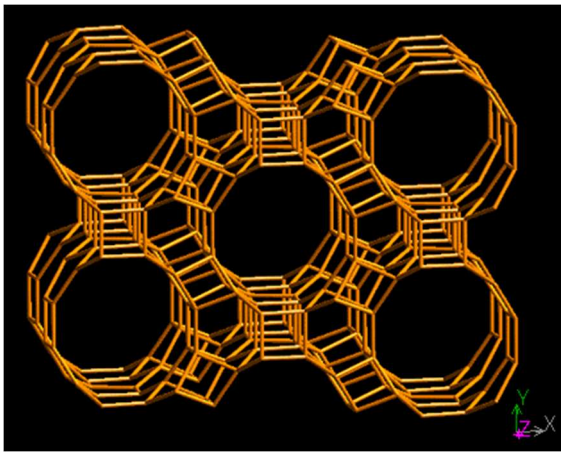

CON

Figure 6 Framework view for FAU; MFI; FER and CON [45]

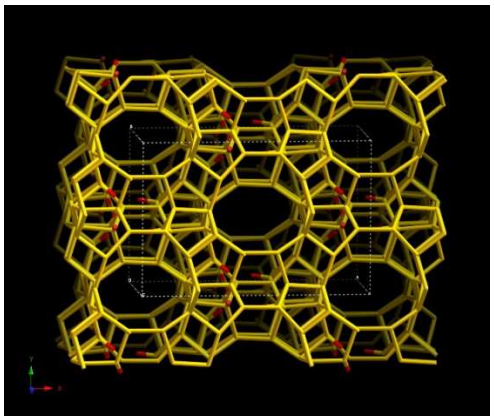

-SVR

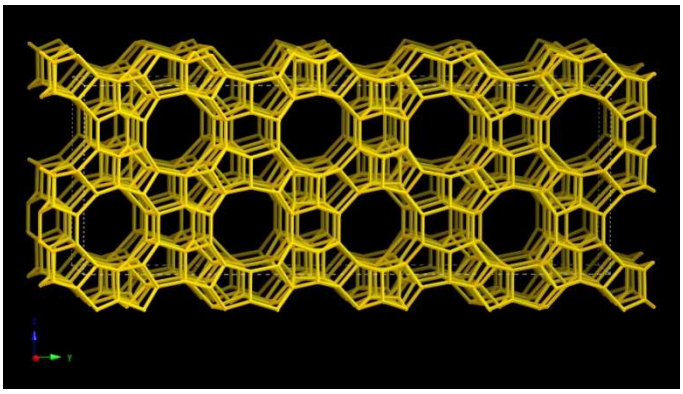

IMF

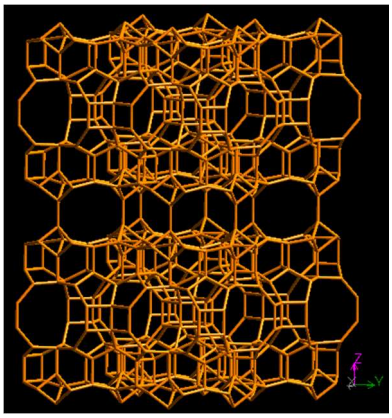

MWW

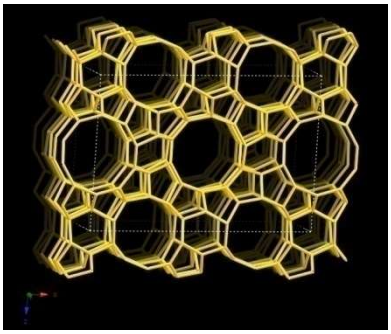

TUN

Figure 7 Framework view for -SVR; IMF; MWW and TUN [45]

3.2 Catalyst characterization

The crystallinity of all samples under investigation were determined by X-ray powder diffraction (XRD) using a Bruker AXS-D8 Advance diffractometer with a graphite monochromator and a position sensitive detector (Våntec-1) using CuKα radiation in Bragg–Brentano geometry.

Nitrogen adsorption/desorption isotherms were measured using an ASAP 2020 (Micromeritics) static volumetric apparatus at liquid nitrogen temperature (–196 °C).

Prior to the sorption measurements, all samples were degassed with a turbomolecular pump at 300 °C for 6 h.

The size and shape of zeolite crystals were examined by scanning electron microscopy (SEM, JEOL JSM-5500LV microscope). For the measurement the crystals were coated with a thin layer of platinum (~ 10 nm) in a BAL-TEC SCD-050 instrument.

The concentration of Lewis (c_L) and Brønsted (c_B) acid sites was determined after adsorption of pyridine (Py) and *d_3*-acetonitrile (ACN) by FTIR spectroscopy using a Nicolet Protégé 460 Magna with a transmission MTC/A detector and Nicolet 6700 instrument equipped with AEM module, respectively. Zeolites were pressed into self-supporting wafers with a density of 8.0 – 12 mg cm–2 and activated in situ at 450 °C and 5·10–5 torr for 4 h. Pyridine adsorption was carried out at 150 °C for 20 min at a partial pressure of 3.5 torr, followed by desorption for 20 min at the same temperature. Before adsorption pyridine was degassed by freezing-pump-thaw cycles. All spectra were recorded with a resolution of 4 cm^{-1} by collecting 128 scans for a single spectrum at room temperature. Spectra were recalculated using a wafer density of 10 mg cm^{-2}. The adsorption of *d_3*-acetonitrile was carried out at room temperature for 20 min at partial pressure 5 torrs followed by desorption for 20 min. Before adsorption, ACN was degassed by freezing and thawing cycles.

3.3 Catalyst evaluation

Hydrotreated Arab Light VGO procured from a domestic refinery was used as the feed in all MAT runs. For the properties of VGO, see Table 4. The catalytic cracking of VGO was carried out in a fixed-bed microactivity test (MAT) unit, manufactured by Sakuragi Rikagaku, Japan according to test methods ASTM D-3907 and D-5154. Schematic

diagram and a picture of MAT unit are given in Figures 8 and 9. For each MAT run, a full mass balance was obtained. If the material balance was less than 96% or greater than 101%, the test was repeated. All MAT runs were performed at a cracking temperature of 550°C and a time-on-stream of 30 s. Conversion was varied by changing catalyst/oil (C/O) ratio in the range of 1.0 to 6.0 g/g, while keeping the amount of VGO (1.0 g) constant. After the reaction mode, the stripping of the catalyst was carried out for 11 min using 30 cc/min of N_2.

Table 4 Properties of Arabian Light hydrotreated vacuum gas oil

Property	Value
Density (g/cm^3) (15 °C)	0.896
Sulfur (ppm)	300
Nitrogen (ppm)	170
Saturates (wt.%)	59
Aromatics (wt.%)	40
Residue (wt.%)	0.8
Simulated Distillation (°C)	
Initial boiling point	308
5%	348
25%	376
50%	420
90%	507
Final boiling point	568

A thorough gas chromatographic analysis of the products was conducted to provide detailed yield patterns and to assess the selectivity of the reaction for different catalyst/additives tested. Gaseous products, dry gas (H_2 and C_1-C_2) and LPG (C_3-C_4) were

analyzed using two Varian gas chromatographs (GC) equipped with 50 m (0.32 mm diameter) Alumina Plot capillary column and FID/TCD detectors. The amount of coke on catalyst was determined by a Horiba carbon analyzer. For liquid products, three different cuts were considered: gasoline (C_5, 221°C), LCO (light cycle oil, 221–343°C), and HCO (heavy cycle oil, +343°C). The weight percentage of liquid products was determined by a simulated distillation GC equipped with 10 m (0.53 mm diameter) RTX-2887 capillary column and FID detector according to ASTM D-2887. Gasoline composition of paraffins, iso-paraffins, olefins, naphthenes, and aromatics was determined using a Shimadzu gas chromatograph equipped with 50 m (0.15 mm diameter) BP-1 PONA capillary column and FID detector. VGO conversion was defined as the sum of yields for dry gas, LPG, gasoline and coke. The unconverted material is defined as all liquid products with boiling point above 221 °C (LCO and HCO).

To analyze the effect of additives on MAT performance, different catalytic parameters were assessed. Ratio ($\%C_3^=$/gasoline) gives the percent increase in propylene per unit decrease in gasoline. This indicates the gasoline penalty in forming more propylene. Another parameter was considered to measure C_3olefinicity, which is the relative amount of propylene within C_3 and LPG. For the relative importance of hydrogen transfer reactions (HTC) and their strong influence on both the product distribution and the octane number, HTC was used and defined as yield of butanes / yield of butenes.

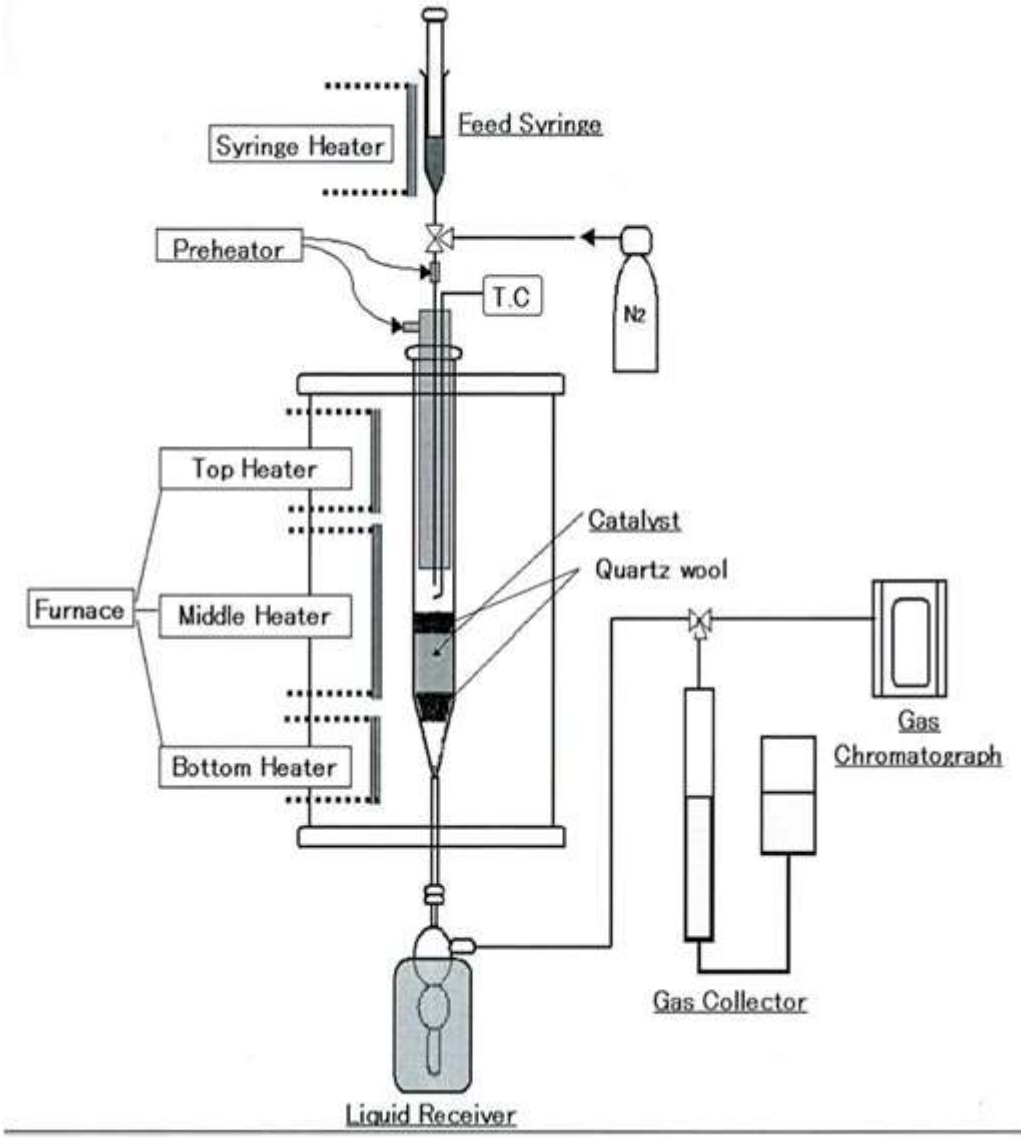

Figure 8 Flow diagram of ASTM MAT unit

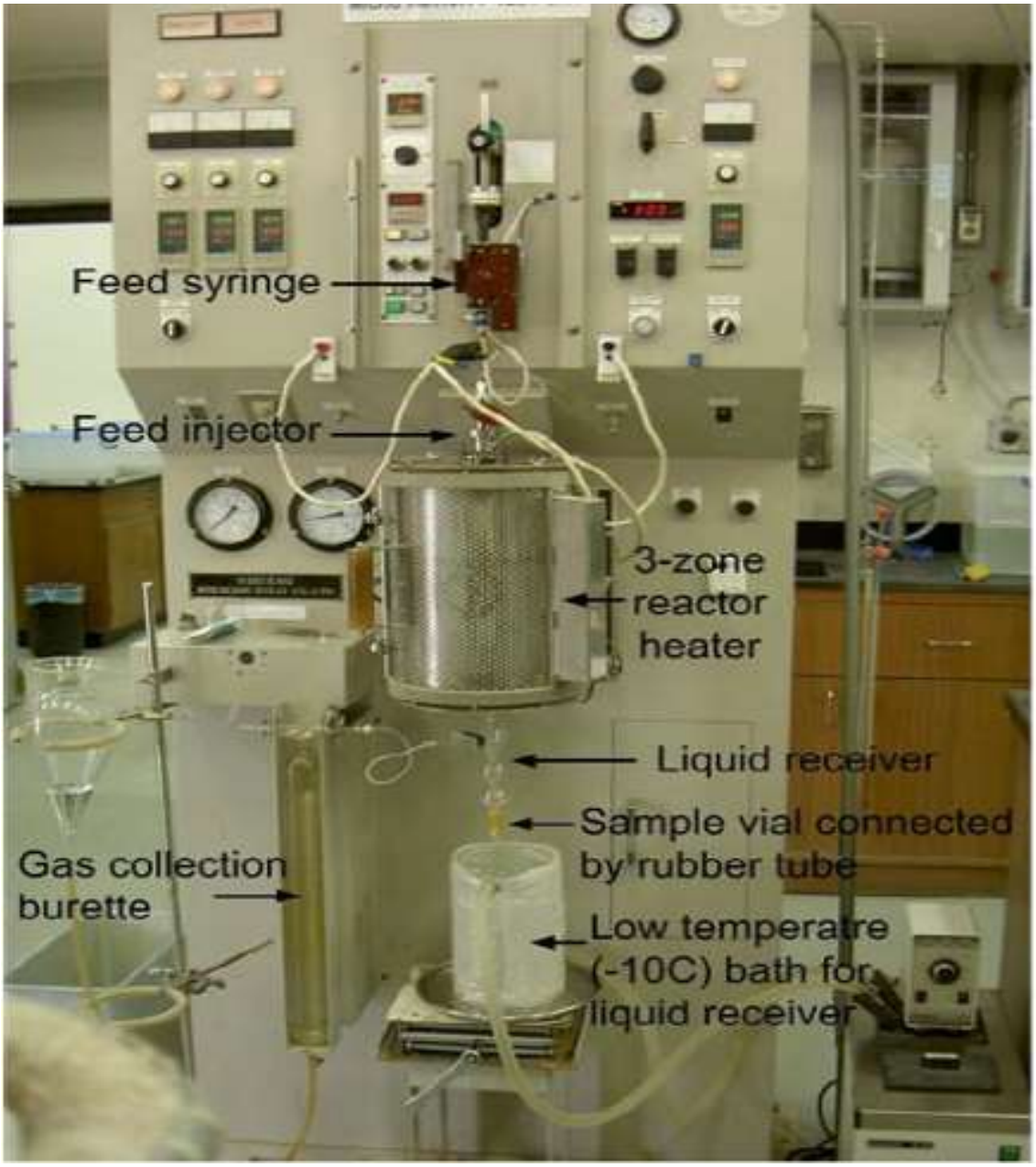

Figure 9 Photo of MAT unit used in this study

CHAPTER 4

EFFECT OF ZEOLITE PORE STRUCTURE

4.1 Catalyst characterization

All zeolites used in this study were characterized for their structure (X-ray powder diffraction), size of the crystals (Scanning electron microscopy), textural properties (sorption capacity for nitrogen), and concentration and type of acid sites (Infrared spectroscopy using pyridine and d_3-acetonitrile as probe molecules).

X-ray diffraction (XRD) patterns of all zeolites are depicted in Figure 10. All XRD patterns show a high crystallinity of studied zeolites and absence of any other crystalline or amorphous phase. Diffraction lines are consistent with those in IZA [54]. In the case of MCM-36, a new interlayer peak is seen at a low angle below 2 theta degree, which is typical for pillared materials and indicates an increase in layer spacing.

The adsorption isotherms for zeolites are given in Figure 11. The shapes of nitrogen isotherms for all zeolites are rather similar consisting of substantial increase in the adsorbed amount of nitrogen at very low partial pressures due to the adsorption in micropores. This is followed by almost constant plateaus over the remaining range of pressures. A little increase in the adsorbed amount at pressures between 0.9 and 1.0 is due to the adsorption in interparticle space. This strongly contrasts with the adsorption isotherm of MCM-36. MCM 36 shows an increase in the adsorbed amount at relative pressures between 0.05 and 0.30 due to filling of pores with diameter of 2.5 – 3.0 nm.

This is even accompanied by a hysteresis loop, typical for pillared zeolites [55]. Textural properties of catalysts studied are summarized in Table 5.

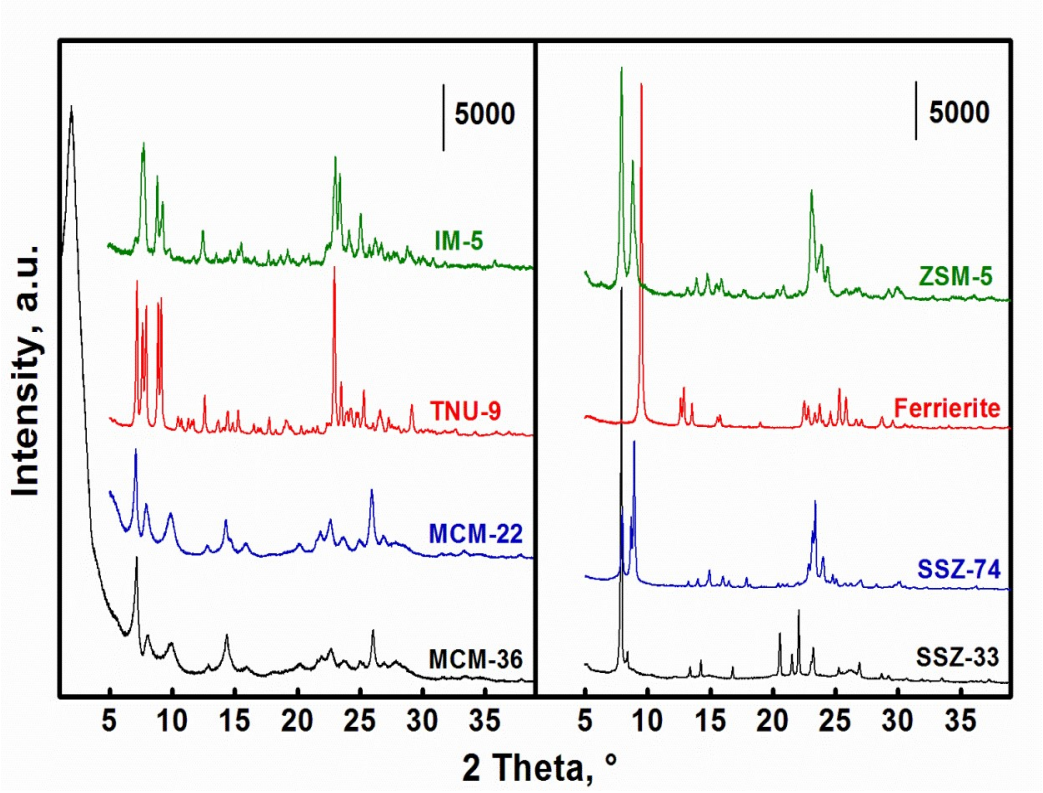

Figure 10 XRD patterns of zeolites under study

Scanning electron microscope images are presented in Figure 12. Crystals of zeolites TNU-9 and IM-5 are of similar size with one dimension slightly larger than 1 μm while other two dimensions are shorter. SSZ-74 is typical for its 5-6 μm long crystals with other two dimensions shorter than 1 μm. SSZ-33 is characteristic of agglomerates consisting of small crystals around 0.2-0.3 μm. The crystals of ZSM-5 zeolite have typical hexagonal shape with the size of 1x0.5 μm forming larger agglomerates.

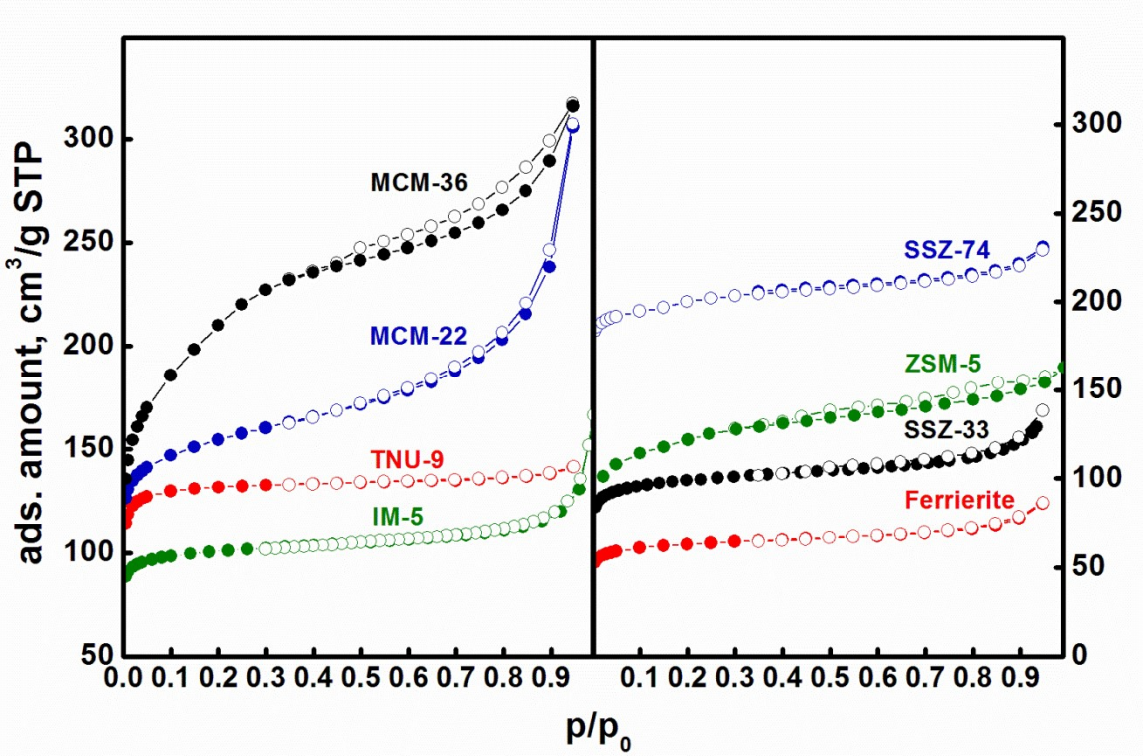

Figure 11 Nitrogen adsorption desorption isotherms

Table 5 Structural and textural properties of zeolites used

Sample	size of the channels (nm) [a]	BET (m^2/g)	V_{mic} (cm^3/g) [b]	V_{tot} (cm^3/g)
ZSM-5	0.51 x 0.55; 0.53 x 0.56	414	0.16	0.25 [d]
MCM-22	0.40 x 0.55; 0.41 x 0.51	529	0.18	0.47 [c]
SSZ-33	0.64 x 0.70; 0.59 x 0.70; 0.45 x 0.51	506	0.20	0.50 [c]
SSZ-74	0.55 x 0.57; 0.52 x 0.59; 0.52 x 0.56	341	0.14	0.20 [c]
MCM-36	MWW layers, D_{meso} = 2.5 nm	741	0.09	0.49 [c]
IM-5	0.55 x 0.56; 0.53 x 0.59	336	0.14	0.23 [d]
Ferrierite	0.42 x 0.54; 0.35 x 0.48	316	0.13	0.18 [c]
TNU-9	0.55 x 0.60 + 0.52 x 0.60; 0.54 x 0.55	445	0.19	0.22 [c]

[a] taken from http://www.iza-structure.org/databases/;[b] V_{mic} = micropore volume; [c] V_{tot} = total pore volume (at p/p_0 = 0.95); [d] V_{tot} = total pore volume (at p/p_0 = 0.99)

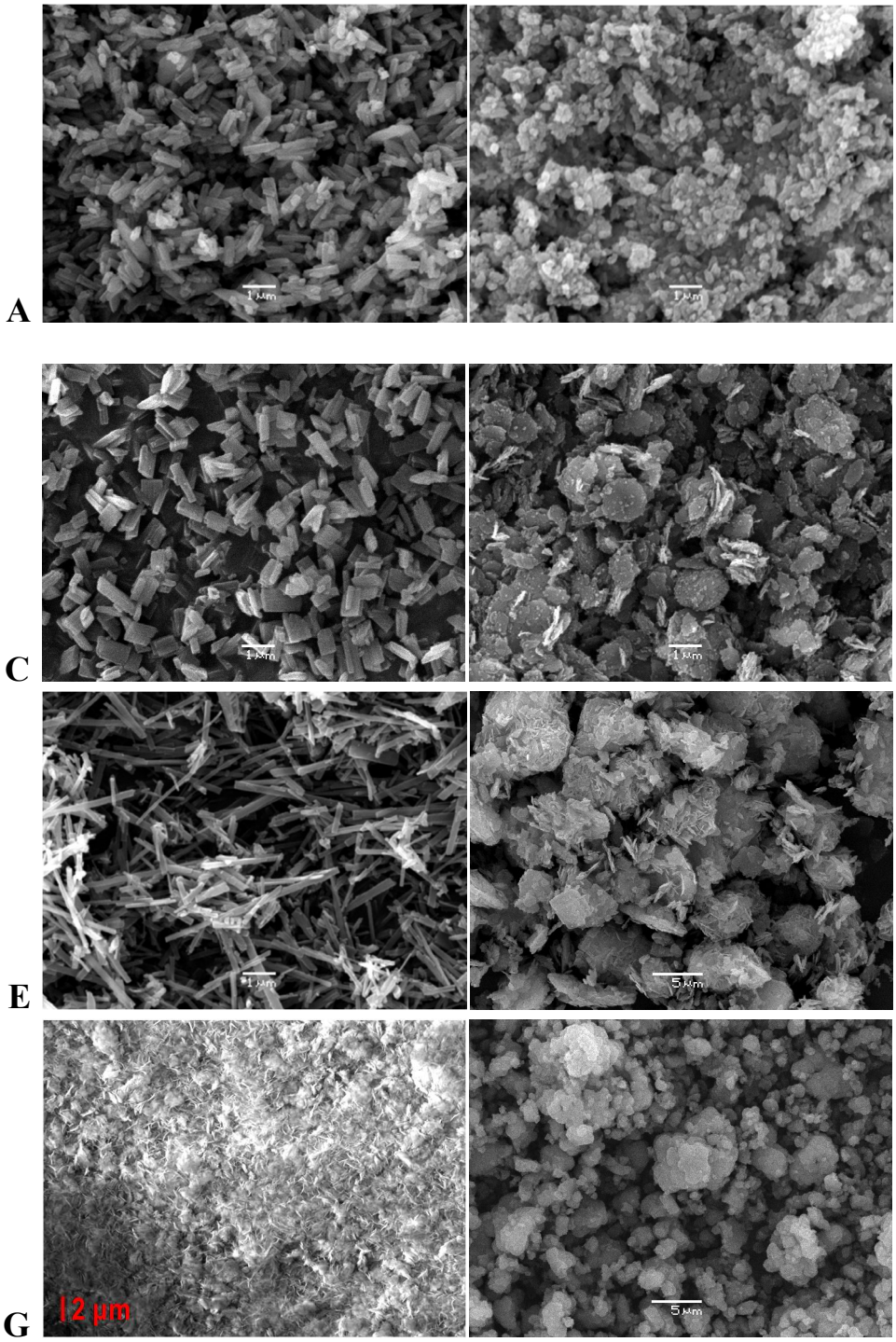

Figure 12 SEM images of (A) TNU-9, (B) SSZ-33, (C) IM-5, (D) MCM-36, (E) SSZ-74, (F) ferrierite, (G) MCM-22 and (H) ZSM-5.

In contrast, ferrierite, MCM-22 and MCM-36 exhibited sheet-like shapes of their crystals, which is particularly typical for MCM-22 and MCM-36 formed from MCM-22 layers by swelling with surfactant. It is generally accepted that size and shape of zeolite crystals together with size of zeolite windows influence the rate of reactions on zeolites. However, there is no straightforward trend to relate conversion or yield to any of these parameters. Not overall zeolite inner volume is involved in the reactions and with smaller size of the crystals reactions can preferentially proceed on their external surface.

Concentrations and type of acid sites for all zeolites studied were determined using FTIR spectroscopy with pyridine or d_3-acetonitrile as probe molecules, Figures 13 and 14 [56]. While pyridine with its kinetic diameter about 0.55 nm can penetrate into 10-ring channels, it is not unable to interact with acid sites located in elliptic 10-ring channels or in 8-ring channels. Therefore, d_3-acetonitrile was especially used to study acidic properties of ferrierite. Hydroxyl region of the spectra consists of two characteristic absorption bands around 3740-45 cm^{-1} and 3610-3625 cm^{-1}. The former band is attributed to the vibrations of silanol groups while the latter one is typical for acidic bridging OH groups. In the case of SSZ-74, we can see here an additional band at about 3725 cm^{-1}. This band is due to the interaction of silanol groups in silanol nests due to the missing one T atom per unit cell of this zeolite [57].

The interaction of bridging Si-OH-Al groups in 10-ring zeolites with both pyridine and d_3-acetonitrile resulted in complete disappearance of this band (cf. the spectra before and after adsorption of probe molecule, Figures 13 and 14. Interaction of pyridine with Brønsted acid sites gave rise to an absorption band around 1545 cm^{-1} while interaction with Lewis acid sites resulted in the appearance of a new band at 1450-1455 cm^{-1}.

Interaction of d_3-acetonitrile provided also two additional bands around 2300 cm^{-1} via interaction with Brønsted acid sites and 2325 cm^{-1} due to interaction with Lewis acid sites. Quantitative evaluation of the concentrations Brønsted and Lewis acid sites is given in Table 6. SSZ-33 and MCM-36 possess the highest concentrations of acid sites, although in the case of MCM-36 around 30 % of the sample is formed by amorphous silica pillars. The highest concentrations of Brønsted acid sites were found for ferrierite, MCM-22, ZSM-5, TNU-9 and IM-5 zeolite. Simultaneously, ferrierite, TNU-9 and IMF zeolites exhibit also the lowest concentrations of Lewis acid sites.

Table 6 Lewis (C_L) and Bronsted (C_B) acid sites concentration

Additive Sample	Si/Al (IR)	C_L (mmol/g)	C_B (mmol/g)
ZSM-5	19.9	0.21	0.37
SSZ-33	18.8	0.32	0.19
SSZ-74	42.1	0.11	0.17
MCM-22	23.0	0.14	0.41
MCM-36	21.6	0.28	0.17
Ferrierite	29.3	0.06	0.44
IM-5	30.5	0.10	0.33
TNU-9	28.1	0.11	0.35

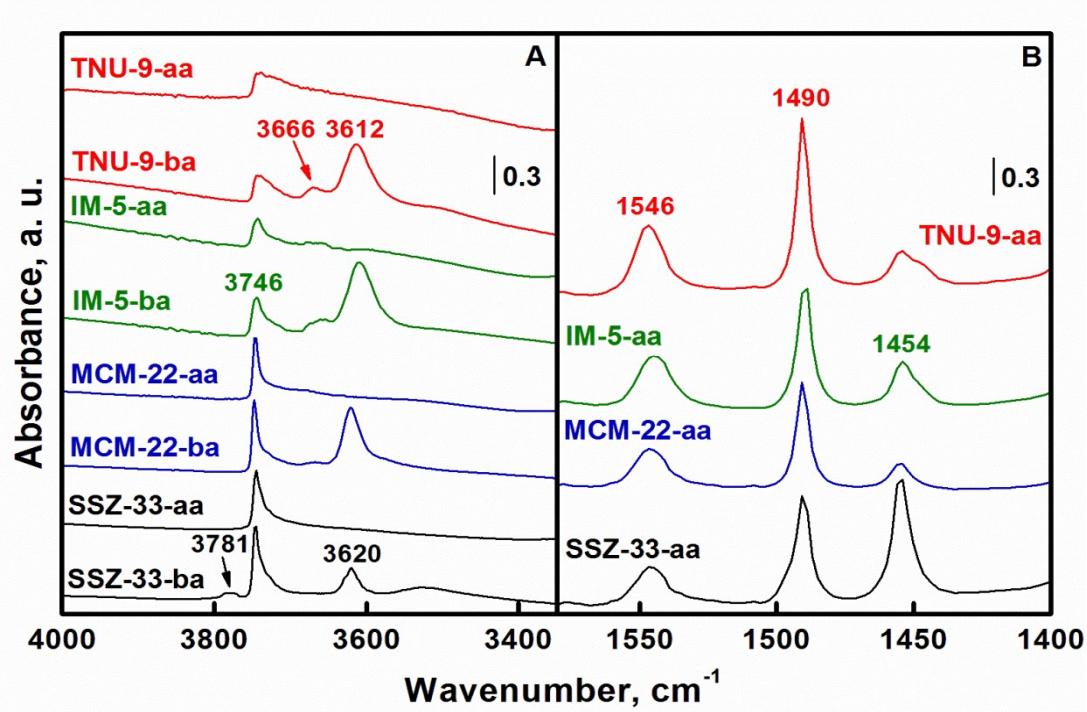

Figure 13 IR spectra of TNU-9, IM-5, MCM-22, and SSZ-33, adsorption of pyridine; (A) region of hydroxyl vibration, (B) region of pyridine vibration. Before (ba) and after (aa) adsorption

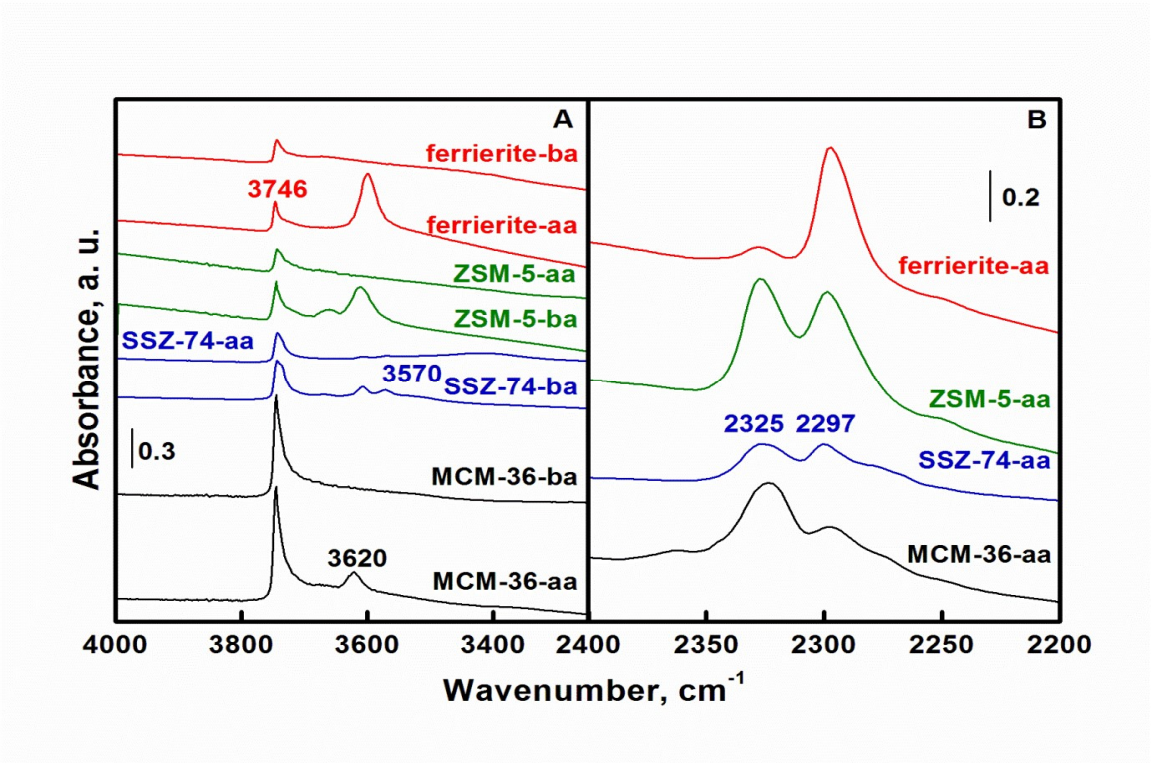

Figure 14 IR spectra of MCM-36, SSZ-74, ZSM-5 and ferrierite zeolite, adsorption of acetonitrile; (A) region of hydroxyl vibration,(B) region of acetonitrile vibration. Before (ba) and after (aa) adsorption.

4.2 Catalyst evaluation

4.2.1 Conversion and yields

The product yield distribution of VGO cracking over E-Cat and E-Cat/additives is shown in Table 7. Product yields were assessed at constant conversion of 70% to distinguish the catalytic performance of different additives.

The conversion versus C/O ratio over E-Cat and E-Cat/additives is shown in Figure 15. The conversion increased with increasing C/O ratio for all E-Cat and E-Cat/additives. The increase in the conversion was substantial for C/O ratio between 2 and 4 followed by a slow increase or even plateau for some additives (Figure 15). This indicates that the effect of experimental conditions on conversion is higher at milder conditions, and this effect is less visible as the severity of conditions gradually increases [58]. Over E-Cat, the conversion increased from 62% to 76% as the C/O ratio increased from 2 to 6. In the case of E-Cat/additives, the conversions ranged between 63% and 82%.

C/O ratio at a constant conversion indicates the activity of each catalyst. Table 7 shows that the conversions over E-Cat/additives decreased in the following order: MCM-36>IM-5>TNU-9>ZSM-5>ferrierite=MCM-22>SSZ-33>SSZ-74. Catalyst activity is influenced by the acidic properties and the pore structure [25]. The high conversion over MCM-36 is attributed to high concentration of acid sites and the mesoporous character of this additive favoring the diffusion of reactants and products [59]. High activity of IM-5 and TNU-9 was also due to high amount of acid sites and more open channel structure than in the case of ZSM-5 (Table 6). Although ferrierite exhibited the highest concentration of Brønsted acid sites, the limited pore structure openings of this zeolite

hindered the accessibility of reactant molecules to acidic sites. Lower activity of SSZ-33 and SSZ-74 may be attributed to the low concentration of Brønsted acid sites (Table 6).

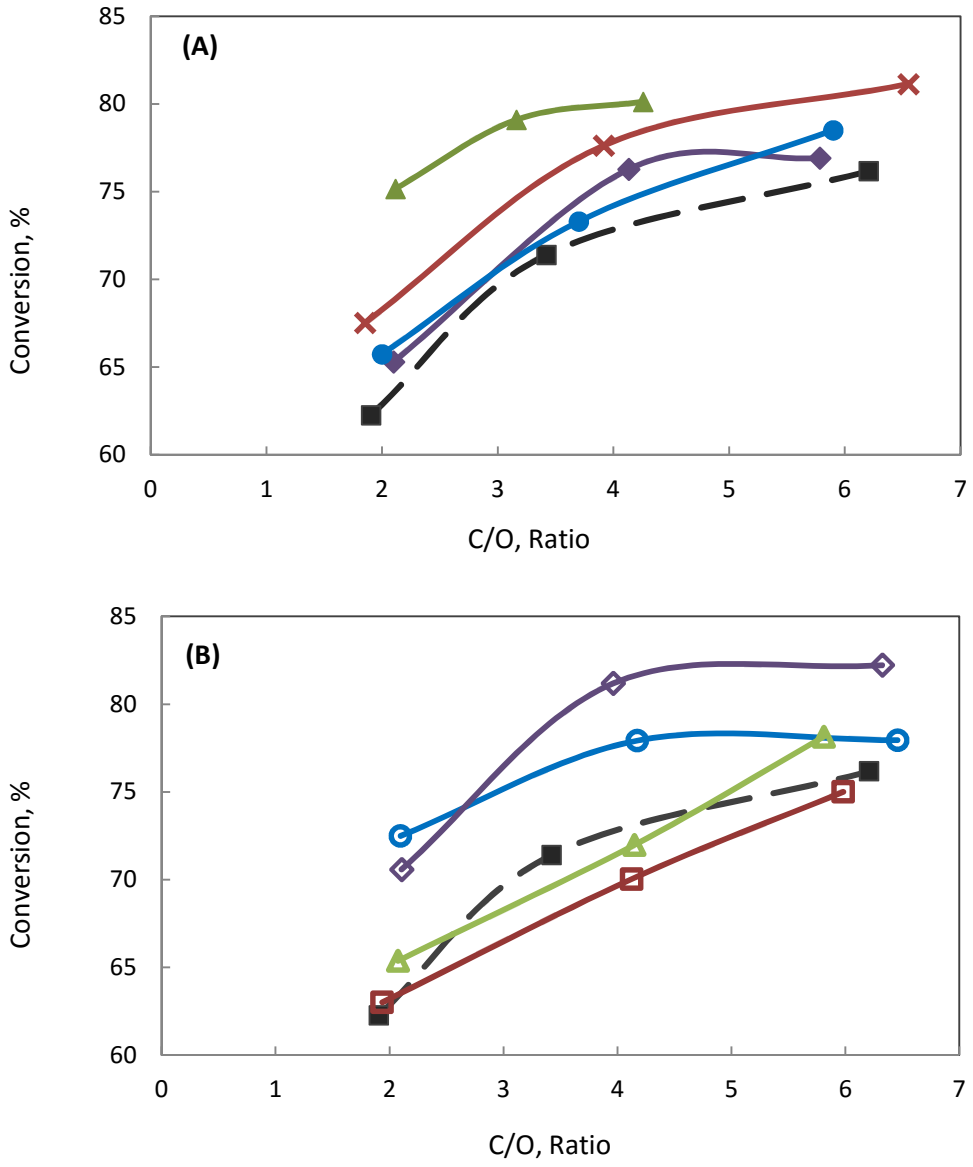

Figure 15 Comparison of MAT conversion over E-Cat and E-Cat/additives (A), (■) E-Cat; (×) ZSM-5; (●) MCM-22; (▲) MCM-36 and (♦) Ferrierite. (B), (■) E-Cat; (Δ) SSZ-33; (□) SSZ-74 (○) IM-5 and (◊) TNU-9.

Table 7 Comparative MAT data at constant conversion (70%) and 550 °C over E-Cat and E-cat/additives

Catalyst	Base E-Cat	E-Cat/ 25wt.% additive							
		ZSM-5	SSZ-33	SSZ-74	MCM-22	MCM-36	Ferrierite	IM-5	TNU-9
(C/O)ratio(g/g)	3.1	2.3	3.6	4.0	2.9	1.7	2.9	1.8	2.1
Product yields (wt.%)									
Dry gas	3.3	6.1	3.4	3.8	4.6	4.5	4.1	6.1	6.1
H_2	0.08	0.15	0.08	0.09	0.12	0.08	0.07	0.11	0.13
C_1	0.9	1.1	0.9	0.8	0.9	1.0	0.9	1.0	1.0
C_2=	**1.4**	**3.4**	**1.5**	**2.0**	**2.7**	**2.5**	**2.2**	**3.7**	**3.6**
C2	0.9	1.4	1.0	0.9	0.9	1.0	1.0	1.3	1.3
LPG	22.6	36.1	22.4	29.2	34.7	32.2	28.1	36.2	36.5
C_3=	**7.0**	**8.8**	**7.0**	**8.9**	**9.5**	**10.8**	**10.9**	**8.6**	**9.0**
C_3	1.1	9.6	0.9	2.6	5.7	2.8	1.3	9.8	9.1
C_4=	**7.7**	**7.4**	**10.2**	**10.4**	**8.6**	**10.0**	**11.0**	**6.9**	**7.4**
n-C_4	2.6	3.1	0.7	1.4	2.2	1.3	0.7	3.2	3.0
i-C_4	4.2	7.2	3.7	5.8	8.8	7.3	4.2	7.7	8.0
C_2=-C_4=	**16.1**	**19.6**	**18.7**	**21.3**	**20.7**	**23.3**	**24.0**	**19.2**	**20.0**
Gasoline	42.9	26.5	42.4	34.9	28.1	30.4	36.4	25.8	23.2
LCO	16.8	13.9	16.6	13.6	13.5	13.4	14.8	13.3	13.0
HCO	13.0	16.2	13.4	16.4	16.5	16.6	15.2	16.7	17.0
Coke	1.4	1.2	1.6	2.1	2.6	2.9	1.5	1.9	4.2
HTC[a]	0.9	1.4	0.4	0.7	1.3	0.9	0.4	1.6	1.5
C_3=/ LPG[b]	0.31	0.24	0.31	0.31	0.27	0.34	0.39	0.24	0.25
C_3olefinicity[c]	0.86	0.48	0.89	0.77	0.6	0.80	0.89	0.47	0.50
%C_3=/ gasoline[d]	Base	1.6	0.8	3.8	2.5	4.5	8.7	1.4	1.5

[a] Hydrogen transfer coefficient (butanes/butenes).
[b] Propylene selectivity within LPG.
[c] C3=/total C3s.
[d] Percent increase in propylene per unit decrease in gasoline.

All product yields exhibited increasing trend upon adding zeolite additives. Gasoline is the only exception due to the formation of more gaseous products by cracking of C_6-C_8 olefins to lighter olefins [53,60]. The drop in gasoline yield over all E-Cat/additive catalysts was associated with a slight change in the yield of LCO and HCO (Table 7).

The variety in pore topology among different additives has a great impact on product distribution, as they provide different accessibility of cracking VGO and intermediates.

4.2.2 LPG and light olefins yields

LPG (C_3-C_4) yield increased with increasing conversion for all E-Cat and E-Cat/additives as shown in Figures 16 and 17, with exception for SSZ-33. At 70% conversion, LPG increased from 22.6 wt.% over E-Cat to about 36 wt.% over E-Cat blended with TNU-9, IM-5 and ZSM-5 (Table 7). Improvements were also reported but at lower extent over MCM-22 (34.7 wt.%), MCM-36 (32.2 wt.%), SSZ-74 (29.2 wt.%) and ferrierite (28.1 wt.%). However, the composition of LPG was different among various additives.

Ferrierite and MCM-36 yielded the highest amount of propylene at ~ 11 wt.% compared with 7.0 wt.% over E-Cat (Table 7). The high yield of propylene over ferrierite might be ascribed to the suppression of hydrogen transfer (HT) reactions saturating olefins to paraffins [58,61]. It has been reported that the smaller the pore size of the zeolite, the greater the suppression of HT reactions. Smaller pore openings do not accommodate bulky bimolecular reaction intermediates and hence, zeolite additives with smaller pore structures are more shape selective in producing propylene [24–26,44]. High enhancement in propylene yield over MCM-36 demonstrates the advantages of the inherent mesoporous character of this pillared zeolite. Mesopores enhanced mass transport and reduced HTC due to shorter residence time and rapid elution of olefins [62].

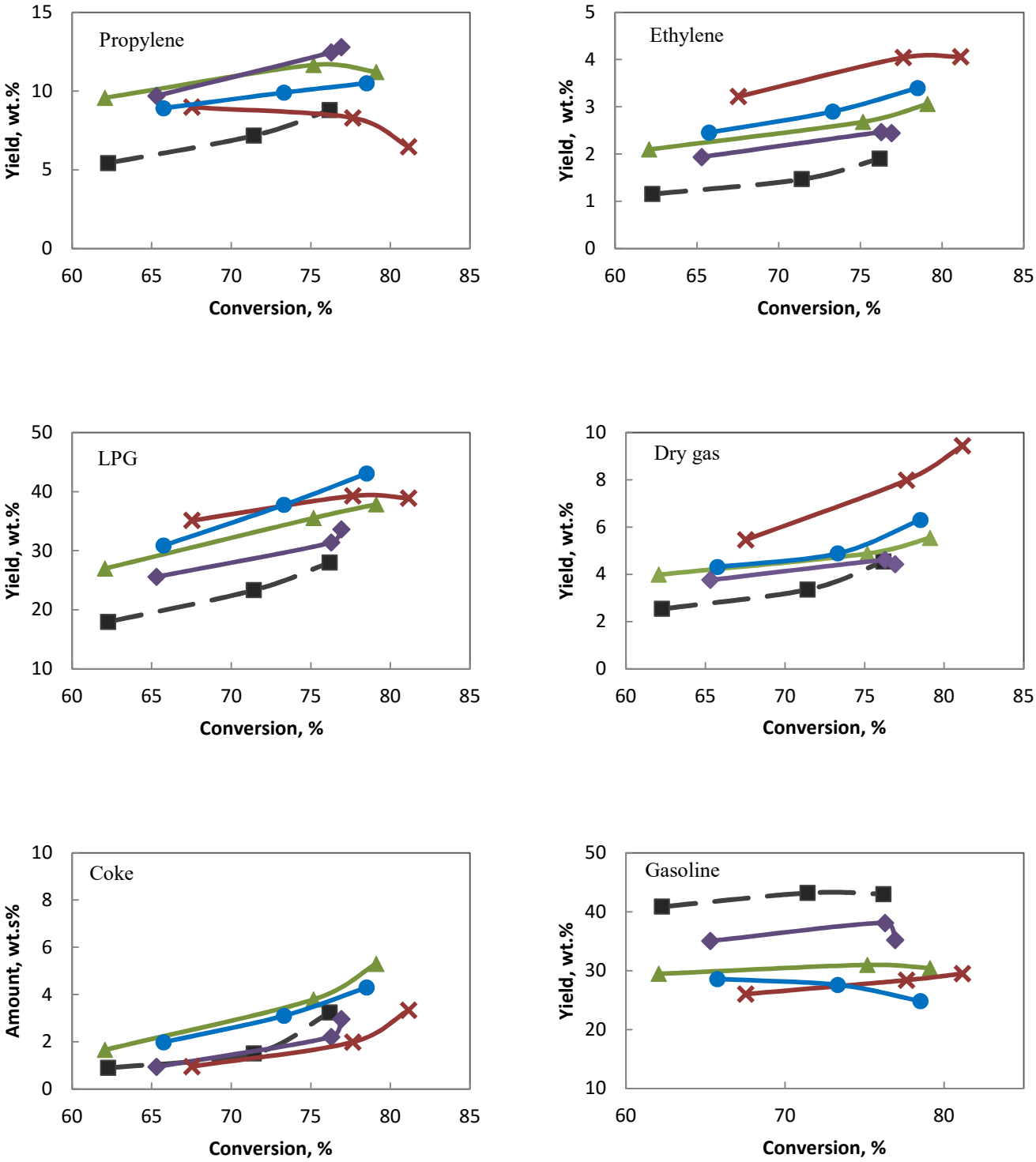

Figure 16 Product yields over E-Cat and E-Cat/additives: (■) E-Cat; (×) ZSM-5; (●) MCM-22; (▲) MCM-36 and (♦) Ferrierite.

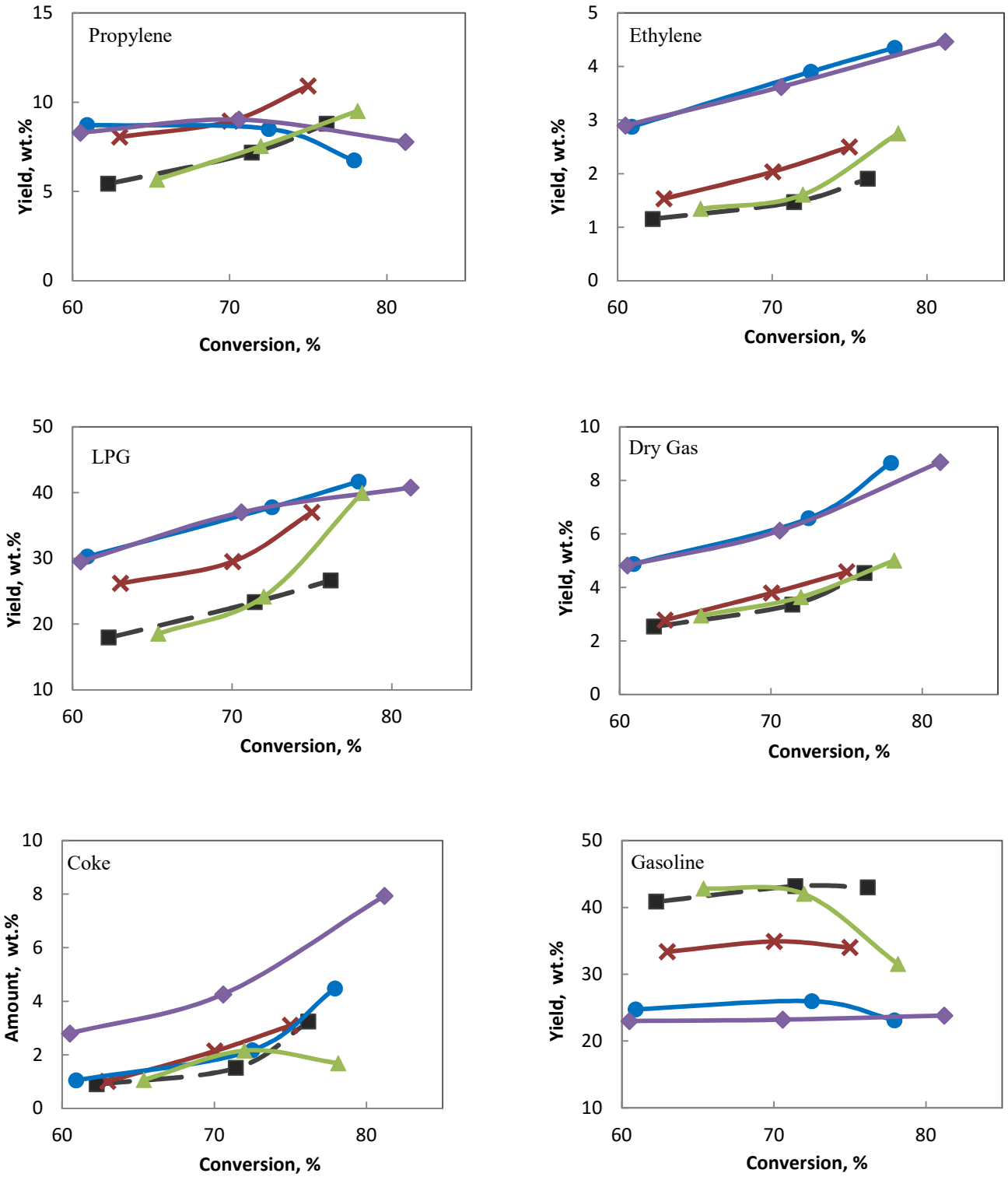

Figure 17 Product yields over E-Cat and E-Cat/additives: (■) E-Cat; (Δ) SSZ-33; (□) SSZ-74 (○) IM-5 and (◊) TNU-9.

MCM-22 showed lower propylene yield at 9.5 wt.% and higher HTC compared to MCM-36 (Table 7). It seems that 10-ring zeolites or even zeolites with 10- and 8-ring channels decrease the rate of bimolecular reactions (lower HTC). The presence of mesopores lowered the real contact time between hydrocarbons and catalyst surface having similar effect on propylene yield (e.g. MCM-36).

Although ZSM-5 zeolite is known to be shape-selective to produce propylene [33], the excessive concentration of acid sites on the zeolite favored secondary reactions resulting in low enhancement in propylene yield at 8.8 wt.% [21,61]. SSZ-74 yielded almost the same amount of propylene as ZSM-5 at 8.9 wt.% (Table 7), however, HTC was much lower for SSZ-74 due to its lower acid site density compared with ZSM-5 (Table 6). IM-5 and TNU-9 exhibited the highest HTC owing to their higher acid site density and slightly large pore entrances than in ZSM-5. As a consequence, they favored bimolecular reactions resulting in a low enhancement in propylene yield [35,49].

Propylene selectivity within LPG (C_3=/LPG) decreased in the following order: ferrierite > MCM-36 > E-Cat = SSZ-33 = SSZ-74 > MCM-22 > TNU-9 > IM-5 = ZSM-5. This is explained by the inverse correlation between HTC and propylene yield as shown in Table 7. High HTC decreases propylene selectivity within LPG due to excessive conversion of propylene to propane.

Propylene yield increased with increasing conversion over zeolite additives having low HTC. Over E-Cat, propylene yield increased from 5.4 to 8.8 wt.% upon increasing conversion from 62 to 76% as shown in Figures 16 and 17. Ferrierite showed the highest increase in the propylene yield from 9.7 to 12.8 wt.% with increasing conversion from 65 to 77%. Similar trend was observed over SSZ-74, SSZ-33, MCM-22 and MCM-36. In contrast, additives having high HTC

exhibited a drop in propylene yield with increasing conversion. For instance, propylene yield over ZSM-5 decreased from 8.9 to 6.5 wt.% as the conversion increased from 67 to 81%. TNU-9 and IM-5 followed a similar trend. However, at constant conversion of 70%, all additives boosted propylene yield compared to E-Cat. The results suggest a strong relationship between C_3 olefinicity and HTC. Ferrierite and SSZ-33 showed high C_3 olefinicity, followed by MCM-36 and SSZ-74 (Table 7). This is caused by high yield of propylene and low propane yield. Compared with E-Cat, C_3 olefinicity decreased in additives with high HTC (ZSM-5, IM-5, MCM-22 and TNU-9), as they produced high yield of propane. The results clearly show that propylene yield can be related not only to zeolite topology but also to the concentration of acid sites (reversely to Si/Al ratio). While smaller zeolite pores limit generally the rate of bimolecular reactions (lower HTC values), lower Si/Al ratios enhance the rate of bimolecular reactions.

Ethylene yield increased with increasing conversion for all E-Cat/additives (Figures 16 and 17). However, at constant conversion of 70%, ethylene yield over IM-5, TNU-9 and ZSM-5 increased more than twice compared with E-Cat. Ethylene yield increased from 1.4 wt.% over E-Cat to 3.4-3.7 wt.% over these additives. To a lower extent, ethylene yield was enhanced to 2.0-2.7 wt.% over MCM-22, MCM-36, ferrierite and SSZ-74. SSZ-33 did not show much enhancement in ethylene yield (1.5 wt.%).

The yield of light olefins (C_2-C_4) showed a similar behavior to propylene yield. At conversion of 70%, maximum light olefins yield was obtained over ferrierite (24.0 wt.%) compared with 16.1 wt.% over E-Cat. This was followed by MCM-36 (23.3 wt.%), SSZ-74 (21.3 wt.%), MCM-22 (20.7 wt.%) and TNU-9 (20.0 wt.%). ZSM-5, IM-5 and SSZ-33 yielded 18-19 wt.% of light olefins. Over all additives, the largest contribution of light olefins was from propylene and butenes, as shown in Figure 18.

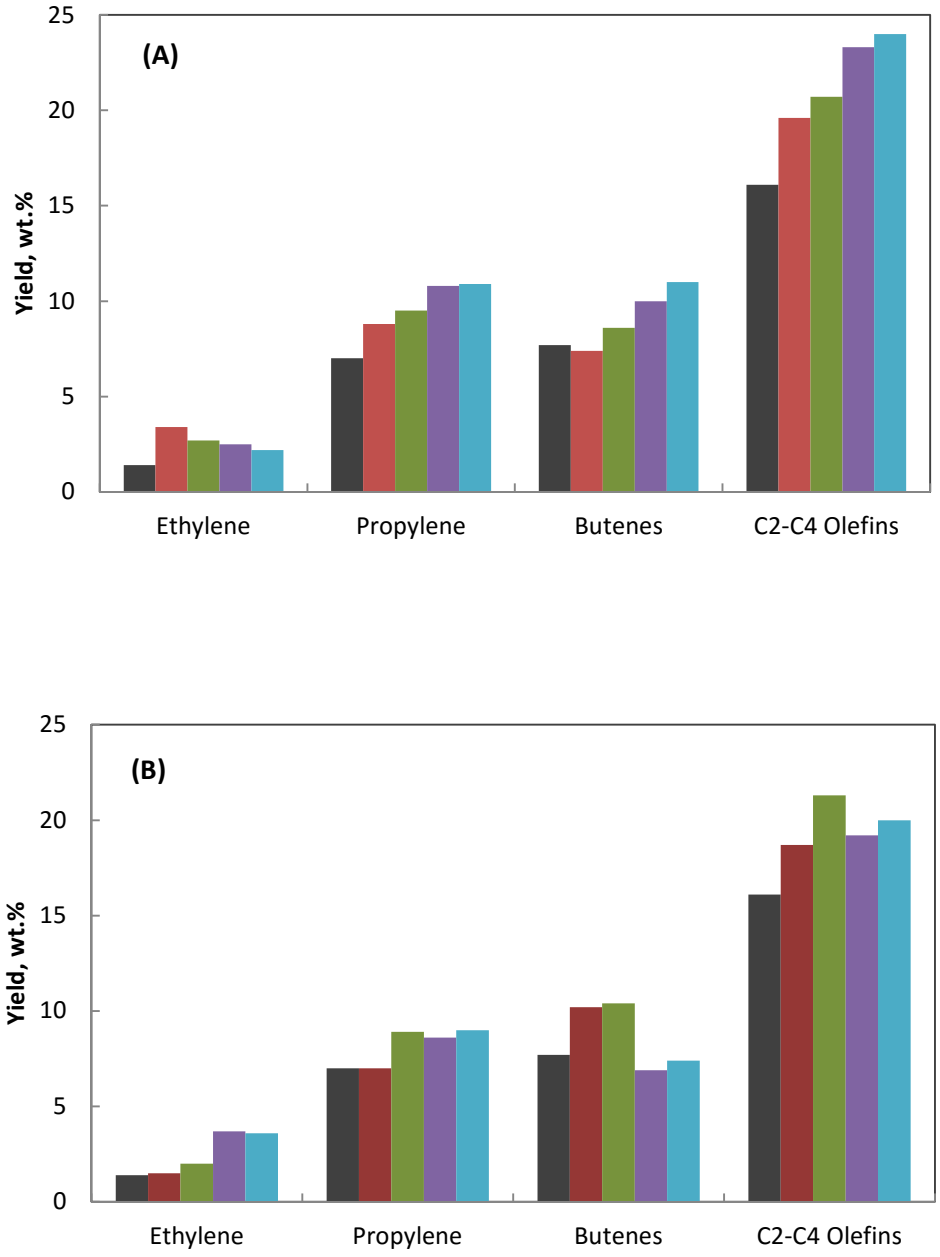

Figure 18 Light olefins yield over E-Cat and E-Cat/additives (A), (■) E-Cat; (■) ZSM-5; (■) MCM-22; (■) MCM-36 and (■) Ferrierite. (B), (■) E-Cat; (■) SSZ-33; (■) SSZ-74; (■) IM-5 and (■) TNU-9.

The increase in the light olefins yield may be attributed to the conversion of reactive gasoline-range species (mainly iso-paraffins and olefins) [17]. Over E-Cat/additives, the observed increase in *i*-C_4 may be assigned to secondary conversion of isobutylene via hydrogen transfer mechanism. It has been reported that the rate of hydrogenation is much higher for the *i*-olefins rather than *n*-olefins [63]. This behavior affected butenes yield and the yield of light olefins (Table 7). Ferrierite produced the highest yield of butenes at 11 wt.% compared with 7.7 wt.% over E-Cat. SSZ-74, SSZ-33, and MCM-36 produced high yield of butenes at ~10 wt.%. To a lower extent butenes yield was enhanced over MCM-22 at 8.6 wt.%. Other additives showed decreased yield of butenes or no change.

4.2.3 Dry gas yields and coke formation

Dry gas (H_2, C_1-C_2) yield increased with increasing conversion over E-Cat and E-Cat/additives. The increase in the dry gas yield may be attributed mainly to the increase in the ethylene yield. The change in other dry gas components was insignificant as they were produced in low yields. Hence, dry gas yield variation among E-Cat/additives followed the same trend of ethylene. For E-Cat, it increased from 2.5 wt.% to 4.5 wt.% within conversion range of 62-76% (Figures 16 and 17). All additives increased dry gas yield compared to E-Cat except for SSZ-33. At 70% conversion, ZSM-5, IM-5 and TNU-9 showed the highest yield of dry gas at 6.1 wt.% compared to 3.3 wt.% over E-Cat. MCM-22, MCM-36 and ferrierite yielded 4-5 wt.%. SSZ-74 yielded 3.8 wt.% (Table 7).

The amount of coke formed was the highest over TNU-9 (4.2 wt.%) compared with 1.4 wt.% over E-Cat. Other E-Cat/additives did not show significant change in coke amount.

4.2.4 Gasoline yield and composition

At VGO conversion of 70 %, gasoline yield decreased in the following order: E-Cat = SSZ-33 > ferrierite > SSZ-74 > MCM-36 > MCM-22 > ZSM-5 > IM-5 > TNU-9. This was associated with a substantial increase in LPG yield (Table 7). The percentage increase in propylene yield for a unit decrease in the gasoline yield (%$C_3^=$/gasoline) gives the best selective additive for propylene from conversion of gasoline-range reactive species to lighter products (C_2-C_4). Ferrierite provides the highest ratio of 8.7% increase in propylene yield per unit decrease in gasoline. MCM-36, SSZ-74, and MCM-22 showed propylene enhancement of 4.5 %, 3.8 % and 2.5 % respectively, per unit decrease in gasoline. The ratios over ZSM-5, IM-5 and TNU-9 were low (1.4-1.6 %). These results showed a strong inverse correlation between %$C_3^=$/gasolineand HTC. High values of (%$C_3^=$/gasoline) were accompanied by low HTC values. The lower ability to carry bimolecular reactions allowed product molecules to desorb as olefins (i.e. less conversion of propylene to propane). SSZ-33 did not enhance propylene yield and hence gave the lowest value for this ratio (0.8%).

The composition of gasoline fraction (n-paraffins, iso-paraffins, olefins, naphthenes and aromatics) over all catalysts at 70% conversion is shown in Tables 8 and 9. Over all E-Cat/additives, there was no significant change in the n-paraffins content of gasoline fraction compared to E-Cat. The zeolite additives enhanced cracking of iso-paraffins as it decreased by more than 50%, as compared to E-Cat except for SSZ-33. The conversion of gasoline-range olefins to light olefins (C_2-C_4), is possible by direct cracking at the high temperature 550 ^oC [26,64]. Additives having high HTC cracked most of the gasoline-range olefins but, they did not show much enhancement in light olefins yield. For instance, gasoline-olefins content dropped from 20.9 wt.% over E-Cat to 1.8 - 3.8 wt.% over IM-5, ZSM-5, TNU-9 and MCM-22 (Tables 8

and 9). However, these additives yielded 19-20 wt.% light olefins compared with 16.1 wt.% over E-Cat (Table 7). In contrast, MCM-36 and SSZ-74 decreased gasoline-olefins to 17.5 wt.% and 10.0 wt.%, respectively, but, they boosted light olefins yield to 23.3 wt.% and 21.3 wt.% respectively. Only ferrierite and SSZ-33 increased gasoline-range olefins content.

Gasoline naphthenes were consumed by dehydrogenation reactions to aromatics and by cracking to olefins [26,63]. This explains the similar decrease in naphthenes content and olefins over E-Cat/additives, with the increase in aromatics content. Only ferrierite, SSZ-33 and MCM-36 showed the increase in naphthenes yield from 7.7 wt.% over E-Cat to 10.0-12.7 wt.%, most probably due to the largest available reaction volumes.

Aromatics content over IM-5, TNU-9 and MCM-22 was more than doubled compared with E-Cat. These zeolite additives increased aromatics content to ~ 89 wt.% compared with 41.9 wt.% over E-Cat. Over MCM-36, SSZ-74 and ZSM-5 aromatics content increased to 62.4 wt.%, 80.9 wt.% and 81.1 wt.% respectively. There was no change in aromatics content over ferrierite while SSZ-33 showed a drop to 26.3 wt.% (Tables 8 and 9).

Research octane number (RON) of gasoline was enhanced over E-Cat/ additives by direct correlation to the increase in aromatics content. RON was 80 over E-Cat, while it increased by 17 numbers over TNU-9 and IM-5 (Tables 8 and 9). The additives ZSM-5, MCM-22, SSZ-33 and SSZ-74 exhibited RON values in the range 88-92. The aromatics content ferrierite (82) increased only slightly. In contrast, MCM-36 decreased its gasoline RON to 76, which is attributed to the decrease in the concentration of iso-paraffins with medium increase in aromatics compared with E-Cat.

Table 8 Gasoline composition at (70%) conversion over E-Cat and additives ZSM-5, SSZ-33, SSZ-74 and MCM-36

Catalyst	Base E-Cat	E-Cat/ 25wt.% additive			
		ZSM-5	SSZ-33	SSZ-74	MCM-22
Compositions (wt.%)					
n-paraffins	2.1	0.9	1.6	1.8	1.3
iso-paraffins	27.3	12.8	20.0	3.0	5.1
Olefins	20.9	3.6	42.1	10.0	3.4
Naphthenes	7.7	1.6	10.0	4.4	1.7
Aromatics	41.9	81.1	26.3	80.9	88.5
RON[a]	80.0	92.0	88.0	89.0	88.0

[a] Research Octane Number by GC PIONA.

Table 9 Gasoline composition at (70%) conversion over E-Cat and additives MCM-36, FER, IM-5 and TNU-9

Catalyst	Base E-Cat	E-Cat/ 25wt.% additive			
		MCM-36	FER	IM-5	TNU-9
Compositions (wt.%)					
n-paraffins	2.1	4.2	2.3	1.5	2.3
iso-paraffins	27.3	6.2	11.7	6.7	2.8
Olefins	20.9	17.5	31.5	1.8	3.8
Naphthenes	7.7	9.6	12.7	1.0	1.9
Aromatics	41.9	62.4	41.8	88.8	89.0
RON[a]	80.0	76.0	82.0	96.2	97.5

[a] Research Octane Number by GC PIONA.

4.3 Kinetic study

4.3.1 Model development

Kinetic study was performed to evaluate activation energies for VGO catalytic cracking over E-Cat/SSZ-74 and compared to E-Cat. Kinetic description of the catalytic cracking of VGO comprises a large number of reactants and products from different chemical families and from different distillation cuts. There are many reaction possibilities with different mechanisms and steps involved [65,66]. Simplifying rate equations through lumping strategy is effective for kinetic modeling of catalytic cracking. 4-lump kinetic model is suitable representative of VGO cracking kinetics [67], which is proposed by the following reaction scheme:

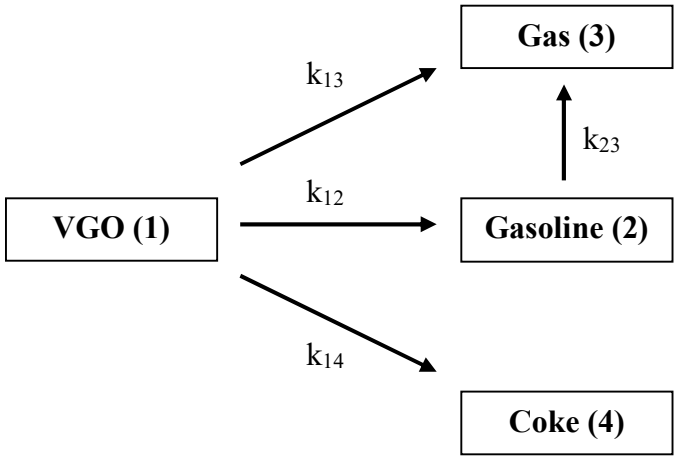

This model accounts for the cracking of VGO to gasoline, gases and coke, and the overcracking of gasoline to gases. Previous studies found that the kinetic constants for the cracking reactions of gasoline to coke and gases to coke were many orders of magnitudes smaller than the others

[67,68]. Taking this into account, we assumed that the formation of coke is only from the reaction of VGO lump.

Based on this proposed scheme, the governing equations for VGO cracking, gasoline, gas and coke formation are:

$$-dY_1/dt = [k_{12} + k_{13} + k_{14}] (Y_1)^2\varphi \quad (1)$$

$$dY_2/dt = [k_{12}Y_1^2 - k_{23}Y_2] \varphi \quad (2)$$

$$dY_3/dt = [k_{13}Y_1^2 + k_{23}Y_2] \varphi \quad (3)$$

$$dY_4/dt = k_{14} (Y_1)^2\varphi \quad (4)$$

$$\varphi = \exp (- \alpha t_{os}) \text{ (deactivation function)} \quad (5)$$

The model equations were formulated under the assumption that the cracking of VGO is the second-order reaction, while gasoline cracking is the first-order reaction. This is a widely adopted assumption in the literature based on the fact that VGO molecules are with changing reactivity [69,70]. At low conversion, most of the VGO reactive molecules crack more rapidly, while as the conversion increases, the reactivity of the feed molecules decreases. On the other hand, gasoline contains a restricted fraction of hydrocarbons with narrower boiling ranges, hence, will exhibit smaller ranges of cracking rates [71].

A catalyst decay function φ is incorporated in the rate equations to account for the loss in catalyst activity due to deactivation from cocking. Exponential decay function which depends on time-on-stream (t_{os}) is used to represent the catalyst decay term φ, as given in Eq. (5). Since cracking of VGO and gasoline is taking place on the same acidic sites, the deactivation function, φ for all the four reaction steps (Eqs. (1) - (4)) was assumed to be identical and independent of

temperature, as been shown in others works [68,72]. This assumption introduces great simplifications in model parameters estimation with narrow errors [73].

k_{ij} are temperature dependent rate constants given by Arrhenius formula:

$$k_{ij} = k_{o\text{-}ij} \exp[(-E_{ij}/R)\,(1/T - 1/T_o)] \quad (6)$$

The temperature T_o is centering temperature introduced to reduce interaction between parameters [74]. The reactor was assumed to operate under isothermal conditions due to negligible temperature change observed during the reactions.

4.3.2 Determination of kinetic model parameters

Kinetic expression of VGO catalytic cracking based on 4-lump model (Equations 1-4), incorporating deactivation equation (Equation 5) and Arrhenius relation (Equation 6) were combined and solved numerically. Nonlinear regression analysis (MATLAB, ODE 45-4th order Runge-Kutta method and least-square curve fitting "lsqcurvefit" routine) was used to evaluate the kinetic parameters. The centering temperature T_o in Arrhenius relation was set equal to 550 ^oC. The regression algorithm restricted the estimated rate constants and activation energies to be positive in consistence with physical principles. The optimization criteria was set to minimize sum of squares of the differences between calculated and experimental values of the mass fractions of reaction components. The data points were taken at different C/O ratios ranging from 2 to 6, and at three different temperatures (500, 550 and 600 ^oC).

The estimated rate constants and apparent activation energies are shown in Table 10, along with their 95 % confidence level which shows that the values are estimated quite precisely. The values for the apparent activation energies obtained in this study are found to be comparable with the literature values [67,75,76], as presented in Table 11. Experimental and calculated VGO

conversions as a function of reaction temperature at different C/O ratios are shown in Figure 19. It can be seen that the model prediction of experimental values is satisfactory.

Table 10 Estimated kinetic parameters for VGO catalytic cracking over E-Cat and E-Cat/SSZ-74

Catalyst	E-Cat		E-Cat/SSZ-74	
Parameter	E_{ij} (kcal/mol)	$k_{o\text{-}ij}$[a]	E_{ij} (kcal/mol)	$k_{o\text{-}ij}$[a]
k_{12}	14.2 ± 0.1	58.4 ± 1.5	16.1 ± 0.08	56.4 ± 0.9
k_{13}	18.0 ± 0.3	19.6 ± 0.2	21.4 ± 0.9	33.5± 0.3
k_{14}	12.2 ± 0.4	1.7 ± 0.01	12.4 ± 0.5	2.4 ± 0.01
k_{23}	17.3 ± 0.2	8.6 ± 0.2	14.6 ± 0.1	13.4 ± 0.2
α (h^{-1})	12.1 ± 0.04		15.3 ± 0.1	

[a] $k_{o\text{-}12}$, $k_{o\text{-}13}$ and $k_{o\text{-}14}$ in (weight fraction h)$^{-1}$; $k_{o\text{-}23}$ in h^{-1}.

Table 11 Comparison of activation energies with literature values

Reaction step	Present study[a]		Literature[a]		
	E-Cat	E-Cat/SSZ-74	A[b]	B[c]	C[d]
VGO-gasoline	14.2	16.1	16.3	14.3	15.2
VGO-gas	18.0	21.4	21.3	11.4	16.3
VGO-coke	12.2	12.4	15.4	7.4	22.7
Gasoline-gas	17.3	14.6	12.6	16.5	15.6

[a]All values in (kcal/mol)
[b]Taken from reference [67].
[c]Taken from reference [75].
[d]Taken from reference [76].

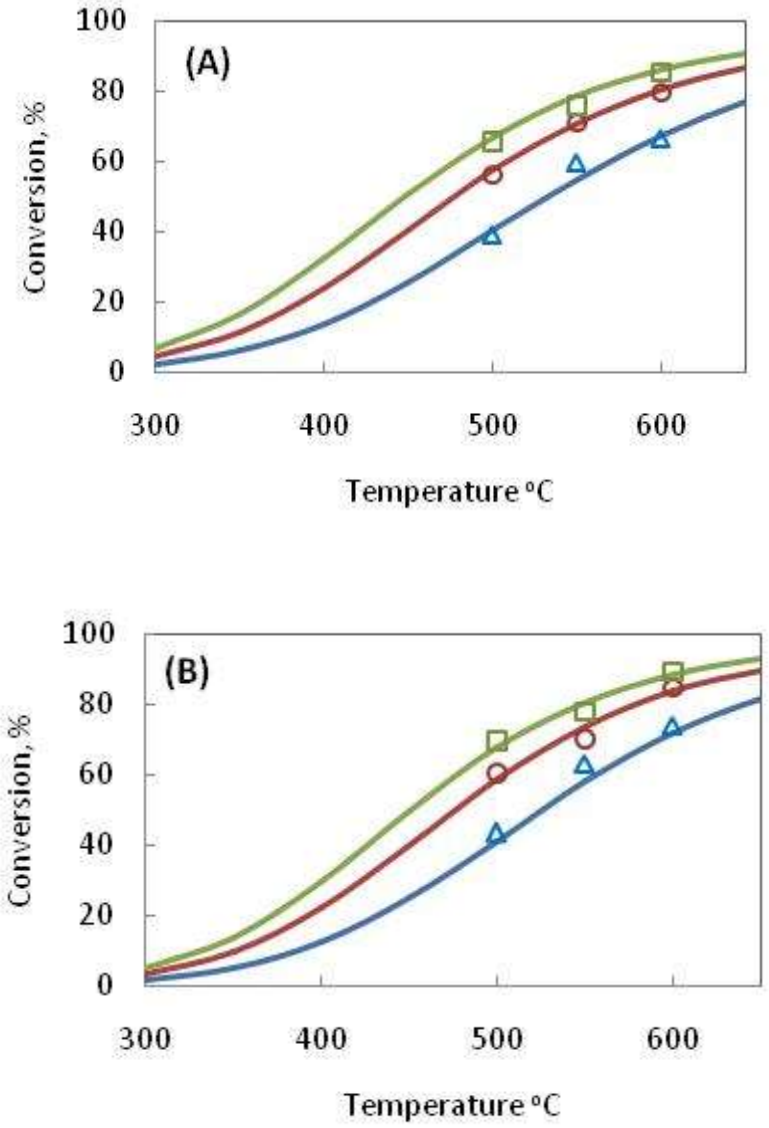

Figure 19 Predicted (lines) and experimental (symbols) conversion for (A) E-Cat and (B) E-Cat/SSZ-74 at C/O ratio of (Δ) 2; (○) 4 and (□) 6.

Comparison between experiments and model prediction for gasoline and gas yields as a function of conversion at different temperatures is shown in Figures 20 and 21. The model successfully predicted the effect of increasing reaction temperature from 500 to 600 ºC is to promote more gases and less gasoline, which is in agreement with experimental results. A drop in gasoline yield curve is observed at high conversions above 75% (Figure 20). In contrary, gases yield increased continuously with increasing conversion (Figure 21). This trend is attributed to the overcracking of gasoline to gases.

Over E-Cat, the apparent activation energies for cracking of VGO to gasoline (E_{12}) and VGO to gas (E_{13}) were 14.2 kcal/mol and 18.0 kcal/mol, respectively (Table 10). While over E-Cat/SSZ-74, the values were 15.3 kcal/mol and 21.4 kcal/mol for E_{12} and E_{13}, respectively. The slightly increased values of E_{12} and E_{13} over E-Cat/SSZ-74 as compared to E-Cat indicate that the cracking of VGO is easier over E-Cat. This might be attributed to the larger pore structure of E-Cat (based on 12-ring Y-zeolite) compared to SSZ-74 (10-ring zeolite) allowing to accommodate higher concentrations of bulky molecules of VGO lump in the catalyst channel system [77,78].

In contrast, the activation energy for reaction of gasoline to gas (E_{23}) dropped from 17.3 kcal/mol over E-Cat, to 14.6 kcal/mol over E-Cat/SSZ-74 (Table 10). This might be due to more restricted pore structure of SSZ-74 which provided more interactions between gasoline molecules and the catalytic surface [72]. This enhanced the reaction of gasoline and hence, lower apparent activation energy (E_{23}) over SSZ-74 is observed. Furthermore, the total acidity of E-Cat was estimated at about 0.04 mmol/g, in agreement with previous studies [16,79]. Adding SSZ-74 with a total acidity of 0.28 mmol/g (Table 6), almost doubled the concentration of acid sites in E-Cat/SSZ-74. Most likely, the increased concentration of acid sites over E-Cat/SSZ-74 has also played a role in decreasing apparent activation energy (E23) compared to E-Cat [78].

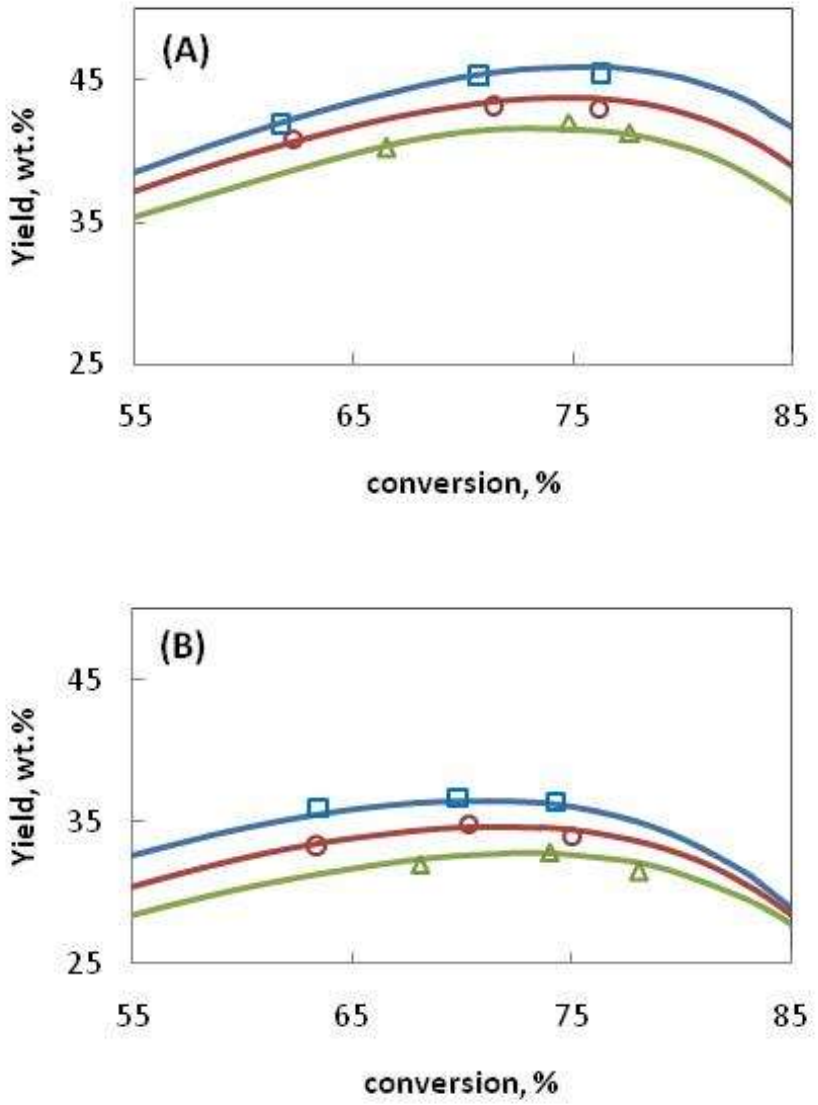

Figure 20 Predicted (lines) and experimental (symbols) gasoline yield for (A) E-Cat and (B) E-Cat/SSZ-74 at temperature of (□) 500 ºC; (○) 550 ºC and (Δ) 600 ºC.

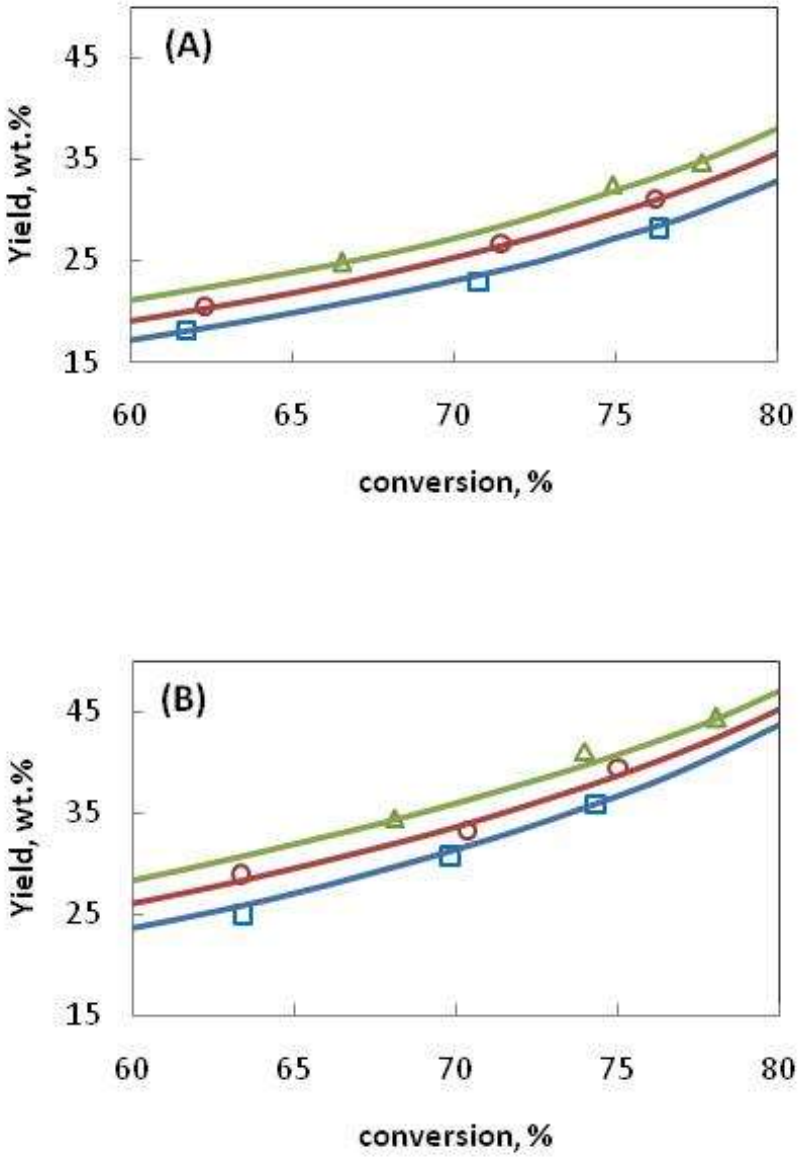

Figure 21 Predicted (lines) and experimental (symbols) gas yield for (A) E-Cat and (B) E-Cat/SSZ-74 at temperature of (□) 500 ºC; (○) 550 ºC and (Δ) 600 ºC.

CHAPTER 5

EFFECT OF ZEOLITE Si/Al MOLAR RATIO

5.1 Catalyst characterization

Framework tetrahedral aluminum is the source of zeolite acidity. Therefore, zeolite Si/Al molar ratio has a major impact on its performance as catalysts [33]. This chapter presents the results on correlation between zeolite Si/Al molar ratio, activity and selectivity. Three framework types were investigated with varying Si/Al molar ratio, namely MFI, -SVR and FER. Table 12 summarizes the samples used for this purpose.

Table 12 Zeolites under study with varying Si/Al molar ratio

Framework type	Number of samples	Range of Si/Al molar ratio
MFI	9	23-2000
-SVR	4	40-900
FER	2	9-27

Samples are named as (framework type-Si/Al molar ratio). For example, MFI-80 corresponds to an MFI zeolite with Si/Al molar ratio of 80.

Textural properties obtained from N_2 adsorption/desorption isotherms are summarized in Table 13. For the same framework type, there was no major variation in textural properties with changing Si/Al ratio. Quantitative evaluation of the concentrations Brønsted and Lewis acid sites obtained from FTIR spectroscopy of adsorped pyridine or d3-acetonitrile is given in Table 14. There is an observed decrease in total number of acid sites along with the increase in zeolite

Si/Al ratio. This is true for all framework types. In the case of MFI zeolites with Si/Al ratio >80, the acid sites were very weak and could not be detected by FTIR spectroscopy (i.e. Signal/noise ratio is very low and hence high percentage of experimental error).

Table 13 Textural properties of zeolites with varying Si/Al molar ratio under study

Sample-Si/Al	BET (m^2/g)[a]	V_{mic} (cm^3/g) [b]	V_{tot} (cm^3/g)
MFI framework type			
MFI-23	322	0.13	0.21[c]
MFI-30	352	0.11	0.29[c]
MFI-55	371	0.11	0.31[c]
MFI-80	399	0.13	0.26[c]
MFI-280	372	0.07	0.22[c]
MFI-500	359	0.08	0.21[c]
MFI-1200	337	0.07	0.20[c]
MFI-2000	320	0.14	0.20[c]
-SVR framework type			
SVR-40	341	0.14	0.20[d]
SVR-80	409	0.15	0.22[d]
SVR-120	340	0.13	0.21[d]
SVR-Silica	341	0.14	0.20[d]
FER framework type			
FER-9	306	0.13	0.17[d]
FER-27	316	0.13	0.18[d]

[a] BET method using p/p_0 0.05-0.20; [b] Vmic = micropore volume using *t-plot* method; [c] Vtot = total pore volume (at p/p0 = 0.99); [d] Vtot = total pore volume (at p/p0 = 0.95).

Table 14 Lewis (C_L) and Brønsted (C_B) acid sites concentration of zeolites with varying Si/Al molar ratio

Additive Sample	Si/Al (IR)	C_L (mmol/g)	C_B (mmol/g)	Total (mmol/g)
MFI-23[a]	-	0.023	0.98	1.003
MFI-30[a]	-	0.21	0.37	0.58
MFI-55[a]	-	0.031	0.424	0.455
MFI-80[a]	-	0.04	0.165	0.205
SVR-40[a]	42.1	0.11	0.17	0.28
SVR-80[a]	87	0.08	0.03	0.11
SVR-120[a]	109	0.04	0.05	0.09
SVR-Silica[a]	926	0.003	0.012	0.015
FER-9[b]	14	0.33	0.42	1.09
FER-27[b]	29.3	0.06	0.44	0.5

[a] Adsorption of pyridine; [b] adsorption of acitonitrile.

5.2 Catalyst evaluation

5.2.1 Conversion and yields

The product yield distribution of VGO cracking for MFI is shown in Table 15, while -SVR and FER are shown in Table 16. Product yields were assessed at constant conversion of 70% to distinguish the catalytic performance of additives with different Si/Al ratios.

Figure 22 shows the conversion versus C/O ratio for selected MFI samples (30, 80, 280 and 2000) to cover the wide range of Si/Al ratio investigated. The other samples (23, 55, 150, 500 and 1200) followed a similar trend. Figure 23 shows the conversion versus C/O ratio for -SVR and FER. The conversion increased with increasing C/O ratio for E-Cat and all the additives.

Table 15 Comparative MAT data at constant conversion (70%) and 550 °C over MFI additives with varying Si/Al molar ratio

Catalyst	Base E-Cat	E-Cat/ 25wt.% additive								
		MFI-23	MFI-30	MFI-55	MFI-80	MFI-150	MFI-280	MFI-500	MFI-1200	MFI-2000
C/O Ratio (g/g) [a]	3.1	2.3	2.3	2.4	2.5	2.0	2.2	3.5	3.4	3.0
Product yields (wt.%)										
Dry gas	3.3	5.6	6.1	6.1	6.2	5.7	5.0	3.5	3.5	3.4
H2	0.1	0.1	0.2	0.1	0.1	0.1	0.1	0.1	0.1	0.1
C1	0.9	1.0	1.1	0.9	1.0	0.8	0.8	0.7	0.7	0.8
C2=	**1.4**	**3.1**	**3.4**	**3.8**	**3.9**	**3.7**	**3.1**	**1.9**	**1.9**	**1.7**
C2	0.9	1.3	1.4	1.3	1.2	1.1	1.0	0.9	0.9	0.8
LPG	22.6	34.1	36.1	37.3	35.3	34.2	33.8	31.6	31.1	31.0
C3=	**7.0**	**8.0**	**8.8**	**9.8**	**10.9**	**11.0**	**12.9**	**12.1**	**12.0**	**11.6**
C3	1.1	9.4	9.6	8.5	6.0	5.2	2.6	1.5	1.5	1.3
C4=	**7.7**	**6.9**	**7.4**	**8.6**	**9.9**	**10.1**	**12.7**	**12.4**	**12.7**	**13.2**
nC4	2.6	3.0	3.1	3.1	2.4	2.2	1.2	0.8	0.9	0.8
iC4	4.2	6.8	7.2	7.2	6.1	5.8	4.4	4.8	4.1	4.2
C2= - C4=	**16.1**	**18.0**	**19.6**	**22.2**	**24.7**	**24.8**	**28.7**	**26.4**	**26.5**	**26.5**
LPG-paraffins	7.9	19.2	19.9	18.9	14.5	13.2	8.2	7.1	6.5	6.2
Gasoline	42.9	28.7	26.5	25.5	26.9	29.0	29.9	33.4	33.6	34.2
LCO	16.8	13.5	13.9	12.7	12.8	14.2	13.1	14.6	14.6	14.2
HCO	13.0	16.5	16.2	17.3	17.3	15.7	17.0	15.4	15.3	15.8
Coke	1.4	1.6	1.2	1.2	1.4	1.1	1.2	1.5	1.7	1.5
HTC [b]	0.89	1.42	1.39	1.20	0.86	0.79	0.44	0.45	0.39	0.38
C_3=/LPG [c]	0.31	0.24	0.24	0.26	0.31	0.32	0.38	0.38	0.38	0.37
C_3 olefinicity [d]	0.86	0.46	0.48	0.54	0.65	0.68	0.83	0.89	0.89	0.90
C_2 olefinicity [e]	0.62	0.70	0.71	0.75	0.76	0.77	0.76	0.68	0.69	0.67
%C_3=/ gasoline [f]	Base	1.08	1.64	2.36	3.57	4.18	6.63	7.81	7.82	7.71

[a] Catalyst to oil ratio; [b] Hydrogen transfer coefficient (butanes/butenes); [c] Propylene selectivity within LPG.
[d] C3=/total C3s; [e] C2=/total C2s; [f] Percent increase in propylene per unit decrease in gasoline.

Table 16 Comparative MAT data at constant conversion (70%) and 550 ºC over -SVR and FER additives with varying Si/Al molar ratio

Catalyst	Base E-Cat	E-Cat/ 25wt.% additive					
		-SVR-40	-SVR-80	-SVR-120	-SVR-silica	FER-9	FER-27
C/O Ratio (g/g) [a]	3.1	4.0	4.6	2.4	6.0	4.7	2.9
Product Yields (wt.%)							
Dry gas	3.3	3.8	4.0	4.0	3.1	7.6	4.1
H2	0.1	0.09	0.08	0.06	0.08	0.21	0.07
C1	0.9	0.8	0.8	0.6	0.7	1.3	0.9
C2=	**1.4**	**2.0**	**2.3**	**2.6**	**1.6**	**4.6**	**2.2**
C2	0.9	0.9	0.8	0.7	0.5	1.5	1.0
LPG	22.6	29.2	29.8	35.6	26.4	33.5	28.1
C3=	**7.0**	**8.9**	**10.9**	**13.5**	**9.1**	**12.7**	**10.9**
C3	1.1	2.6	2.0	2.6	1.2	4.8	1.3
C4=	**7.7**	**10.4**	**10.5**	**12.8**	**11.2**	**9.1**	**11.0**
nC4	2.6	1.4	1.2	1.6	0.9	1.1	0.7
iC4	4.2	5.8	5.2	5.1	4.1	5.8	4.2
C2=-C4=	**16.1**	**21.3**	**23.7**	**28.9**	**21.9**	**26.4**	**24.0**
LPG-paraffins	7.9	9.8	8.4	9.3	6.1	11.7	6.2
Gasoline	42.9	34.9	34.1	28.9	39.1	26.5	36.4
LCO	16.8	13.6	13.9	12.7	14.3	12.8	14.8
HCO	13.0	16.4	16.1	17.3	15.7	17.2	15.2
Coke	1.4	2.1	2.1	1.5	1.4	2.4	1.5
HTC [b]	0.9	0.7	0.6	0.5	0.4	0.8	0.4
C3=/LPG [c]	0.31	0.31	0.37	0.38	0.34	0.38	0.39
C3 olefinicity [d]	0.86	0.77	0.85	0.84	0.89	0.73	0.89
C2 olefinicity [e]	0.61	0.70	0.74	0.79	0.76	0.76	0.69
%C3=/ gasoline [f]	Base	3.8	6.9	7.0	9.7	5.2	8.7

[a] Catalyst to oil ratio; [b] Hydrogen transfer coefficient (butanes/butenes); [c] Propylene selectivity within LPG.
[d] C3=/total C3s; [e] C2=/total C2s; [f] Percent increase in propylene per unit decrease in gasoline.

Through all catalysts, the conversion ranged between 60-82 % as C/O ratio increased from 2 to 6. All MFI additives enhanced VGO conversion compared to E-Cat despite the dilution effect of the additives (Figure 22). -SVR and FER exhibited lower conversion compared to E-Cat and MFI additives, except for -SVR-120 and FER-27 (Figure 23). Over all catalysts, the increase in conversion was more significant for C/O ratio between 2 and 4 followed by a slow increase from 4 to 6. Which proves that the effect of experimental conditions on conversion is higher at milder conditions, and this effect is less to observe as the severity of conditions are gradually increased [58].

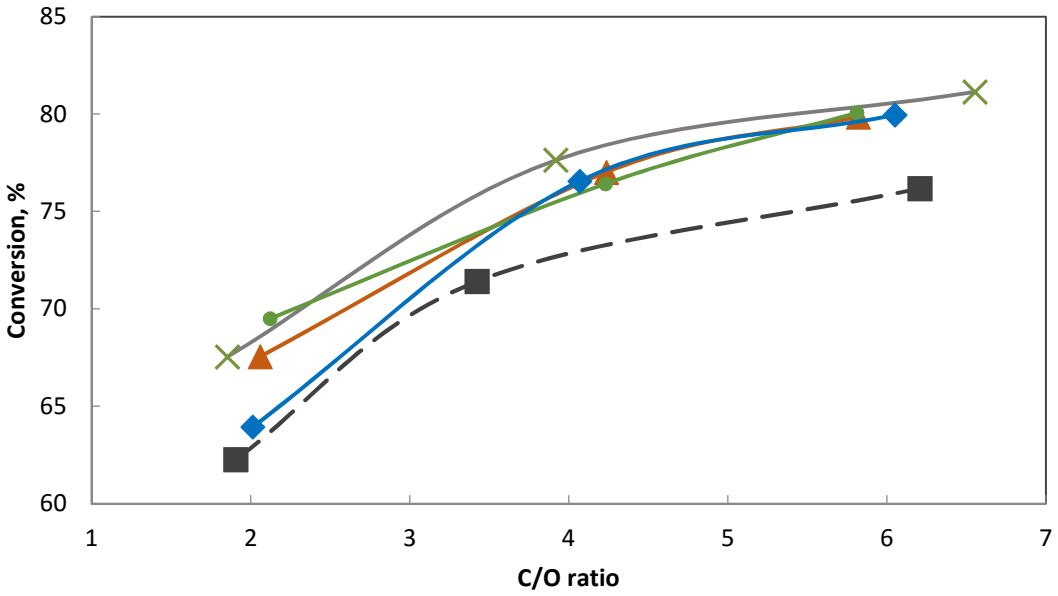

Figure 22 Comparison of MAT conversion over, (■) E-Cat; (×) MFI-30; (▲) MFI-80; (●) MFI-280 and (♦) MFI-2000.

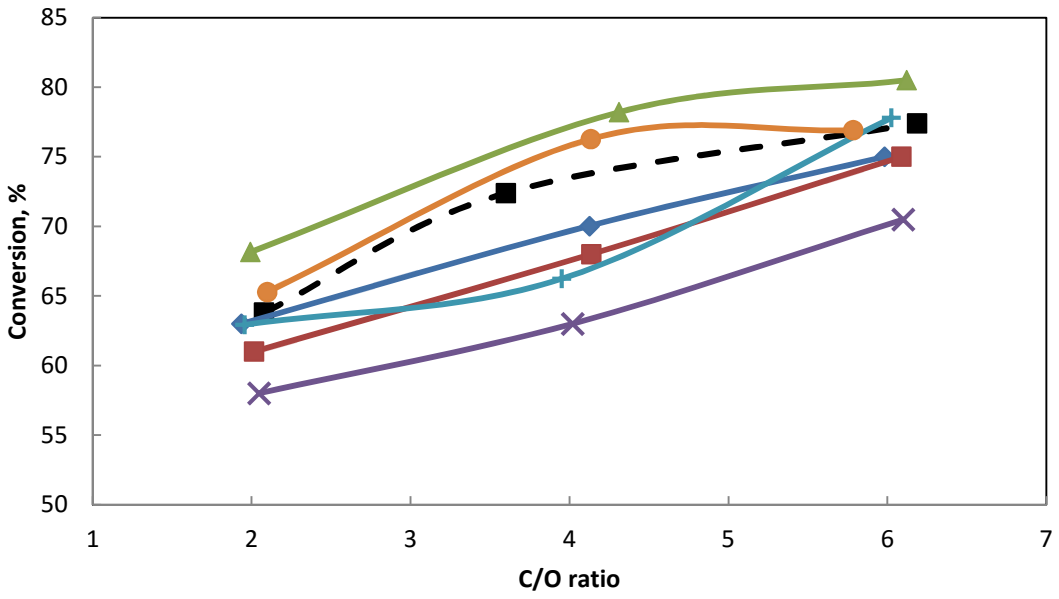

Figure 23 Comparison of MAT conversion over, (■) E-Cat; (♦) -SVR-40; (■) -SVR-80; (▲) -SVR-120; (×) -SVR-silica; (+) FER-9 and (●) FER-27

Catalyst to oil (C/O) ratio at constant conversion gave an indication about the activity of each catalyst. As shown in (Table 15), this value was not affected significantly by the change in MFI Si/Al ratio. However, it ranged between 2-2.5 for MFI-23 to MFI-280, and between 3-3.5 for MFI 500 to MFI-2000 (Table 15). The value for E-Cat was 3.1. The relatively lower values over MFI-23 to MFI-280 may be explained by the higher amount of acid sites in these additives compared to the additives MFI-500 to MFI-2000. It is known that the acidity of FCC catalyst plays a key role in VGO conversion [80]. C/O ratio at 70 % conversion ranged in 2.4-4.6 g/g over -SVR-40 to -SVR-120. The value was higher over -SVR-silica at 6.0 g/g. This can be attributed to lower acid sites density over -SVR-silica compared to other -SVR samples (Table 14). Over FER framework type, C/O ratio at 70 % conversion ranged in 2.9-4.7 g/g (Table 16).

The results showed that the general effects of adding the additives to E-Cat are to produce more gaseous products with increases in propylene and light olefins yields compared to E-Cat.

Gasoline yield is tending to decrease over the additives, however, with gain in research octane number (RON). Detailed discussion on product yields is given in the following sections.

For all framework types, hydrogen transfer reactions were minimized by increasing Si/Al ratio. As shown in Table 15, HTC was the highest over MFI-23 at 1.42; and decreased continuously with increasing Si/Al ratio to the minimum value of 0.38 over MFI-2000. The same trend is observed over -SVR and FER (Table 16). HTC decreased continuously from 0.7 over -SVR-40 to 0.4 over -SVR-silica. Similarly, HTC was 0.8 over FER-9 and decreased to 0.4 over FER-27 (Table 16). High Si/Al ratio gave the advantage of lowering the concentration of acid sites and, positively weakening the acidic function of the zeolite. At low density of acid sites, the adsorption of hydrocarbons is lowered which favor monomolecular reactions, i.e. cracking, rather than bimolecular reactions, i.e. hydrogen transfer [27].

5.2.2 LPG and light olefins yields (MFI framework type)

Products distribution showed that LPG was the main product from gasoline over-cracking over MFI additives. At 70% conversion, LPG yield was 22.6 wt.% over E-Cat and this increased upon adding MFI additives (Table 15). LPG yield increased gradually from 34.1 wt.% over MFI-23 to reach a maximum at 37.3 wt.% over MFI-55 followed by a gradual decrease to 31.0 wt.% over MFI-2000. Ethylene yield exhibited a maximum over MFI-80 at 3.9 wt.% compared with 1.4 wt.% over E-Cat. Ethylene yield was 3.1 wt.% and 1.7 wt.% over MFI-23 and MFI-2000, respectively (Table 15).

Figure 24 shows the yields of propylene and propane versus conversion over E-Cat, MFI-55 and MFI-280. Over E-Cat, propylene yield increased from 5.4 wt.% to 8.8 wt.% with increasing conversion from 62 % to 76 % (Figure 24). Upon adding MFI additives, changing in propylene

yield with increasing conversion followed two scenarios. The first is a continuous drop in propylene yield with increasing conversion. This trend was observed over the additives with the lower Si/Al ratios, MFI-23, MFI-30 and MFI-55. In this case, the decrease in propylene yield with increasing conversion was side by side with a dramatic increase in propane yield. As shown in Figure 24 over MFI-55, upon increasing conversion from 68% to 81%, propylene yield decreased from 10.0 wt.% to 8.2 wt.% with a sharp increase in propane yield from 7.9 wt.% to 15.0 wt.%. This is attributed to the high hydrogen transfer activity over the additives with low Si/Al ratios (high density of acid sites) which caused excessive saturation of propylene to propane.

The second scenario is continuous increase in propylene yield with increasing conversion. This trend was observed over all MFI additives with Si/Al ratios of 80 and above. Figure 24 shows this case over MFI-280 where upon increasing conversion from 69% to 80%, propylene yield increased from 12.8 wt. % to 14.6 wt.% with a slow increase in propane yield from 2.5 wt.% to 5.3 wt.%. In this case, low density of acid sites hindered hydrogen transfer reactions, as a result, limited propylene saturation to propane [18,28]. However, despite the two observed trends in changing of propylene yield with increasing conversion, at 70% conversion, all MFI samples increased propylene yield compared to E-Cat.

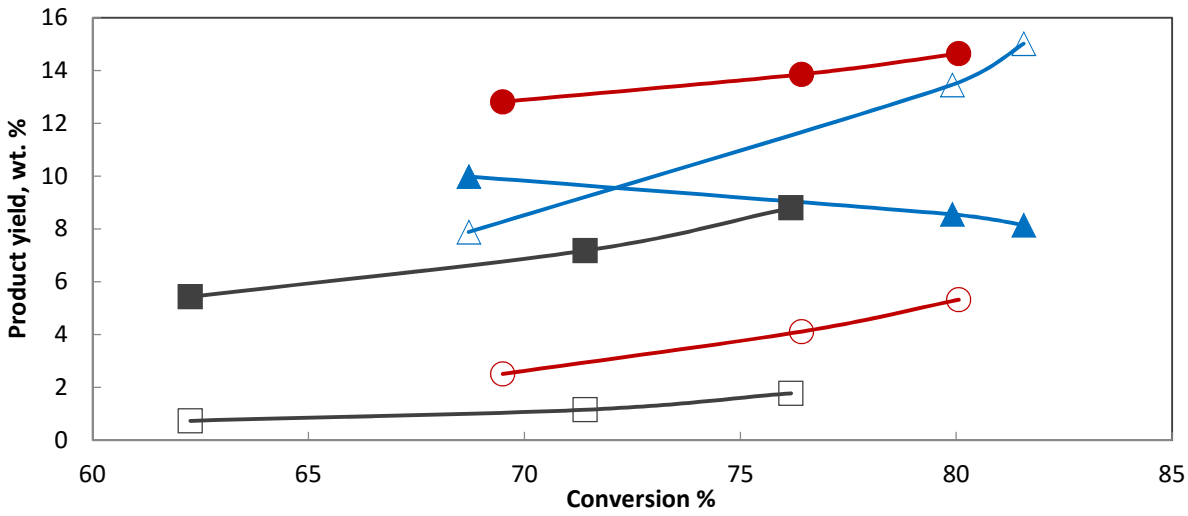

Figure 24 Yields of propylene (solid fill) and propane (no fill) over, (■) E-Cat; (▲) MFI- 55 and (●) MFI-280.

Figure 25 shows the important product yields at 70% conversion (Propylene, light olefins and gasoline) as a function of Si/Al ratio of MFI additives. At 70% conversion, propylene yield over E-Cat was 7.0 wt.% and increased to 8.0 wt.% over MFI-23 (Table 15). Propylene yield continue to increase with increasing Si/Al ratio to reach a maximum of 12.9 wt.% over MFI-280 followed by slow decrease to 11.6 wt.% over MFI-2000 (Table 15 and Figure 25).

C3 olefinicity over E-Cat was 0.86. This value dropped significantly to 0.46 over MFI-23 and then starts to increase gradually with increasing Si/Al ratio to reach a maximum of 0.90 over MFI-2000 (Table 15). The results showed a strong relationship between C3 olefinicity and HTC. The lowest value of C3 olefinicity over MFI-23 is attributed to the high HTC value (1.42) where high yield of propane is produced with low enhancement in propylene yield compared to E-Cat (Table 15). The gradual increase in C3 olefinicity from MFI-23 to MFI-2000 may be explained by the decrease in HTC as Si/Al ratio increases.

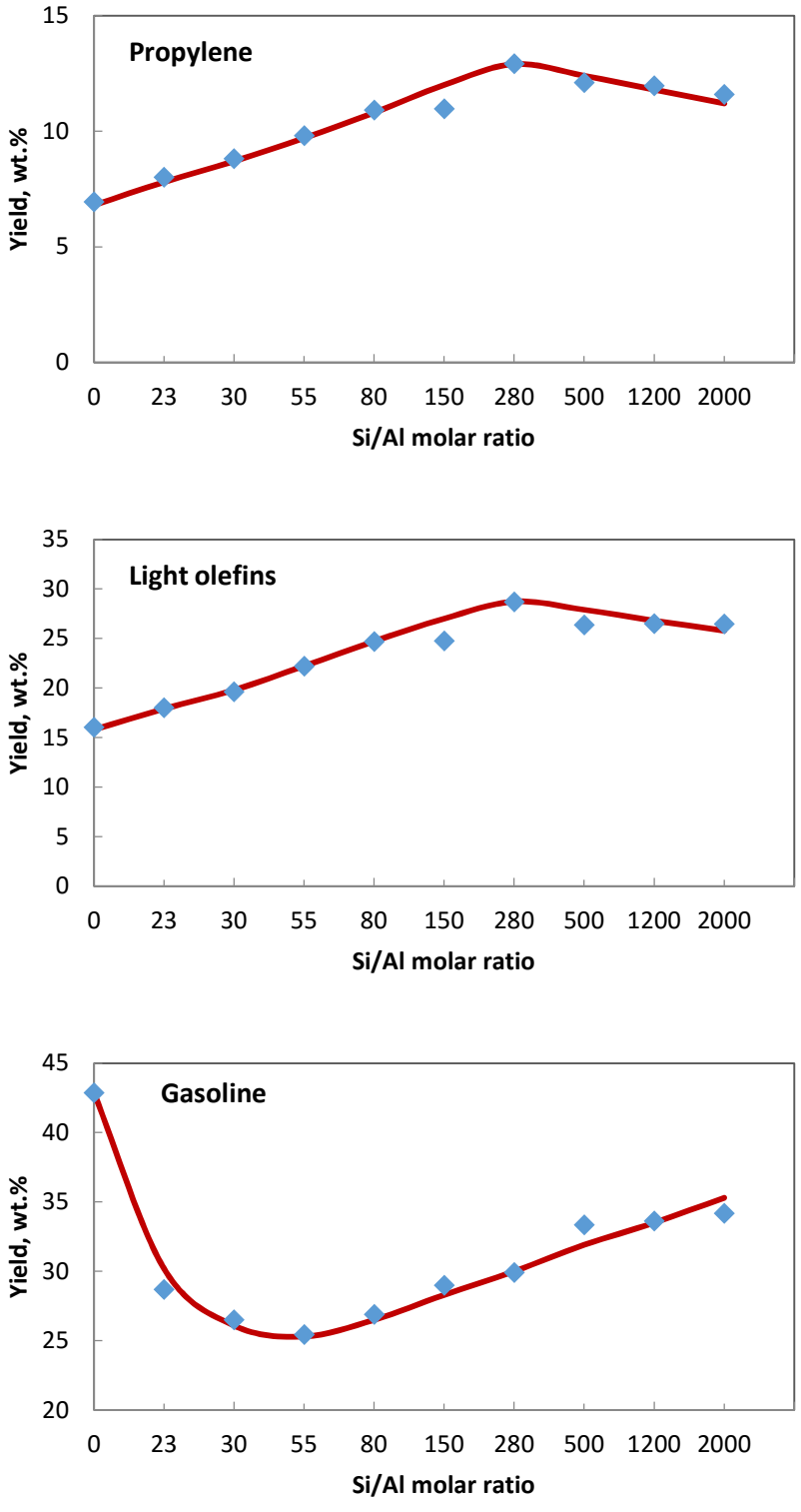

Figure 25 Propylene, light olefins and gasoline yields vs. MFI Si/Al molar ratio

Butenes yield was 7.7 wt.% over E-Cat and decreased to 6.9 wt.% over MFI-23 (Table 15). However, butenes yield increased with increasing Si/Al ratio to reach a maximum of 13.2 wt.% over MFI-2000. It has been reported that the rate of hydrogenation is much higher for i-olefins rather than n-olefins [63]. By this, it is expected that the effect of HTC is more to observe on butenes compared to other light olefins (ethylene and propylene). This explains the continues increase in butenes yield with increasing Si/Al ratio (along with HTC decreases) while ethylene and propylene yields both exhibited a maximum.

The largest contribution of light olefins (C2-C4) was from propylene and butenes. Over E-Cat light olefins yield was 16.1 wt.% and increased to 18.0 wt.% over MFI-23. Light olefins yield increased with increasing Si/Al ratio to a maximum of 28.7 wt.% over MFI-280. This is followed by a slight decrease to 26.5 wt.% over MFI-2000. The increase in light olefins yield maybe attributed to the conversion of reactive gasoline-range species (mainly iso-paraffins and olefins).

As shown in Figure 25, the observed trends in propylene and light olefins yields with increasing Si/Al ratio, i.e. continuous increase in the product yield up to a maximum value followed by a decrease as Si/Al ratio is further increased, suggest the presence of two affecting factors balanced against each other: the catalyst activity in cracking gasoline range reactive species to produce light olefins, and the ability to preserve light olefins from saturation to paraffins. The contentious enhancement in propylene and light olefins yields in the more acidic region from 23 to 280 (Figure 25), suggests that the affecting factor is the continuous suppression of hydrogen transfer reactions as Si/Al ratio increases. However, in the low acidic region from 280 to 2000, the yields of propylene and light olefins starts to slightly decrease despite the fact that HTC is still getting lower. Most probably, the weak and low density acid sites on these additives are less able to over-crack the gasoline. This is supported by the increase in gasoline yield from Si/Al

ratio of 55 to 2000 (Figure 25). The results present MFI-280 as the point that strikes a balance between suppression of hydrogen transfer reactions and catalyst activity in over-cracking gasoline for maximum propylene production.

5.2.3 LPG and light olefins yields (-SVR and FER framework type)

LPG yield increased gradually with increasing Si/Al ratio from 29.2 wt.% over -SVR-40 to reach a maximum at 35.6 wt.% over -SVR-120 followed by a decrease to 26.4 wt.% over -SVR-silica (Table 16). Ethylene yield exhibited a maximum over -SVR-120 at 2.6 wt.% compared with 1.4 wt.% over E-Cat. Ethylene yield was 2.0 wt.% and 1.6 wt.% over -SVR-40 and -SVR-silica, respectively (Table 16). FER-9 yielded more LPG at 33.5 wt.% compared to 28.1 wt.% for FER-27. Ethylene yield over FER-9 was the highest among all the additives at 4.6 wt.%.

Figure 26 shows the important product yields at 70% conversion (Propylene, light olefins and gasoline) as a function of -SVR Si/Al ratio. -SVR showed a similar pattern to MFI (Figure 2 and 3). At 70% conversion, propylene yield over E-Cat was 7.0 wt.% and increased to 8.9 wt.% over -SVR-40 (Table 16 and Figure 26). Propylene yield continue to increase with increasing Si/Al ratio to reach a maximum of 13.5 wt.% over -SVR-120 followed by a decrease to 9.1 wt.% over -SVR-silica. Over E-Cat, light olefins yield was 16.1 wt.% and increased to 21.3 wt.% over -SVR-40. Light olefins yield increased with increasing Si/Al ratio to a maximum of 28.9 wt.% over -SVR-120. This is followed by a decrease to 21.9 wt.% over -SVR-silica. Similar to MFI zeolites, the increase in propylene and light olefins yields with the increase in Si/Al ratio between -SVR-40 and -SVR-80 is attributed to the decrease in HTC from 0.7 to 0.5 (Table 16). However, over -SVR-silica, the yields of propylene and light olefins decreased despite the fact

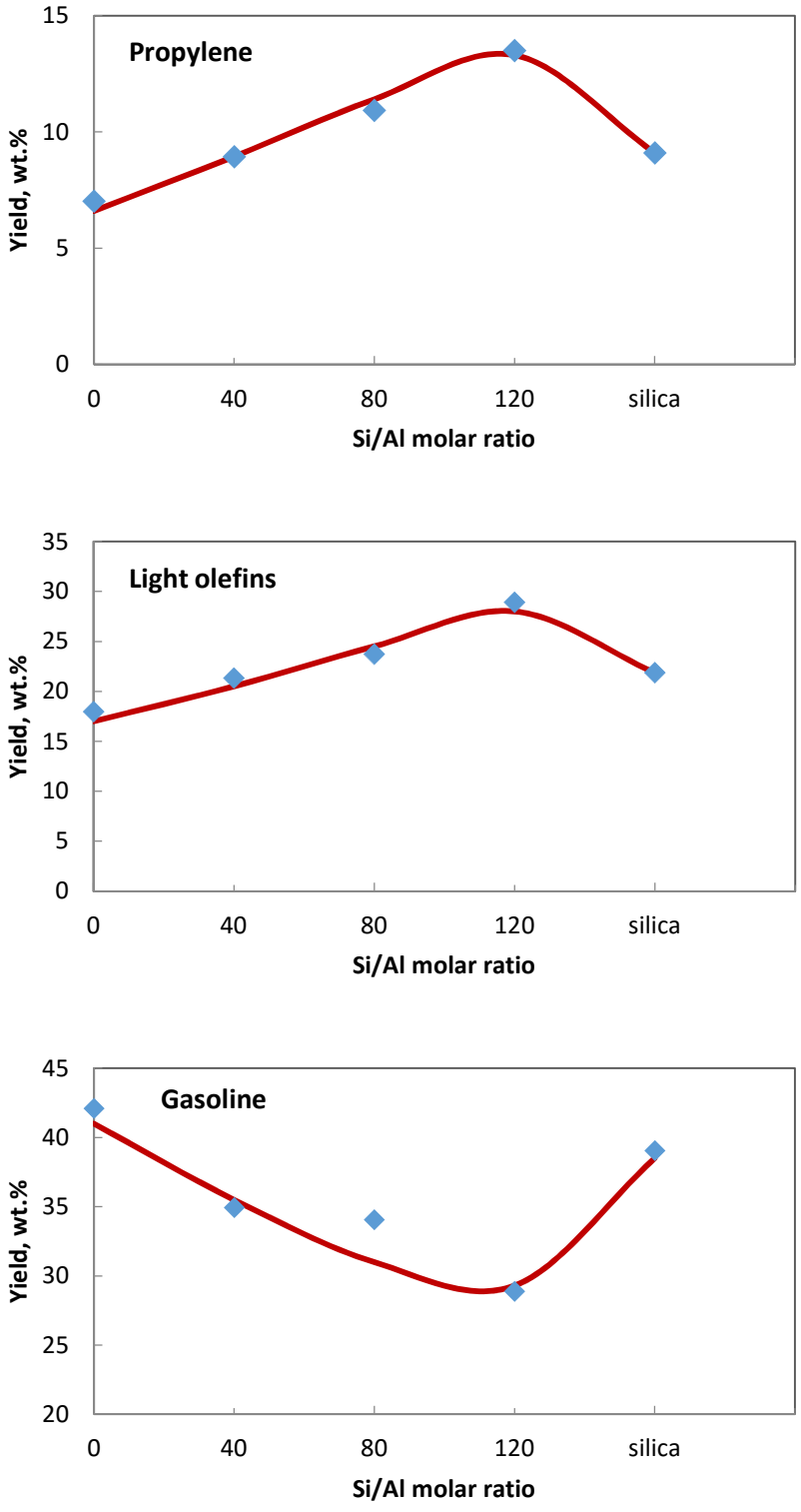

Figure 26 Propylene, light olefins and gasoline yields vs. -SVR Si/Al molar ratio

that HTC is still getting lower. Most probably, the weak and low density acid sites on -SVR-silica are less able to over-crack the gasoline. This is supported by the increase in gasoline yield between -SVR-120 and -SVR-silica (Figure 26).

For FER, the decrease in Si/Al ratio favored the production of propylene and light olefins. FER-9 yield of propylene and light olefins was 12.7 wt.% and 26.4 wt.%, respectively, compared to 10.9 wt.% and 24.0 wt.%, respectively, over FER-27 (Table 16). Lower Si/Al ratio increased the density of acid sites and as a result, enhanced the cracking of gasoline range reactive species to light olefins. This is supported by the lower yield of gasoline over FER-9 at 26.5 wt.% compared to 36.4 wt.% over FER-9 (Table 16).

The results showed a strong relationship between C3 olefinicity and HTC for both -SVR and FER. C3 olefinicity increased from 0.77 over -SVR-40 to 0.89 over -SVR-silica and, from 0.73 over FER-9 to 0.89 over FER-27 (Table 16).

5.2.4 Dry gas yield and coke formation

For all zeolite framework types, the increase in dry gas yield may be attributed mainly to the increase in ethylene yield. Other dry gas components (H2, C1 and C2) were produced in low yields with insignificant changes compared to E-Cat and with changing Si/Al ratio (Tables 15 and 16). Hence, dry gas variation with changing Si/Al ratio followed the same trend of ethylene. Over MFI, dry gas yield exhibited a maximum over MFI-80 at 6.2 wt.% compared with 3.3 wt % over E-Cat. Dry gas yield was 5.6 wt.% and 3.4 wt.% over MFI-23 and MFI-2000, respectively (Table 15). Over -SVR, dry gas yield varied between 3.1 wt.% and 4.0 wt.%. FER-9 exhibited the highest dry gas yield among all additives at 7.6 wt.%. Dry gas yield was 4.1 wt.% over FER-27 (Table 16).

The low yields of methane, ethane and ethylene, is attributed to the carbenium ion mechanism [18]. The formation of these products requires the reaction to proceed through primary carbenium ion, which is very unstable. However, the increases in ethylene yield over the additives maybe attributed to their smaller pore structure compared to E-Cat. Smaller pore structure provides more interactions between the catalytic surface and the carbenium ion. This provides more stabilization to reaction intermediates and, as a result, enhancement in ethylene yield [26].

Coke amount did not change much upon adding the additives and did not show much correlation with Si/Al ratio. Over E-Cat and all framework types, coke amount was in the range of 1.1-2.4 wt.% (Tables 15 and 16).

5.2.5 Gasoline yield and composition

Gasoline yield was 42.9 wt.% over E-Cat and dropped over all additives as compared to E-Cat. Over MFI, gasoline yield dropped to 28.7 wt.% and 25.5 wt.% over MFI-23 and MFI-55, respectively. This is followed by a continuous increase in gasoline yield with increasing Si/Al ratio to 34.2 wt.% over MFI-2000 (Table 15 and Figure 25). Figure 27 shows LPG and gasoline yields as a function of MFI Si/Al ratio. The decrease in gasoline yield was balanced by an increase in LPG yield. For instance, the lowest gasoline yield of 25.5 wt.% over MFI-55 was associated with the highest LPG yield at 37.3 wt.% (Table 15).

Hydrogen transfer reactions consume the gasoline-range olefins to less reactive species, i.e. aromatics. As a result, gasoline reactivity to gaseous products decreases. This might explains the higher yield of gasoline over MFI-23 and MFI-30 compared to MFI-55.

Over -SVR, gasoline yield was 34.9 wt.% over -SVR-40 and decreased gradually to 28.9 wt.% over -SVR-120. This is followed by an increase to 39.1 wt.% over -SVR-silica (Table 16 and Figure 26). Gasoline yield was 26.5 wt.% and 36.4 wt.% over FER-9 and FER-27, respectively (Table 16).

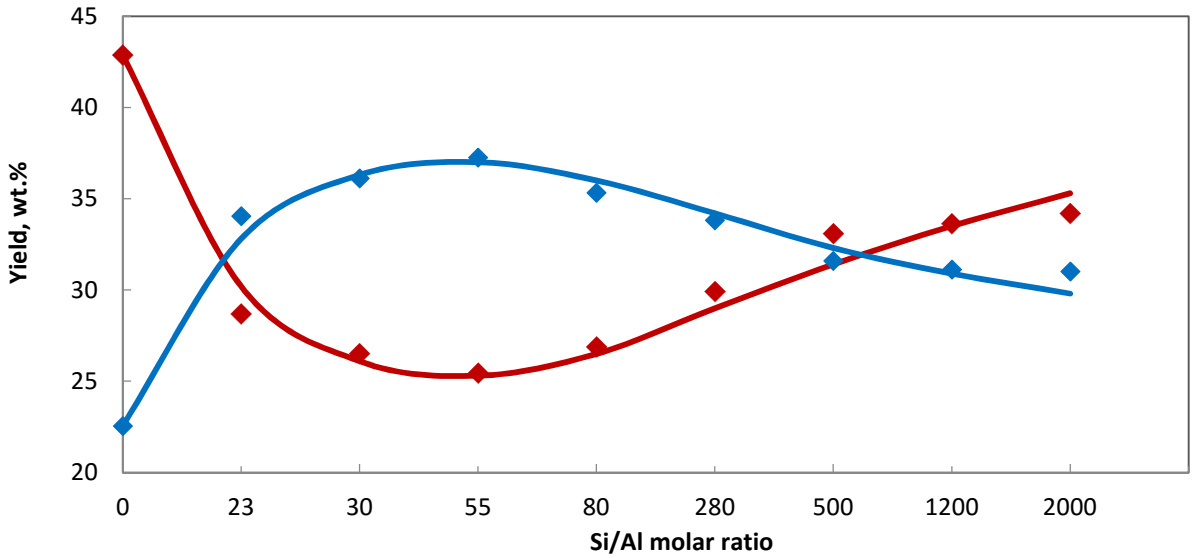

Figure 27 Yields of (♦) LPG and (♦) gasoline vs. MFI Si/Al molar ratio

The percentage increase in propylene yield for a unit decrease in gasoline yield (%C3=/gasoline) gives an indication about selectivity for propylene from conversion of gasoline-range reactive species to lighter products (C2-C4). Over MFI additives, (%C3=/gasoline) was the lowest over MFI-23 at 1.08% and increased gradually with increasing Si/Al ratio to reach a maximum of ~7.8% in the region of high Si/Al ratio (500-2000). Over -SVR, (%C3=/gasoline) increased step by step from 3.8% over -SVR-40 to 9.7% over -SVR-silica. Similarly, (%C3=/gasoline) increased with increasing Si/Al ratio for FER. The values were 5.2% and 8.7% over FER-9 and

FER-27, respectively. The results showed a strong inverse correlation between (%C3=/gasoline) and HTC. Additives with high Si/Al ratio have less density of acid sites. This allowed product molecules to desorb as olefins, i.e. less conversion of propylene to propane.

The composition of gasoline fraction (n-paraffins, iso-paraffins, olefins, naphthenes and aromatics) over E-Cat, MFI-30, MFI-280 and MFI-2000 at 70% conversion is shown in Table 17. Gasoline compositions over -SVR and FER are shown in Table 18. For all framework types, iso-paraffins and olefins were the most reactive species in gasoline fraction, while n-paraffins content did not change much compared to E-Cat. Cracking of iso-paraffins was enhanced remarkably over the additives as it contents dropped to 4.0-17 wt.% in gasoline fraction compared to 27.3 wt.% over E-Cat. However, no trend was observed in iso-paraffins with changing Si/Al ratio (Tables 17 and 18).

Table 17 Gasoline compositions at (70%) conversion over E-Cat and MFI additives.

Catalyst	Base E-Cat	E-Cat/ 25wt.% additive			
		MFI-30	MFI-80	MFI-280	MFI-2000
Compositions (wt.%)					
n-paraffins	2.1	0.9	1.2	2.7	3.5
iso-paraffins	27.3	12.8	11.9	13.3	17.5
Olefins	20.9	3.6	7.3	14.7	18.5
Naphthenes	7.7	1.6	2.4	8.1	9.2
Aromatics	41.9	81.1	77.2	61.3	51.4
RON[a]	80.0	92	90	86	81

[a] Research Octane Number by GC PIONA.

The conversion of gasoline-range olefins to light olefins (C2-C4) was possible by direct cracking at the high temperature 550 ^{o}C [64]. Gasoline-olefins were heavily consumed over MFI with low Si/Al ratio. Gasoline-olefins content was 3.6 wt.% over MFI-30 and increased gradually with increasing Si/Al ratio to 18.5 wt.% over MFI-2000 (Table 17). Similar trend to MFI is observed

over -SVR. Gasoline-olefins content was 10.0 wt.% over -SVR-40 and increased to 26.1 wt.% over -SVR-silica. FER-9 gasoline-olefins content was 7.2 wt.% and increased to 31.5 wt.% over FER-27 (Table 18).

Gasoline naphthenes were consumed by dehydrogenation reactions to aromatics and by cracking to olefins [63]. Naphthenes were almost completely consumed over MFI-23 and MFI-80 as it content dropped to ~2%. Naphthenes content did not change much over MFI-280 and MFI-2000 (Table 17). Naphthenes content ranged between 4.0-7.9 wt.% over -SVR and between 9.7-12.7 wt.% over FER. For all framework types, consumption of olefins and naphthenes matches an increase in aromatic contents. Additives with low Si/Al ratio were more able to hydrogenate naphthenes to aromatics. For instance, aromatics content increased significantly over MFI-23 to 81.1 % and decreased with increasing Si/Al ratio to 51.4 % over MFI-2000 (Table 17).

Table 18 Gasoline compositions at (70%) conversion over -SVR and FER additives.

Catalyst	Base E-Cat	E-Cat/ 25wt.% additive					
		-SVR-40	-SVR-80	-SVR-120	-SVR-silica	FER-9	FER-27
Compositions (wt.%)							
n-paraffins	2.1	1.8	2.6	1.5	1.7	1.1	2.3
iso-paraffins	27.3	3.0	4.8	4.0	10.8	4.4	11.7
Olefins	20.9	10.0	13.6	16.9	26.1	7.2	31.5
Naphthenes	7.7	4.4	4.0	5.2	7.9	9.7	12.7
Aromatics	41.9	80.9	75.0	72.4	53.5	77.6	41.8
RON[a]	80.0	89.0	87.6	84.5	85.0	89.5	82

[a] Research Octane Number by GC PIONA.

Research octane number (RON) of gasoline was enhanced over the additives by direct correlation to the increase in aromatics content. RON was 80 over E-Cat, and increased to 92, 90 and 86 over MFI 30, MFI-80 and MFI-280, respectively (Table 17). MFI-2000 did not increase

RON due to medium increase in aromatics content with decreases in iso-paraffins. RON over -SVR ranged between 85-89 and between 82-89 over FER (Table 18).

5.3 Kinetic study

Kinetic study was performed to investigate the effect of Si/Al ratio on activation energies for VGO catalytic cracking over E-Cat and the additives MFI-30, MFI-280 and MFI-2000. 4-lump kinetic model was used to represent VGO cracking kinetics as described in *Section 4.3*.

The estimated rate constants and apparent activation energies are shown in Table 19, along with their 95 % confidence level which shows that the values are estimated quite precisely. Experimental and calculated VGO conversion as a function of reaction temperature at different C/O ratios is shown in Figure 28. It can be seen that the model prediction of experimental values is satisfactory.

Table 19 Estimated kinetic parameters for VGO catalytic cracking over E-Cat and the additives MFI-30, MFI-280 and MFI-2000

Catalyst	Base E-Cat	E-Cat/ 25wt.% additive		
		MFI-30	MFI-280	MFI-2000
Parameter				
E_{12}[a]	14.2 ± 0.1	13.2 ± 0.3	12.7 ± 0.1	13.1 ± 0.2
k_{o-12}[b]	58.4 ± 1.5	51.9 ± 1.5	59.1 ± 0.9	61.0 ± 0.5
E_{13}[a]	18.0 ± 0.3	18.3 ± 0.9	17.4 ± 0.2	18.3 ± 0.9
k_{o-13}[b]	19.6 ± 0.2	58.1 ± 0.05	45.9 ± 0.1	48.7 ± 0.13
E_{14}[a]	12.2 ± 0.4	16.9 ± 0.1	13.7 ± 0.5	12.3 ± 0.5
k_{o-14}[b]	1.7 ± 0.01	4.2 ± 0.02	3.8 ± 0.2	3.3 ± 0.01
E_{23}[a]	17.3 ± 0.2	14.2 ± 0.1	15.8 ± 0.2	16.3 ± 0.1
k_{o-23}[c]	8.6 ± 0.2	14.1 ± 0.1	14.9 ± 0.08	7.8 ± 0.1
α (h^{-1})	12.1 ± 0.04	16 ± 0.1	15 ± 0.3	12 ± 0.1

[a] kcal/mol

[b] $(\text{weightfraction } h)^{-1}$

[c] h^{-1}

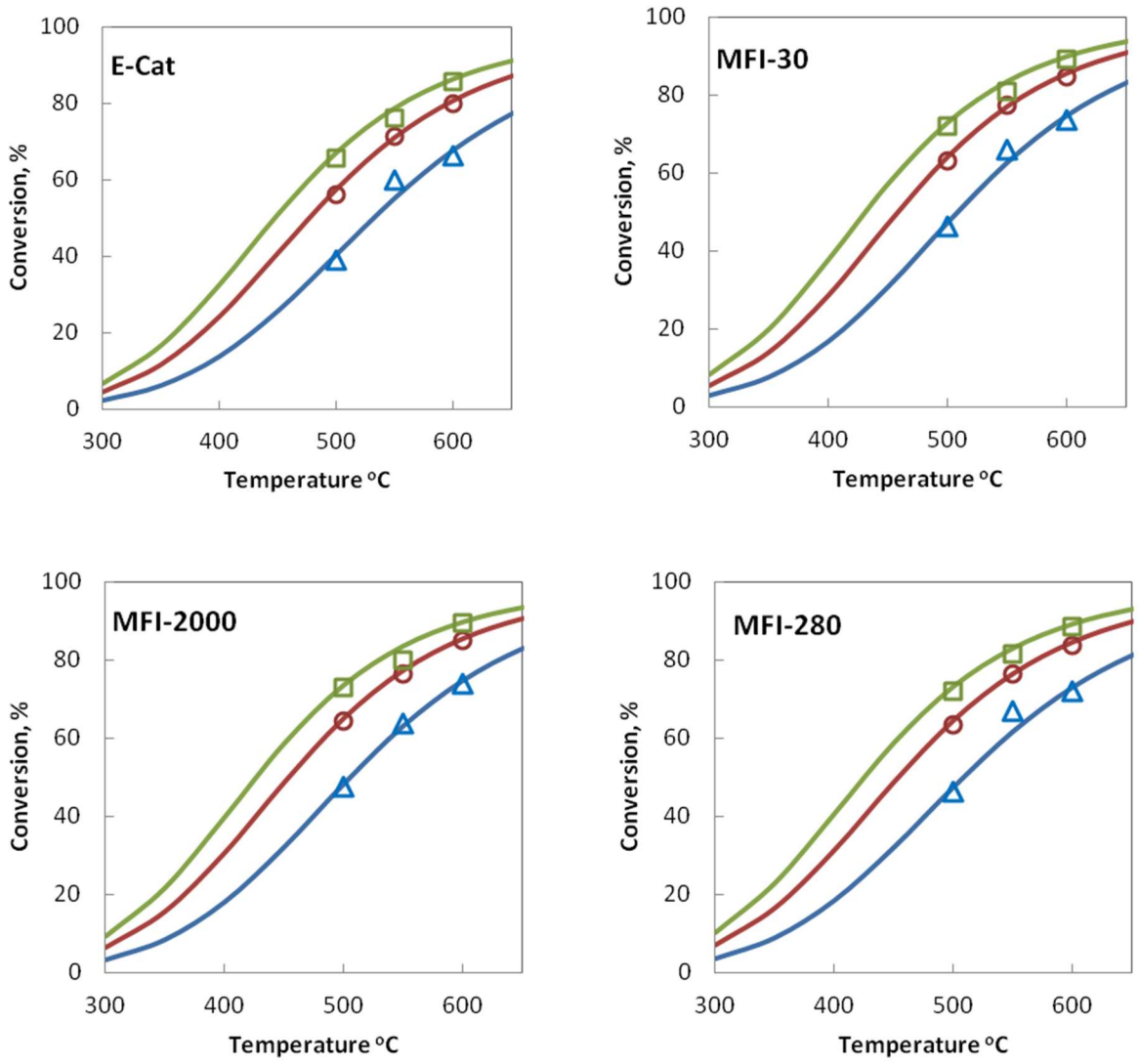

Figure 28 Predicted (lines) and experimental (symbols) conversion for E-Cat and the additives MFI-30, MFI-280 and MFI-2000 at C/O ratio of (Δ) 2; (○) 4 and (□) 6.

Comparison between experiments and model prediction for VGO, gasoline, gas and coke yields as a function of conversion at reaction temperatures 550 °C is shown in Figure 29. A drop in gasoline yield curve is observed at high conversions above 75%. In contrary, gases yield increased continuously with increasing conversion. This trend is attributed to the overcracking of gasoline to gases.

Over E-Cat, the apparent activation energies for cracking of VGO to gasoline (E12) and VGO to gas (E13) were 14.2 kcal/mol and 18.0 kcal/mol, respectively (Table 19). These values did not change much over MFI additives and ranged in 12.7 - 13.2 kcal/mol for E12 and 17.4 - 18.3 kcal/mol for E13.

The effect of Si/Al ratio on activation energies was observed on E23. Over E-Cat, the value was 17.3 kcal/mol and dropped to 14.2, 15.8 and 16.3 kcal/mol over MFI-30, MFI-280 and MFI-2000 respectively (Table 19). The results showed that the continuous increase in acid sites density along with the decrease in Si/Al ratio from 2000 to 30; resulted in the decrease in E23 from 16.3 kcal/mol to 14.2 kcal/mol. The effect of MFI acid sites density on the activation energies E12 and E13 was not observed as E23. This might be attributed to the limited access of VGO molecules to the active sites in MFI structure.

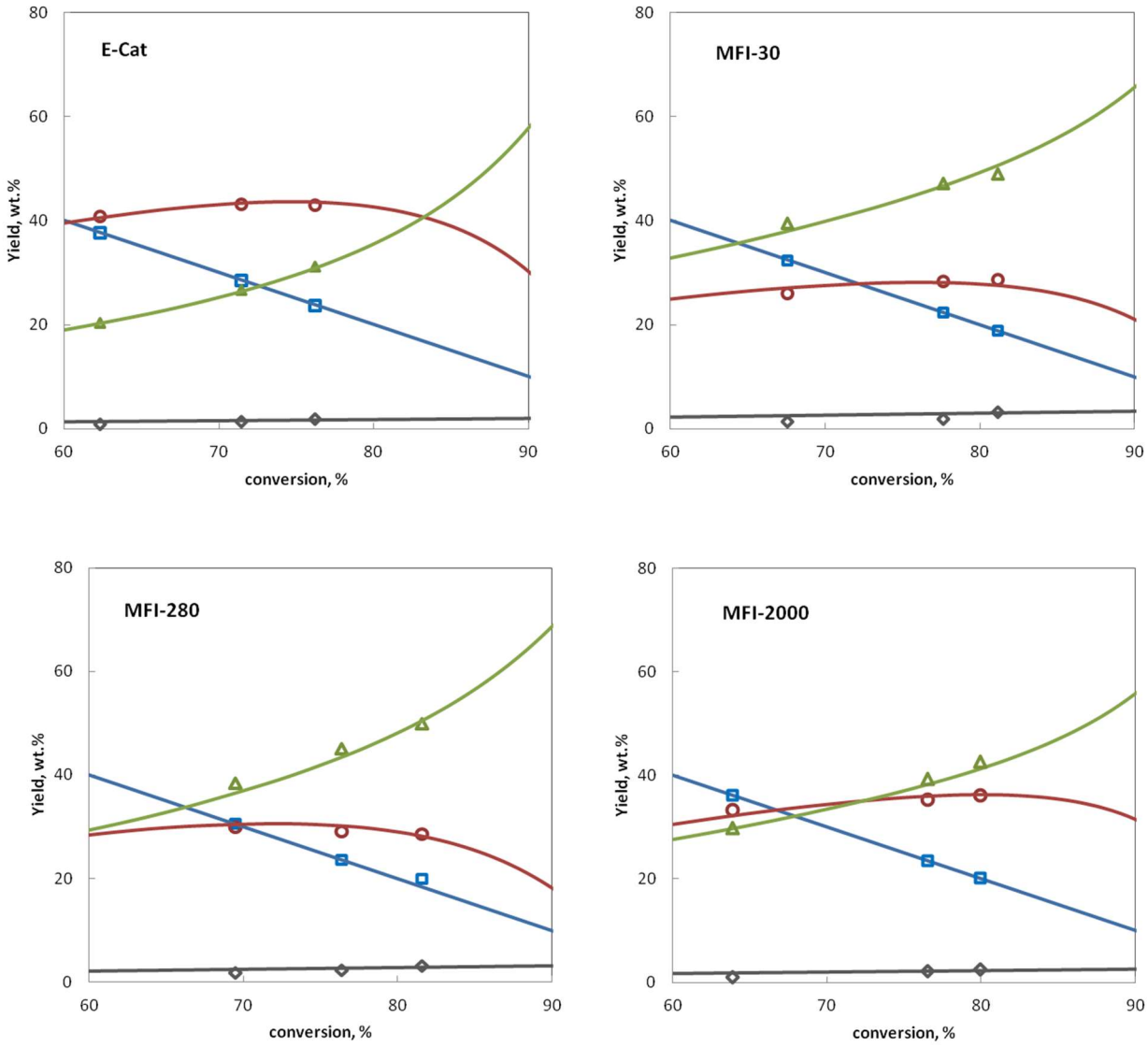

Figure 29 Predicted (lines) and experimental (symbols) for the yields of (□) VGO; (○) gasoline; (Δ) gas and (◊) coke over E-Cat and the additives MFI-30, MFI-280 and MFI-2000 at reaction temperature 550 ºC.

CHAPTER 6

CONCLUSIONS AND RECOMMENDATIONS

6.1 Conclusions

A series of zeolites with different pore structures and different Si/Al molar ratios was used as FCC catalyst additives in the cracking of Arabian Light VGO to enhance propylene productions.

At *comparable Si/Al molar ratios*, main conclusions are summarized as follows:

1. All zeolite additives increased the conversion of the base catalyst. However, mesoporous character of MCM-36 favored the diffusion of reactants and products and hence, the highest conversion among different additives was obtained.
2. Hydrogen transfer reactions (which were monitored by hydrogen transfer coefficient) had a great impact on product yields and quality. Decreased rate of hydrogen transfer reactions increased propylene yield.
3. Maximum propylene and light olefins yields of 10.9 wt.% and 24.0 wt.%, respectively, were achieved over ferrierite compared with 7 wt.% and 16.1 wt.% over E-Cat. Smaller pore size openings of ferrierite suppressed hydrogen transfer reactions as they do not accommodate bulky bimolecular reaction intermediates.
4. High propylene and light olefins yield over MCM-36 as compared to MCM-22, shows the advantages of mesoporous in reducing HTC. Mesoporous lowers the real contact time and as a result, improves products quality.

5. Detailed product analysis showed that the decrease in the gasoline yield was due to the cracking of gasoline-range iso-paraffins and olefins. The increase in gasoline aromatics content over E-Cat/additives increased research octane number.
6. Results of the kinetic study showed that E-Cat/SSZ-74 has lower activation energy for the reaction of gasoline to gases compared to E-Cat.

Main conclusions for the effect of additives Si/Al molar ratio are summarized as follows:

1. Increasing Si/Al molar ratio minimized hydrogen transfer reactions. High Si/Al molar ratio gave the advantage of lowering the concentration of acid sites and, positively weakening the acidic function of the zeolite. This favored monomolecular reactions rather than bimolecular reactions.
2. At high Si/Al molar ratio, over-cracking of gasoline is low due to decreased concentration of acid sites.
3. For maximum propylene production, there is a point that strikes a balance between suppression of hydrogen transfer reactions and catalyst activity in over-cracking gasoline to propylene.
4. The point for maximum propylene production for MFI framework type was over MFI-280 at 12.8 wt.% propylene yield compared to 7.0 wt.% over E-Cat. While for -SVR framework type, maximum propylene yield was over -SVR-120 at 13.5 wt.%.
5. Results of kinetic study showed that the activation energy for cracking reactions from gasoline to gases decreased with decreasing Si/Al molar ratio, in direct relation to the increased concentration of acid sites.

6.2 Recommendations

1. Zeolites SSZ-74, ferrierite and MCM-36 showed superior propylene yield to ZSM-5. It is desired to evaluate these additives in more advanced reactors such as Advanced Cracking Evaluation (ACE) pilot plant.
2. Deactivation of zeolites to investigate their thermal and hydrothermal stability will be with great value. Deactivated zeolites have different activity and selectivity of freshly ones. The rate of dealumination can affect propylene yield during FCC operation.
3. Kinetic modeling based on molecular description is desired. This will give better insight on additives role on different reaction pathways to produce propylene.

REFERENCES

[1] Al-Khattaf S, Ali SA, Aitani AM, Žilková N, Kubička D, Čejka J. Recent Advances in Reactions of Alkylbenzenes Over Novel Zeolites: The Effects of Zeolite Structure and Morphology. Catal Rev Sci Eng 2014;56:333–402.

[2] Aitani AM. Propylene Production. In: S. L, editor. Encycl. Chem. Process., New York: Taylor & Francis; 2006, p. 2461–6.

[3] Schnaith M, Shackleford A, McLean J. Re-inventing the FCC. Annu. Meet. Am. Fuel Petrochemical Manuf., Orlando: 2014.

[4] Lambert N, Ogasawara I, Abba I, Redhwi H, Santner C. HS-FCC for propylene : concept to commercial operation. PTQ 2014:39–45.

[5] Graaf B, Allahverdi M, Evans M, Diddams P. "Snakes and ladders" for maximising propylene. PTQ 2014:1–7.

[6] Moolji S. Petrochemical Scenario Across Continents: What is Happening in the World of Polypropylene? Presented in 10CL Petrochemical Conclave, New Delhi 2014.

[7] Robert M. Handbook of petroleum refining processes, 3rd edn. Focus Catal 2004;2004:8.

[8] Den Hollander MA, Wissink M, Makkee M, Moulijn JA. Synergy effects of ZSM-5 addition in fluid catalytic cracking of hydrotreated flashed distillate. Appl Catal A Gen 2002;223:103–19.

[9] Maadhah A, Fujiyama Y, Redhwi H, Abul-Hamayel M, Aitani A, Saeed M, et al. A new catalytic cracking process to maximize refinery propylene. Arab J Sci Eng 2008;33:17–28.

[10] Sadeghbeigi R. Fluid Catalytic Cracking Handbook. 3rd ed. Elsevier; 2012.

[11] Raseev S. Thermal and Catalytic Processes in Petroleum Refining. CRC Press; 2003.

[12] Biswas J, Maxwell IE. Recent process- and catalyst-related developments in fluid catalytic cracking. Appl Catal 1990;63:197–258.

[13] Harding R., Peters a. ., Nee JR. New developments in FCC catalyst technology. Appl Catal A Gen 2001;221:389–96.

[14] Soni D, Rao MR, Saidulu G, Bhattacharyya D, Satheesh VK. Catalytic cracking process enhances production of olefins. Pet Technol Q 2009;14:95–100.

[15] Kung HH, Williams B a, Babitz SM, Miller JT, Haag WO, Snurr RQ. Enhanced hydrocarbon cracking activity of Y zeolites. Top Catal 2000;10:59–64.

[16] Al-Khattaf S. The influence of Y-zeolite unit cell size on the performance of FCC catalysts during gas oil catalytic cracking. Appl Catal A Gen 2002;231:293–306.

[17] Wallenstein D, Harding RH. The dependence of ZSM-5 additive performance on the hydrogen-transfer activity of the REUSY base catalyst in fluid catalytic cracking. Appl Catal A Gen 2001;214:11–29.

[18] Buchanan JS, Santiesteban JG, Haag WO. Mechanistic considerations in acid-catalyzed cracking of olefins. J Catal 1996;158:279–87.

[19] Dupain X, Makkee M, Moulijn JA. Optimal conditions in fluid catalytic cracking: A mechanistic approach. Appl Catal A Gen 2006;297:198–219.

[20] Vermeiren W, Gilson JP. Impact of zeolites on the petroleum and petrochemical industry. Top Catal 2009;52:1131–61.

[21] Zhao X, Harding RH. ZSM-5 Additive in Fluid Catalytic Cracking. 2. Effect of Hydrogen Transfer Characteristics of the Base Cracking Catalysts and Feedstocks. Ind Eng Chem Res 1999;38:3854–9.

[22] Cerqueira HS, Caeiro G, Costa L, Ramôa Ribeiro F. Deactivation of FCC catalysts. J Mol Catal A Chem 2008;292:1–13.

[23] Dwyer J, Rawlence DJ. Fluid catalytic cracking : chemistry. Catal Today 1993;18:487–507.

[24] Corma A, González-Alfaro V, Orchillés A. The role of pore topology on the behaviour of FCC zeolite additives. Appl Catal A Gen 1999;187:245–54.

[25] Zhu X, Liu S, Song Y, Xu L. Catalytic cracking of C4 alkenes to propene and ethene: Influences of zeolites pore structures and Si/Al2 ratios. Appl Catal A Gen 2005;288:134–42.

[26] Den Hollander MA, Wissink M, Makkee M, Moulijn JA. Gasoline conversion: Reactivity towards cracking with equilibrated FCC and ZSM-5 catalysts. Appl Catal A Gen 2002;223:85–102.

[27] Triantafillidis CS, Evmiridis NP, Nalbandian L, Vasalos I a. Performance of ZSM-5 as a Fluid Catalytic Cracking Catalyst Additive: Effect of the Total Number of Acid Sites and Particle Size. Ind Eng Chem Res 1999;38:916–27.

[28] Buchanan J. The chemistry of olefins production by ZSM-5 addition to catalytic cracking units. Catal Today 2000;55:207–12.

[29] Bortnovsky O, Sazama P, Wichterlova B. Cracking of pentenes to C2–C4 light olefins over zeolites and zeotypes. Appl Catal A Gen 2005;287:203–13.

[30] Lu J, Zhao Z, Xu C, Zhang P, Duan A. FeHZSM-5 molecular sieves - Highly active catalysts for catalytic cracking of isobutane to produce ethylene and propylene. Catal Commun 2006;7:199–203.

[31] Xiaoning W, Zhen Z, Chunming X, Aijun D, Li Z, Guiyuan J. Effects of Light Rare Earth on Acidity and Catalytic Performance of HZSM-5 Zeolite for Catalytic Cracking of Butane to Light Olefins. J Rare Earths 2007;25:321–8.

[32] Xue N, Chen X, Nie L, Guo X, Ding W, Chen Y, et al. Understanding the enhancement of catalytic performance for olefin cracking: Hydrothermally stable acids in P/HZSM-5. J Catal 2007;248:20–8.

[33] Rahimi N, Karimzadeh R. Catalytic cracking of hydrocarbons over modified ZSM-5 zeolites to produce light olefins: A review. Appl Catal A Gen 2011;398:1–17.

[34] Wan J, Wei Y, Liu Z, Li B, Qi Y, Li M, et al. A ZSM-5-based catalyst for efficient production of light olefins and aromatics from fluidized-bed naphtha catalytic cracking. Catal Letters 2008;124:150–6.

[35] Siddiqui MAB, Aitani AM, Saeed MR, Al-Yassir N, Al-Khattaf S. Enhancing propylene production from catalytic cracking of Arabian Light VGO over novel zeolites as FCC catalyst additives. Fuel 2011;90:459–66.

[36] Costa AF, Cerqueira HS, Ferreira JMM, Ruiz NMS, Menezes SMC. BEA and MOR as additives for light olefins production. Appl Catal A Gen 2007;319:137–43.

[37] Tarach K, Góra-Marek K, Tekla J, Brylewska K, Datka J, Mlekodaj K, et al. Catalytic cracking performance of alkaline-treated zeolite Beta in the terms of acid sites properties and their accessibility. J Catal 2014;312:46–57.

[38] Castañeda R, Corma A, Fornés V, Martínez-Triguero J, Valencia S. Direct synthesis of a 9 × 10 member ring zeolite (Al-ITQ-13): A highly shape-selective catalyst for catalytic cracking. J Catal 2006;238:79–87.

[39] Corma A, Gonzàlez-Alfaro V, Orchillès A V. Catalytic cracking of alkanes on MCM-22 zeolite. Comparison with ZSM-5 and beta zeolite and its possibility as an FCC cracking additive. Appl Catal A, Gen 1995;129:203–15.

[40] Corma A, Martinez-Triguero J. The Use of MCM-22 as a Cracking Zeolitic Additive for FCC. J Catal 1997;165:102–20.

[41] AfsharEbrahimi A, Tarighi S. The Influence of Temperature and Catalyst Additives on Catalytic Cracking of a Heavy Fuel Oil. Pet Sci Technol 2015;33:415–21.

[42] Corma A, Martínez-Triguero J, Valencia S, Benazzi E, Lacombe S. IM-5: A Highly Thermal and Hydrothermal Shape-Selective Cracking Zeolite. J Catal 2002;206:125–33.

[43] Corma A, Mengual J, Miguel PJ. IM-5 zeolite for steam catalytic cracking of naphtha to produce propene and ethene. An alternative to ZSM-5 zeolite. Appl Catal A Gen 2013;460-461:106–15.

[44] Bastiani R, Lam YL, Henriques CA, Teixeira da Silva V. Application of ferrierite zeolite in high-olefin catalytic cracking. Fuel 2013;107:680–7.

[45] Web page n.d. http://www.iza-structure.org/databases.

[46] Zones SI. Zeolite SSZ-33. US patent No. 4,963,337, 1990.

[47] Zones SI, Burton AW, Ong K. Molecular sieve SSZ-74 composition of matter and synthesis thereof. US patent No. 2007/0148086 A1, 2007.

[48] Han S, Shihabi DS. Dealumination of aluminosilicate zeolites. US patent No. 4,753910, 1988.

[49] Corma A, Chica A, Guil JM, Llopis FJ, Mabilon G, Perdigon-Melon J a, et al. Determination of the pore topology of zeolite IM-5 by means of catalytic test reactions and hydrocarbon adsorption measurements. J Catal 2000;189:382–94.

[50] Leonowicz ME, Lawton J a, Lawton SL, Rubin MK. MCM-22: A Molecular Sieve with Two Independent Multidimensional Channel Systems. Science (80-) 1994;264:1910–3.

[51] Kresge CT, Roth WJ, Simmons KG, Vartuli JC. Crystalline oxide material. US patent No.5,229,341, 1993.

[52] Hong SB, Min H-K, Shin C-H, Cox P a, Warrender SJ, Wright P a. Synthesis, crystal structure, characterization, and catalytic properties of TNU-9. J Am Chem Soc 2007;129:10870–85.

[53] Adewuyi YG, Klocke DJ, Buchanan JS. Effects of high-level additions of ZSM-5 to a fluid catalytic cracking (FCC) RE-USY catalyst. Appl Catal A, Gen 1995;131:121–33.

[54] International Zeolite Association n.d. www.ize-online.org (accessed March 26, 2015).

[55] Opanasenko M, Parker WON, Shamzhy M, Montanari E, Bellettato M, Mazur M, et al. Hierarchical hybrid organic-inorganic materials with tunable textural properties obtained using zeolitic-layered precursor. J Am Chem Soc 2014;136:2511–9.

[56] Gil B, Zones SI, Hwang SJ, Bejblová M, Čejka J. Acidic properties of SSZ-33 and SSZ-35 novel zeolites: a complex I.R. and MAS NMR study. J Phys Chem C 2008;112:2997–3007.

[57] Baerlocher C, Xie D, McCusker LB, Hwang S-J, Chan IY, Ong K, et al. Ordered silicon vacancies in the framework structure of the zeolite catalyst SSZ-74. Nat Mater 2008;7:631–5.

[58] Li X, Li C, Zhang J, Yang C, Shan H. Effects of Temperature and Catalyst to Oil Weight Ratio on the Catalytic Conversion of Heavy Oil to Propylene Using ZSM-5 and USY Catalysts. J Nat Gas Chem 2007;16:92–9.

[59] Roth WJ, Nachtigall P, Morris RE, Čejka J. Two-Dimensional Zeolites : Current Status and Perspectives. Chem Rev 2014;114:4807–37.

[60] Zhao X, Roberie TG. ZSM-5 Additive in Fluid Catalytic Cracking. 1. Effect of Additive Level and Temperature on Light Olefins and Gasoline Olefins. Ind Eng Chem Res 1999;38:3847–53.

[61] De la Puente G, Sedran U. Evaluation of hydrogen transfer in FCC catalysts. A new approach for cyclohexene as a test reactant. Chem Eng Sci 2000;55:759–65.

[62] Maheshwari S, Martínez C, Teresa Portilla M, Llopis FJ, Corma A, Tsapatsis M. Influence of layer structure preservation on the catalytic properties of the pillared zeolite MCM-36. J Catal 2010;272:298–308.

[63] Scherzer J. Octane-Enhancing, Zeolitic FCC Catalysts: Scientific and Technical Aspects. Catal Rev Sci Eng 1989;31:215–354.

[64] Pujro R, Falco M, Sedran U. Formation of aromatics in heavy gasoline and light LCO ends in FCC. "Applied Catal A, Gen 2015;489:123–30.

[65] Avidan AA, Shinnar R. Development of catalytic cracking technology. A lesson in chemical reactor design. Ind Eng Chem Res 1990;29:931–42.

[66] Pitault I, Nevicato D, Forissier M, Bernard J-R. Kinetic model based on a molecular description for catalytic cracking of vacuum gas oil. Chem Eng Sci 1994;49:4249–62.

[67] Lee L-S, Chen Y-W, Huang T-N, Pan W-Y. Four-lump kinetic model for fluid catalytic cracking process. Can J Chem Eng 1989;67:615–9.

[68] Bollas GM, Lappas AA, Iatridis DK, Vasalos IA. Five-lump kinetic model with selective catalyst deactivation for the prediction of the product selectivity in the fluid catalytic cracking process. Catal Today 2007;127:31–43.

[69] Hagelberg P, Eilos I, Hiltunen J, Lipiäinen K, Niemi VM, Aittamaa J, et al. Kinetics of catalytic cracking with short contact times. Appl Catal A Gen 2002;223:73–84.

[70] Al-Sabawi M, Atias JA, De Lasa H. Kinetic modeling of catalytic cracking of gas oil feedstocks: Reaction and diffusion phenomena. Ind Eng Chem Res 2006;45:1583–93.

[71] Weekman VW, Nace DM. Kinetics of catalytic cracking selectivity in fixed, moving, and fluid bed reactors. AIChE J 1970;16:397–404.

[72] Al-Khattaf S, Lasa H de. Diffusion and reactivity of gas oil in FCC catalysts. Can J Chem Eng 2001;79:341–8.

[73] Bollas GM, Vasalos IA, Lappas AA, Iatridis D. Modeling Small-Diameter FCC Riser Reactors. A Hydrodynamic and Kinetic Approach. Ind Eng Chem Res 2002;41:5410–9.

[74] Schwaab M, Lemos LP, Pinto JC. Optimum reference temperature for reparameterization of the Arrhenius equation. Part 2: Problems involving multiple reparameterizations. Chem Eng Sci 2008;63:2895–906.

[75] Ahari JS, Farshi A, Forsat K. A mathematical modeling of the riser reactor in industrial FCC unit. Pet Coal 2008;50:15–24.

[76] Sertić-Bionda K, Gomzi Z, Fabulić-Ruszkowski M. Kinetics of gas oil catalytic cracking. React Kinet Catal Lett 2006;88:111–8.

[77] Bari Siddiqui MA, Aitani AM, Saeed MR, Al-Khattaf S. Enhancing the production of light olefins by catalytic cracking of FCC naphtha over mesoporous ZSM-5 catalyst. Top Catal 2010;53:1387–93.

[78] Tukur NM, Al-Khattaf S. Catalytic cracking of n-dodecane and alkyl benzenes over FCC zeolite catalysts: Time on stream and reactant converted models. Chem Eng Process 2005;44:1257–68.

[79] Psarras AC, Iliopoulou EF, Kostaras K, Lappas AA, Pouwels C. Investigation of advanced laboratory deactivation techniques of FCC catalysts via FTIR acidity studies. Microporous Mesoporous Mater 2009;120:141–6.

[80] Awayssa O, Al-Yassir N, Aitani A, Al-Khattaf S. Modified HZSM-5 as FCC additive for enhancing light olefins yield from catalytic cracking of VGO. Appl Catal A Gen 2014;477:172–83.

VITAE

Name	Abdelrahman Izzeldin Hussain
Nationality	Sudanese
Date of Birth	5/29/1989
Email	a.izzaldeen@gmail.com
Address	Dammam, Eastern Province, Kingdom of Saudi Arabia
Academic Background	Bachelor of Science, Chemical Engineering (2007-2012) University of Khartoum, Sudan
Publications	A.I. Hussain, A.M. Aitani, Martin Kubů, Jiří Čejka, S. Al-Khattaf. Fuel 167 (2016) 226-239